REMARKS

Applicants thank the Examiner for the courtesy of the interview held on September 16, 2008. The above amendments and following remarks are responsive to the interview and reflect the points discussed at the interview.

Applicants respectfully request reconsideration of the present application in view of the foregoing amendments and in view of the reasons that follow.

Claims 2, 5, and 11 are amended. Claim 1, and 3-4 are cancelled. Support for amendment can be found throughout the Specification, for example, in the paragraph starting from Page 7/Line 27.

After amending the claims as set forth above, claims 2, 5-7, and 11 are now pending for examination. Claims 8-10 and 12-14 remain withdrawn.

Information Disclosure Statement

Applicants enclose a resubmission of an Information Disclosure Statements filed in the above-identified application on October 12, 2005. Copies of the foreign patent documents and literature articles are submitted herewith to ensure consideration thereof by the Examiner. The absence of a full English translation or an English-language counterpart document does not relieve the PTO from its duty to consider any submitted document (37 CFR §1.98 and MPEP§609). Further, the relevance of the foreign language reference is given in the International Search Report filed on August 21, 2007, which meets the "concise explanation" requirement for foreign language documents.

Applicants respectfully request that each listed document be considered by the Examiner and be made of record in the present application and that an initialed copy of Form PTO/SB/08 be returned in accordance with MPEP §609.

Claim Rejections 35 U. S. C. § 112

Claims 5 and 11 are rejected under 35 U.S.C. 112, 2nd paragraph. Claim 5 is amended, without prejudice, to recite "the genome of said mouse, except for the targeted endogenous GLAST gene, is the same as that of a C57BL/6 strain mouse", as the Examiner

suggested in the interview held on September 16, 2008. Claim 11 is a proper product-by-process claim. A product-by-process claim is legally classified by the USPTO as a product claim, and therefore, should be examined with the elected product claims. Applicants respectfully request withdrawal of the 112 rejections in view of above amendments.

Claim Rejections 35 U. S. C. § 102

Applicants acknowledge that the previously granted 102 rejection of claim 11 is withdrawn.

Claim Rejections 35 U. S. C. § 103

Claims 2 and 5-7 are rejected under 35 U.S.C. 103 (a) as being unpatentable over Watase et al. (Eur. J. Neurosci. 10: 976-988, 1998) in view of Chitnis et al. (J. Clin. Invest. 108(5): 739-747, 2001). Applicants respectfully request withdrawal of the 103 rejections in view of following reasons.

(I) Watase and Chitnis fails to disclose the phenotype of the mouse claimed in claims 2 and 11 or to disclose all elements of the method of making the mouse claimed, even if combined.

The Examiner alleged that "it would have been *prima facie* obvious for a person of ordinary skill in this art to combine the teaching of Watase et al. and Chitnis et al. (*as both describe mice with targeted disruption of endogenous genes in a C57BL/6 genetic background*)", and argued that "Applicants have ignored the teaching of Chitnis et al. for the multigenerational backcross to a C57BL/6 genetic background to produce an inbred GLAST knockout mouse having less genotypic and phenotypic background variation." (Page 6, 3rd Paragraph of the Office Action dated on Nov 14, 2007 that is asserted in the presently pending Office Action, and Page 5, 2nd Paragraph of the Office Action dated on Jun 20, 2007, the presently pending Office Action). Applicants respectfully disagree.

Watase is directed to studying function of GLAST and teaches that GLAST may play active roles both in the cerebellar climbing fibre synapse formation and in preventing excitotoxic cerebellar damage after acute brain injury. Watase does teach one to identify heterozygous and homozygous mice by Southern blot analysis, and to obtain homozygous and

heterozygous mice by heterozygote mating. However, Watase *fails* to teach *repeating crossing of heterozygous (GLAST knockout mice) with wild-type C57BL/6 strain mice for at least 5 times*, which is proven to be essential for producing a GLAST knockout mouse, as claimed in claim 2, having an intraocular pressure within a normal range (not greater than 21 mmHg) and 20% - 50% less retinal ganglions cells than a wild-type mouse.

Furthermore, Chitnis is directed to "study effect of targeted disruption of STAT4 and STAT6 on the induction of experimental autoimmune encephalomyelitis and teaches that STAT4 and STAT6 genes play a critical role in regulation the autoimmune response in EAE." Chitnis discloses a method comprising a step of "*backcrossing STAT4 and STAT6 mice* with C57BL/6 background for at least ten generations." There would have been no reasonable expectation of success based on Chitnis that backcrossing would be effective for a totally different combination involving a GLAST knockout mouse.

Note that, although GLAST knockout and STAT4 / STAT6 mice are mice with targeted disruption of endogenous gene, the disclosure of two species (STAT4 and STAT6) does *not* render a third species (GLAST knockout mice) of the same genus (mice with targeted disruption of endogenous gene) obvious.

Thus, even if combined, Watase and Chitnis *fails* to disclose at least above features of method of making the articles claimed in currently pending claims.

(II) It is a surprising result that the method disclosed in this Application produces GLAST knockout mice having an intraocular pressure within normal range (not greater than 21 mmHg) and having at least 20% less retinal ganglions cells than a wild-type mouse.

In contrast to what the Examiner alleges in the Office Actions, the step of "repeating crossing the heterozygous mouse obtained in step 3 with a normal C57BL/6 strain mouse to generate a heterozygous knockout mouse" produces an inbred GLAST knockout mouse *not only* having less genotypic and phenotypic background variation, *but also, surprisingly,* having an intraocular pressure within a normal range (not greater than 21 mmHg) and 20% - 50% less retinal ganglions cells than a wild-type mouse. Chitnis in no way suggests such results would be possible.

Indeed, one of ordinary skill of art in this field would *not* be able to predict, with a reasonable expectation of success, how various types of genetic backgrounds for each mouse strain would affect phenotype of a knockout mouse. For example, the cataracts associated with the phenotype displayed by the Cx50 knockout mouse backcrossed with the C57BL/6J strains become milder than that associated with the phenotype of a mouse backcrossed with the 129S6 strains (see Lines 2-8 in the right column at Page 2671 and Fig. 2 in Invest Ophthalmol Vis Sci 44: 2669-2674, 2003 "Exhibit A"). In such case, the expression of other genes (genetic modifiers) that affect the phenotype of the knockout mouse may be differentiated among different mice strains. (See Lines 4-6 in abstract and line 2 from the bottom in the middle column to Line 6 in the right column in Science 299: 1579, 2003 "Exhibit B", and Lines 6-9 in the abstract and Fig. 2A of Mech Dev 124: 551-558, 2007 "Exhibit C")

In particular, Applicants submit that the GLAST knockout mice backcrossed with the 129sv strains display a different phenotype from the GLAST knockout mice backcrossed with the C57BL/6J strains. For example, in contrast to GLAST knockout mice obtained by backcrossing with the C57BL/6J strains, significant reducing of the number of the retinal ganglion cells was *not* observed on GLAST knockout mice obtained by backcrossing with the 129sv strains, as shown in the Rule 132 Declaration accompanying this Response.

In addition, the induction of neural cell death by ischemic load is believed to be due to a different mechanism than spontaneous neural cell death. In contrast to the degeneration in the neural cells observed in the GLAST knockout mouse backcrossed with the C57BL/6J mouse, when GLT1 (a transporter for glutamic acid other than GLAST) knockout mouse was backcrossed with the C57BL/6J mouse, the degeneration in the neural cells was *not* observed (see Lines 16-20 in the left column at Page 1765 and Lines 2-3 in the right column at Page 1768 of J Clin. Invest. 117: 1763-1770, 2007 "Exhibit D"), although the induction of neural cell death by ischemic load was also observed in the GLT1 knockout mouse as in the GLAST knockout mouse (see Fig. 3 of PNAS 95: 4663, 1998 "Exhibit E").

Thus, Applicants respectfully submit that one of the ordinary skill in the art would not be able to predict that the GLAST knockout mouse backcrossed with the C57BL/6J strains

would result in the phenotype recited in the present claims, with a reasonable expectation of success, at the time of the instant invention.

Conclusion

Applicants believe that the present application is now in condition for allowance. Favorable reconsideration of the application as amended is respectfully requested.

The Examiner is invited to contact the undersigned by telephone if it is felt that a telephone interview would advance the prosecution of the present application.

The Commissioner is hereby authorized to charge any additional fees which may be required regarding this application under 37 C.F.R. §§ 1.16-1.17, or credit any overpayment, to Deposit Account No. 19-0741. Should no proper payment be enclosed herewith, as by a check being in the wrong amount, unsigned, post-dated, otherwise improper or informal or even entirely missing or a credit card payment form being unsigned, providing incorrect information resulting in a rejected credit card transaction, or even entirely missing, the Commissioner is authorized to charge the unpaid amount to Deposit Account No. 19-0741. If any extensions of time are needed for timely acceptance of papers submitted herewith, Applicants hereby petition for such extension under 37 C.F.R. §1.136 and authorize payment of any such extensions fees to Deposit Account No. 19-0741.

Respectfully submitted,

Date November 19, 2008

By [signature] Reg. No 43,438

for Stephen B. Maebius
Attorney for Applicants
Registration No. 35,264

FOLEY & LARDNER LLP
Customer Number: 22428
Telephone: (202) 672-5569
Facsimile: (202) 672-5399

Exhibit A

Genetic Background Influences Cataractogenesis, but Not Lens Growth Deficiency, in Cx50-Knockout Mice

Dwan A. Gerido, Caterina Sellitto, Leping Li, and Thomas W. White

Purpose. Deletion of connexin (Cx)50 produces microphthalmia with nuclear cataracts. To determine whether these two traits are influenced by genetic background and are dependent on each other, mice carrying the Cx50 deletion in two different strains were generated, and the growth defect and severity of cataracts were analyzed.

Methods. Cx50-knockout mice were generated in the 129S6 strain, and back-crossed into the C57BL/6J genetic background. To analyze the influence of genetic background on the observed phenotype, postnatal lens growth, lens clarity, lens histology and crystallin solubility were determined and compared between the two strains of Cx50-knockout mice.

Results. The growth deficiency persisted, regardless of genetic background, but genetic modifiers that differentially altered the solubility of crystallin proteins influenced the severity of cataracts. Expression levels of Cx46 were similar in all animals, regardless of genetic background, indicating that the differences were not due to a compensatory upregulation of Cx46.

Conclusions. Taken together, these data indicate that the two components of the Cx50 phenotype are independent of each other and that cataractogenesis is under the influence of an unidentified genetic modifier. (*Invest Ophthalmol Vis Sci.* 2003;44:2669–2674) DOI:10.1167/iovs.02-1311

The mammalian lens is a multicellular organ in which the cells act as a functional syncytium. The lens is composed of a single layer of epithelial cells located at the anterior surface and a solid mass of elongated fiber cells that extend from the anterior to posterior pole. During differentiation, lens epithelial cells undergo a process of maturation and elongation during which they become new lens fiber cells.[1,2] The mature lens fiber cells are unique in that they have no intracellular organelles and lack a vascular supply of nutrients. The absence of blood supply and intracellular organelles is necessary for transparency, but presents serious homeostatic and metabolic challenges to the cells within the lens. Lens fiber cells have overcome these challenges through gap-junction–mediated intercellular communication, which allows the metabolically active epithelial cells to share ions, second messengers, and metabolites with the lens fiber cells.[3]

Structural proteins belonging to the connexin (Cx) family comprise the intercellular channels present in gap junctions. Functional channels are formed when connexons on adjacent cells align, giving rise to a direct pathway for cell-to-cell communication. Each connexin forms channels with distinctly different physiological properties of permeation, gating, and selective interaction with other members of the connexin family.[4,5] The connexin gene family encodes at least 20 different proteins, of which three are expressed in the lens.[6,7] The lens epithelium predominantly expresses Cx43,[8,9] but during epithelium-to-fiber cell differentiation, Cx43 expression is downregulated and replaced by two different connexins, Cx46 and Cx50.[10–13]

Studies involving the deletion of connexin proteins expressed in the lens have revealed their diverse roles in lens homeostasis. Knockout of Cx43 leads to cardiac malformation and neonatal death.[14] Thus, analysis of a lens phenotype in the absence of Cx43 was limited to prenatal development, which was found to proceed normally, at least until birth.[15,16] Deletion of Cx46 results in a severe, senile-type cataract, with otherwise normal ocular development, whereas deletion of Cx50 produces much milder nuclear pulverulent cataracts, along with a significant reduction in ocular growth.[17–19]

The difference in cataract severity between Cx46- and Cx50-knockout mice has been attributed to abnormal proteolytic cleavage of crystallins. Crystallin proteins comprise the major cytoplasmic component of lens fiber cells, and loss of crystallin solubility leads to cataractogenesis.[20] Deletion of Cx46 resulted in an aberrant cleavage of γ-crystallin, which was not observed in the Cx50-knockout.[17,18] This cleavage resulted from an increase in calcium accumulation and activity of the calcium-dependent protease Lp82 in Cx46-knockout lenses.[21]

Although these studies clearly support different roles for Cx46 and Cx50 in lens development, they do not address the question of whether other genetic factors are able to exert an influence on the phenotype in animals where these genes have been deleted. It has been shown that the deletion of Cx46 in animals of different genetic backgrounds resulted in differences in cataract severity that directly correlated with the relative levels of cleaved γ-crystallin. This finding demonstrated that other genetic factors could profoundly influence the phenotype of connexin-knockout animals. In the current study, we explored whether genetic factors also influence the Cx50-knockout phenotype. We found that the growth deficiency persisted regardless of genetic background, but that the process of the cataractogenesis was markedly different between the two animal strains tested.

Methods

Cx50-Deficient Mice

The study adhered to the ARVO Statement for the Use of Animals in Ophthalmic and Vision Research. The generation of Cx50-deficient mice in the 129S6 and C57BL/6J mouse strains (Taconic Farms Inc., Germantown, NY) has been described.[16,18] Animals were genotyped by PCR screening by a three-primer protocol for the Cx50 allele. A common 5′ flanking primer (pcr 1; 5′-GCCCCCTCCTGCTTATTTCTG-3′) was paired with either a 3′ primer derived from vector sequences unique to the Cx50 replacement cassette (pcr 2; 5′-CGGGCCTCT-

From the Department of Physiology and Biophysics, State University of New York, Stony Brook, New York.

Supported by National Eye Institute Grant EY13163 and National Institute of Deafness and Other Communications Disorders Grant DC05491.

Submitted for publication December 19, 2002; revised January 24, 2003; accepted January 31, 2003.

Disclosure: **D.A. Gerido**, None; **C. Sellitto**, None; **L. Li**, None; and **T.W. White**, None

The publication costs of this article were defrayed in part by page charge payment. This article must therefore be marked "*advertisement*" in accordance with 18 U.S.C. §1734 solely to indicate this fact.

Corresponding author: Thomas W. White, Department of Physiology and Biophysics, State University of New York, T5-147, Basic Science Tower, Stony Brook, NY 11794-8661; thomas.white@sunysb.edu.

TCGCTATTACG-3′), or a third primer derived from the Cx50-coding region (pcr 3; 5′-CTCCATGCGAACGTGGTGTAC-3′). Primers 1+2 amplified a 1370-bp band from Cx50-knockout chromosomes. Amplification of wild-type chromosomes with primers 1+3 produced a 1600-bp band. DNAs isolated from tail biopsy samples were amplified in a thermal cycler (DNA Engine Dyad; MJ Research, Waltham, MA), and amplified products were resolved by agarose gel electrophoresis.

Protein Analysis

For protein expression analysis, lenses were dissected from adult Cx50 wild-type and Cx50-knockout mice from each genetic background. Equal wet weights of wild-type and knockout lenses were homogenized in 1 mL of 0.1 M NaCl, 0.1 M Na_2HPO_4, 10 mM ascorbic acid, and protease inhibitors (10 μg/mL each of chymostatin, leupeptin, and pepstatin). The homogenized tissue was centrifuged at 14,000*g* for 20 minutes at room temperature, after which the soluble fraction was recovered and stored at −80°C. The insoluble fraction was subjected to a second wash with 1 mL of 0.1 M NaCl and 0.1 M Na_2HPO_4, followed by a subsequent wash with 1 mL of 20 mM NaOH. After centrifugation at 14,000*g* for 20 minutes, the insoluble fraction was finally washed in 1 mL of 1 mM Na_2CO_3, after which the pellets were resuspended in 0.1 mL of sample buffer and stored at −80°C.

Equal aliquots of samples from each animal strain and genotype were electrophoresed on 15% polyacrylamide gels, transferred to nitrocellulose membranes, and incubated with antibodies specific for Cx50[12]; Cx46[11]; major intrinsic polypeptide (MIP); and αA-, αB-, β-, and γ-crystallin proteins (αA-, αB- and β-crystallin antibodies were purchased from Stressgen, Victoria, British Columbia, Canada; MIP and γ-crystallin antibodies were generously provided by Joseph Horwitz, Jules Stein Eye Institute, University of California Los Angeles). Primary antibodies were detected with alkaline phosphatase–conjugated goat anti-rabbit IgG (Roche Molecular Biochemicals, Indianapolis, IN) with nitro blue tetrazolium and 5-bromo-4-chloro-3-indolyl phosphate used as substrates (Sigma Chemical Co., St. Louis, MO). Blots were digitized, and band intensities were quantified with image-analysis software (1D; Eastman Kodak, Rochester, NY). Values were normalized to the mean band intensity in the 129S6 strain for each protein analyzed and multiplied by 100 to express a percentage.

Growth and Cataract Analysis

Lens growth in Cx50 wild-type and knockout animals from each mouse strain was studied at 2, 4, and 6 weeks of age. Animals were killed and weighed to determine their overall growth. Eye and lens growth was examined by sequentially dissecting each organ before weighing. Lenses were dissected from wild-type and knockout animals in each mouse strain on a 37°C stage in M199 medium supplemented with Hanks' salts and 10 mM HEPES [pH 7.4]. Cataracts were visualized using a microscope (model SZX9; Olympus Corporation of America, Lake Success, NY) and photographed with a digital camera (model C3030; Olympus).

Histology

Mouse eyes were dissected and fixed in 4% formaldehyde, freshly prepared from paraformaldehyde, in phosphate-buffered saline (PBS) for 16 to 24 hours at room temperature. Fixed eyes were rinsed in PBS, dehydrated through an ethanol series and embedded in paraffin. Sections of 2 to 3 μm were cut on a diamond knife, deparaffinized, and stained with hematoxylin and eosin.[16,18,22] Histologic sections were viewed with 10× and 40× objectives on a microscope (model BX51; Olympus) and photographed with an digital camera (MagnaFire; Optronics, Goleta, CA).

Results

Ocular Growth of Cx50-Knockout Mice

Initial characterization of mice without the Cx50 gene in a mixed genetic background demonstrated deficient eye and lens growth.[18,19] To determine whether these growth abnormalities are influenced by genetic background, the mass of the animals, eyes, and lenses from knockout mice in the 129S6 and C57BL/6J backgrounds were recorded at 2, 4, and 6 weeks of age and compared with wild-type animals. There were no statistically significant differences in the overall postnatal growth of wild-type and Cx50-knockout mice in either the 129S6 or C57BL/6J genetic backgrounds (Fig. 1A). Although the overall growth of knockout mice was similar to the control, growth of both the eyes and lenses of Cx50 knockouts was significantly reduced (Student's *t*-test, $P < 0.05$) when compared with wild-type animals (Figs. 1B, 1C). The reductions in

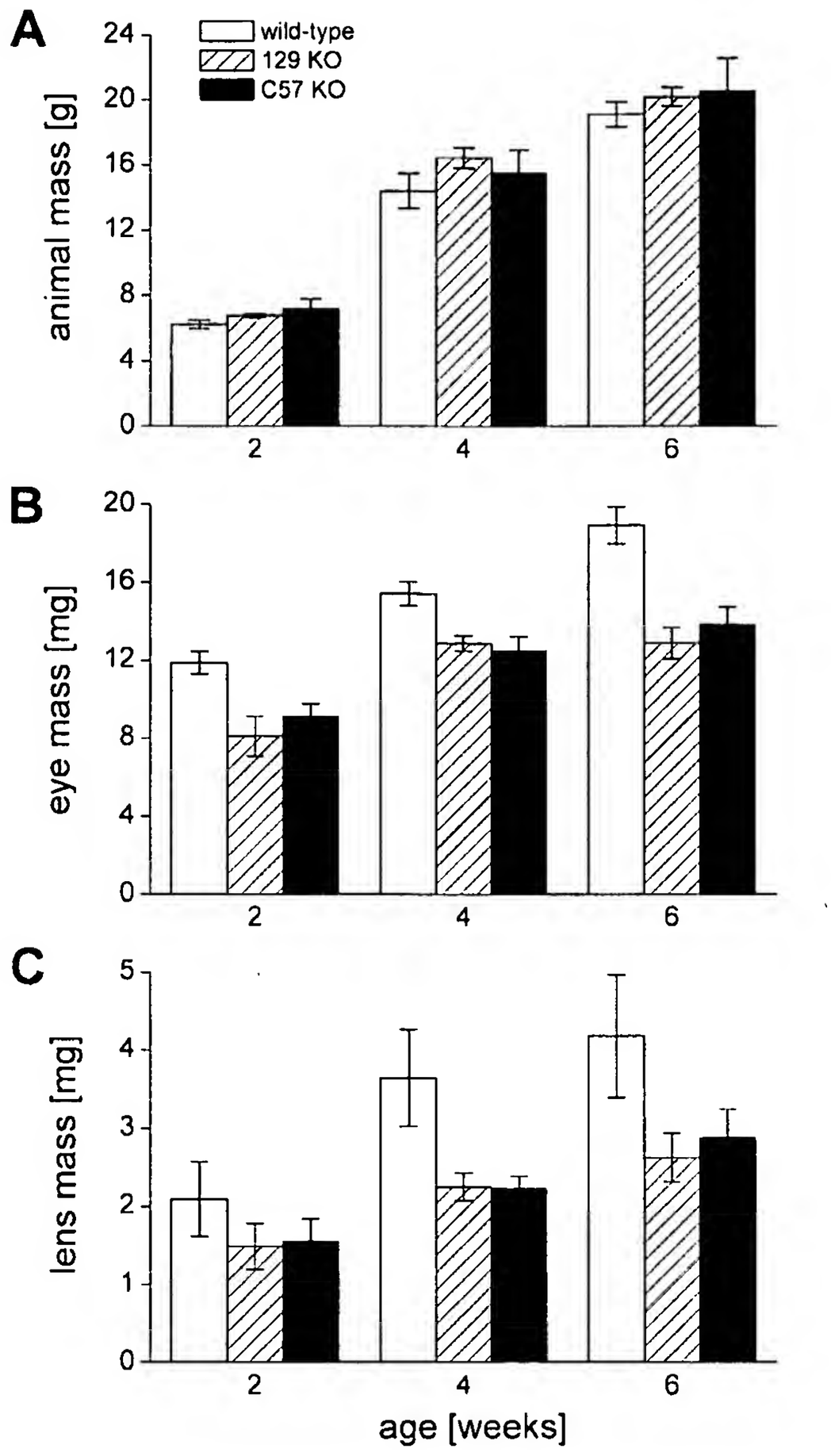

FIGURE 1. Eye and lens growth in Cx50-knockout mice. The mass of the animals, eyes, and lenses were recorded as a function of age. (**A**) Overall postnatal growth was similar between wild-type and knockout animals in both genetic backgrounds. (**B**) Eye growth in Cx50-knockout mice, in each genetic background significantly lagged that of wild-type mice. (**C**) Lens growth was also severely impaired in Cx50-knockout mice in each genetic background. The mass of Cx50-knockout eyes and lenses were not significantly different between the two genetic backgrounds, in both cases knockout lenses displayed a ~42% reduction in growth when compared with wild-type mice. Data are the mean ± SD (n = 4 to 8 animals at each time point).

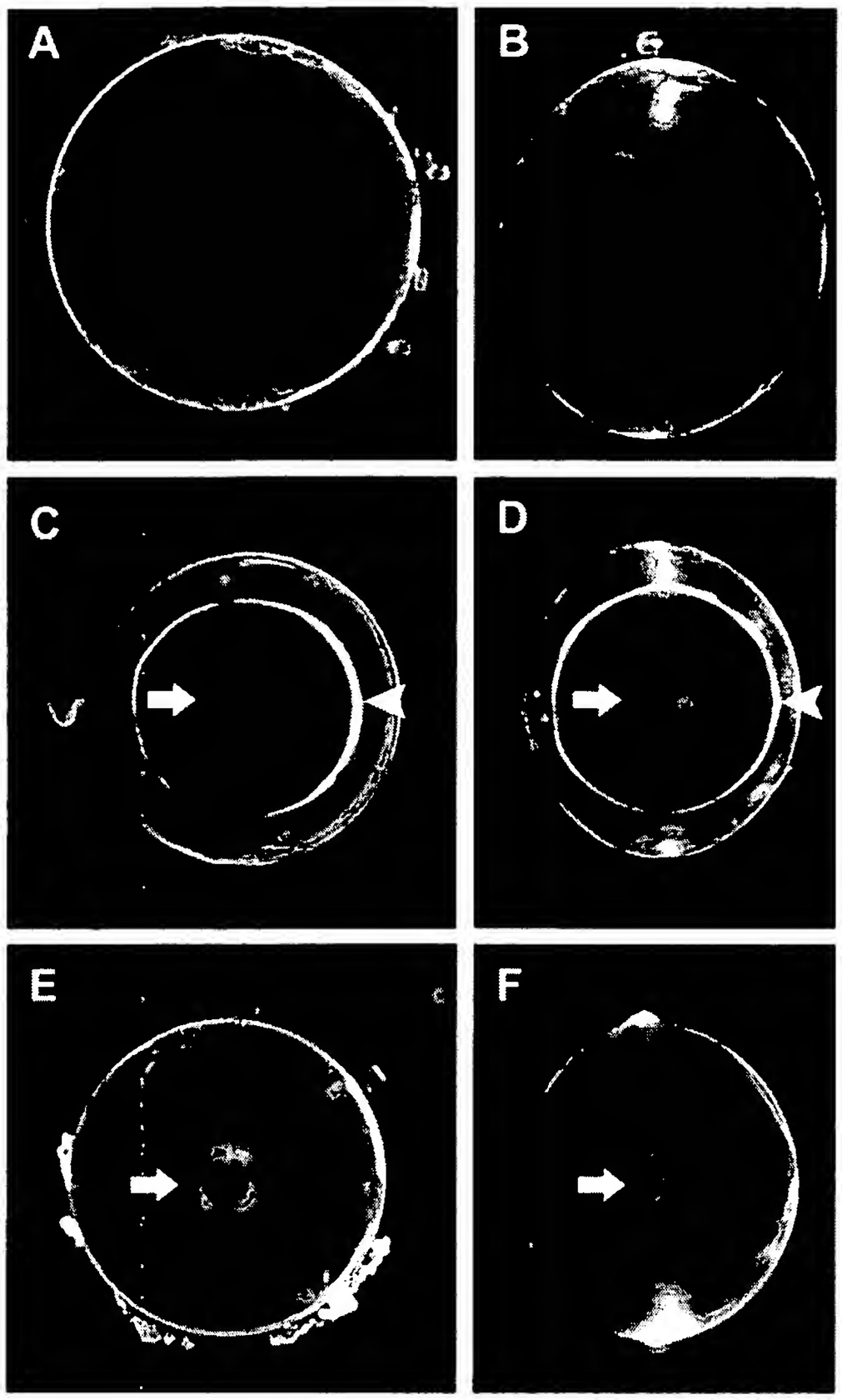

FIGURE 2. Nuclear cataracts in young Cx50-knockout mice. Eight-week-old lenses from each genotype were dissected and photographed for analysis of opacities. Wild-type lenses displayed no opacities when viewed either through the anterior surface (**A**) or on equatorial edge (**B**). Cx50-knockout mice in the 129S6 genetic background (**C**, **D**) displayed pulverulent nuclear cataracts (*arrows*) with a profound lamellar opacity in the lens cortex (*arrowheads*). In contrast, Cx50-knockout mice from the C57BL/6J genetic background (**E**, **F**) showed dense nuclear opacities that were markedly different from the pulverulent cataracts in mice from the 129S6 genetic background (*arrows*) and also showed no cortical lamellar cataract.

both eye and lens mass were similar in either the 129S6 or the C57BL/6J knockout mice at all ages tested, with knockout lenses displaying an approximate 42% reduction in growth compared with wild-type animals. Thus, genetic background did not influence the growth-deficient aspect of the Cx50-knockout phenotype.

Comparison of Lens Clarity

In animals of mixed genetic background, disruption of the Cx50 allele produced cataracts.[18] To determine whether the degree of lens opacity was influenced by genetic background, lenses from 8-week-old wild-type and knockout 129S6 and C57BL/6J animals were dissected and photographed using dark-field microscopy. Wild-type lenses were clear when viewed through the anterior epithelium (Fig. 2A) or through the equatorial edge (Fig. 2B). Disruption of the Cx50 allele produced cataracts in both genetic backgrounds, with distinct differences in the character of lens opacity. Cx50-knockout mice from the 129S6 genetic background displayed pulverulent nuclear cataracts with a prominent lamellar opacity (Figs. 2C, 2D). In contrast, Cx50-knockout mice from the C57BL/6J genetic background contained an irregular nuclear opacity with a greatly reduced, or absent, lamellar cataract (Figs. 2E, 2F). To determine whether a lamellar cataract develops in the C57BL/6J knockout lenses later in life, lenses from 6-month-old mice were also examined. We found that the cataract phenotypes of older 129S6 (Figs. 3A, 3B) and C57BL/6J (Figs. 3C, 3D) lenses were quite comparable to those of 8-week-old animals and that the differences in opacities did not simply result from a similar process operating with different kinetics. These results indicate that the cataract phenotype of Cx50-knockout mice was influenced by genetic factors that produced differences in the degree of lens opacity and that the differences in lens opacity were constant at least up to 6 months of age.

Analysis of Crystallin Solubility

Deletion of either Cx46 or Cx50, results in the loss of crystallin solubility and produces cataracts.[17-19] In the case of Cx46, it was subsequently shown that cataract severity is influenced by genetic background, with 129SvJ (129S4) Cx46-knockout mice having more severe cataracts than C57BL/6J Cx46-knockout mice.[23] To ascertain whether crystallin precipitation in Cx50-knockout mice is influenced by genetic background, the solubility of crystallin proteins was examined in 129S6 and C57BL/6J animals. Control and knockout lenses of adult mice in both backgrounds were separated into soluble and insoluble components,[18] and equal volumes of these fractions were

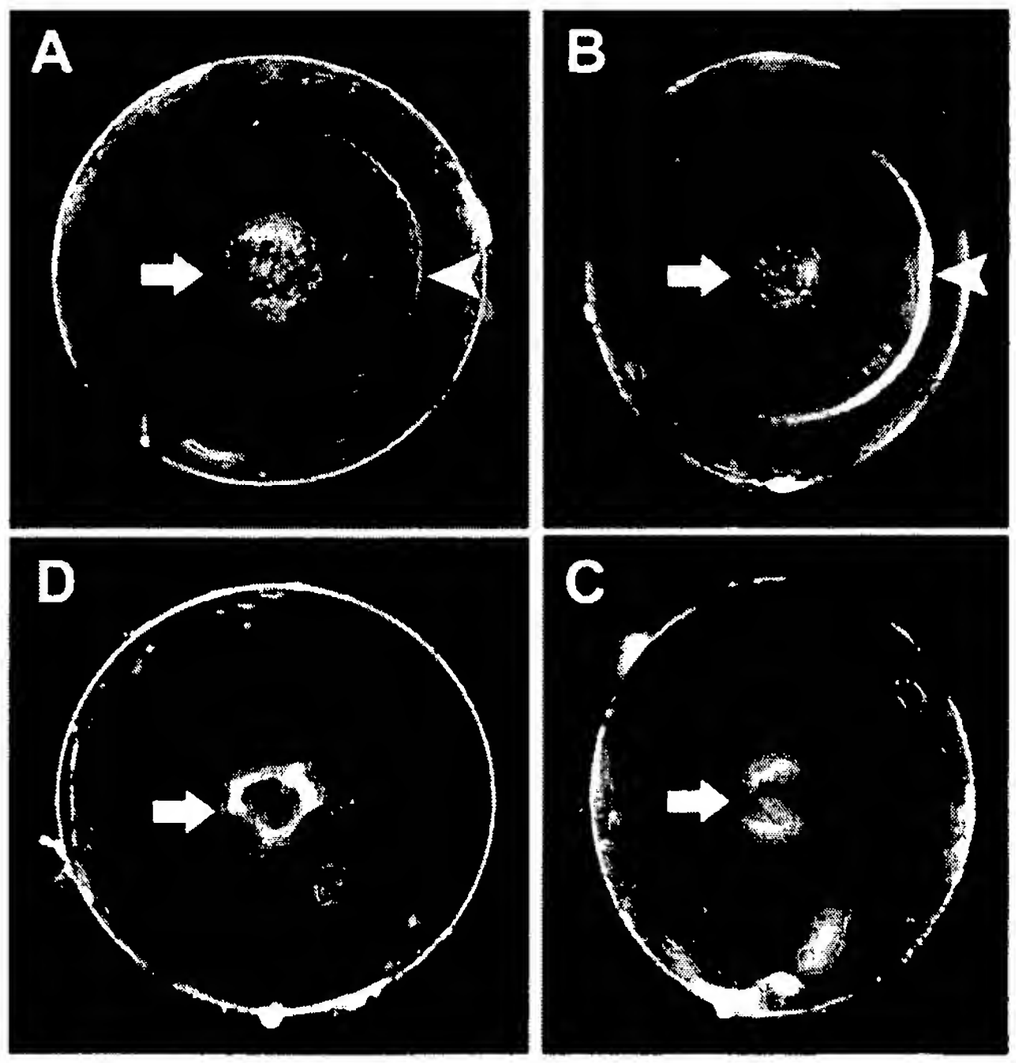

FIGURE 3. Nuclear cataracts in older Cx50-knockout mice. Six-month-old lenses from Cx50-knockout animals in both genetic backgrounds were dissected and photographed for analysis. Lenses from 129S6 mice (**A**, **B**) showed little difference in the severity or pattern of crystallin precipitation from that observed at 8 weeks of age, displaying pulverulent nuclear cataracts (*arrows*) with a profound lamellar opacity in the lens cortex (*arrowheads*). Adult lenses from Cx50-knockout animals in the C57BL/6J genetic background differed from the 129S6 mice in the same manner as the younger lenses, displaying an irregular nuclear cataract (*arrows*) and an absence of lamellar opacity (**C**, **D**).

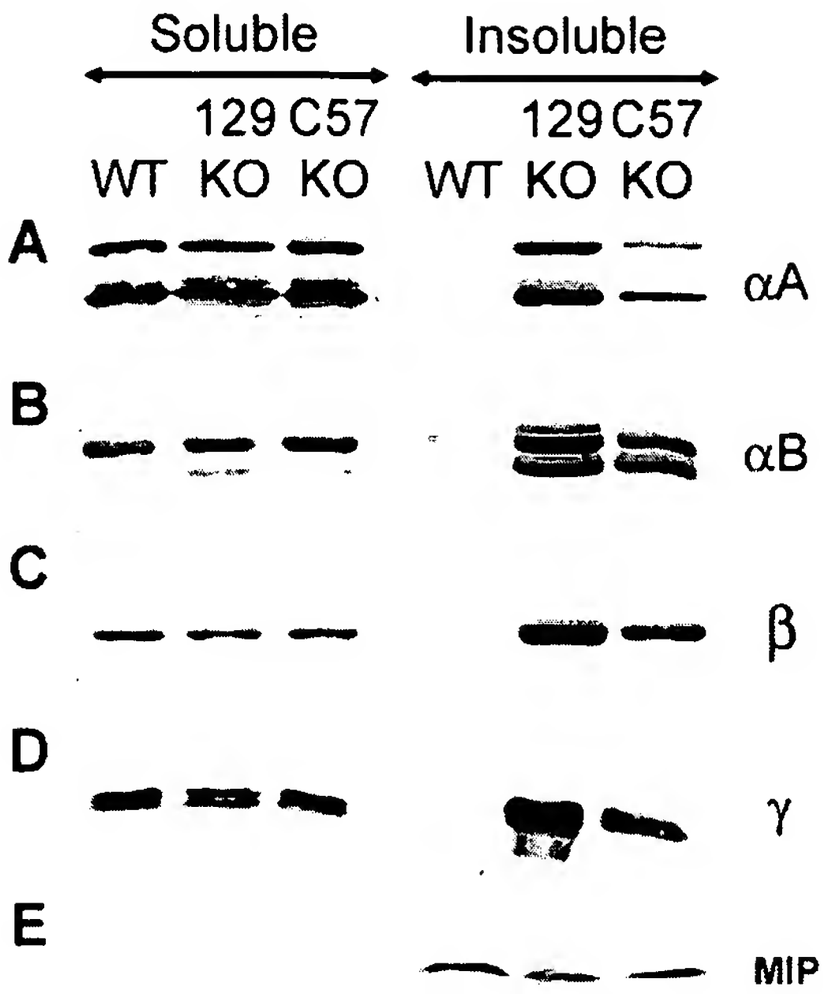

FIGURE 4. Biochemical analysis of crystallin solubility. Lenses were separated into soluble and insoluble fractions and subjected to Western blot analysis. Equal volumes of lens homogenates were probed with antibodies specific for αA- (**A**), αB- (**B**), β- (**C**), and γ-crystallin (**D**). Crystallin proteins were abundant in the soluble fractions of wild-type and knockout animals, as expected. The insoluble fractions of wild-type mice contained little or no crystallin proteins, whereas the insoluble fractions of the 129Sv and C57BL/6J knockout mice contained precipitates of all three crystallin proteins. In addition, for each crystallin examined, there was qualitatively more present in the insoluble fraction from 129S6 than C57BL/6J knockout lenses. MIP expression levels (**E**) were unchanged in all mice, independent of the deletion of Cx50.

electrophoresed, analyzed by Western blot, and probed with antibodies to different crystallins. All the crystallin proteins examined were abundant in the soluble fractions from either wild-type or knockout lenses in both backgrounds (Figs. 4A–D, left). Consistent with the presence of opacities, αA-, αB-, β-, and γ-crystallins were present in the insoluble fraction of Cx50-knockout lenses, but not in wild-type lenses (Figs. 4A–D, right). There also appeared to be clear differences in the relative amounts of precipitated crystallin proteins in the two backgrounds, with more crystallins being present in the insoluble fraction of 129S6 than in that of C57BL/6J Cx50-knockout mice. In contrast, MIP was absent from the soluble fractions of all animals and equally abundant in the insoluble fractions of wild-type and Cx50-knockout lenses from both genetic backgrounds (Fig. 4E).

Differences in band intensity were quantified to determine the relative amounts of precipitated crystallin proteins in the two strains (Fig. 5). Cx50-knockout animals from the 129S6 genetic background displayed significantly increased amounts of αA-, αB-, and β-crystallin proteins when compared with Cx50-knockout mice from the C57BL/6J background (Student's *t*-test, $P < 0.05$). In a similar fashion, γ-crystallin was qualitatively more abundant in the 129S6 background, but statistical significance could not be ascertained because of the lack of sufficient antibody to perform multiple analyses. As a loading control for the insoluble fractions, we analyzed levels of MIP, and they not differ significantly between 129S6 and C57BL/6J lenses ($P = 0.75$). Thus, 129S6 Cx50-knockout mice displayed a significant increase in the amount of precipitated

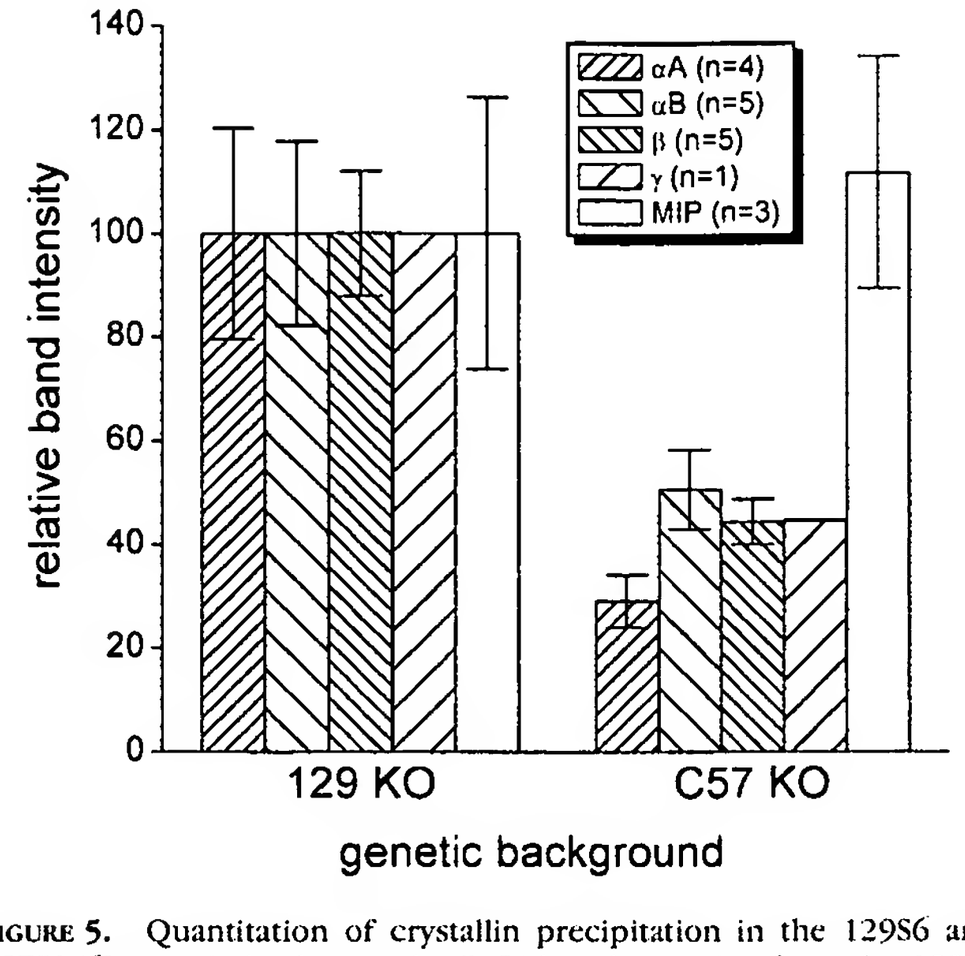

FIGURE 5. Quantitation of crystallin precipitation in the 129S6 and C57BL/6J genetic backgrounds. Cx50-knockout mice from the 129S6 genetic background displayed significantly greater precipitation of αA-, αB-, and β crystallins that did Cx50-knockouts in the C57BL/6J genetic background (Student's *t*-test, $P < 0.05$). Precipitation of γ-crystallin was also reduced in the C57BL/6J strain in one experiment. Relative amounts of MIP in the insoluble fractions were not significantly different. Data are the mean ± SD of the indicated number of experiments.

crystallins when compared with levels in the C57BL/6J animals. This finding is consistent with the more prominent opacities that were observed in the 129S6 knockout lenses, and supports the notion that a genetic modifier results in milder cataracts in the C57BL/6J mice.

Analysis of Connexin Synthesis

One possible explanation for the difference in cataractogenesis between Cx50-knockout mice in the 129S6 and C57BL/6J backgrounds is that different levels of Cx46 are normally present in the two strains. To test whether Cx46 was differentially expressed in the Cx50-knockout mice, the insoluble fractions used for crystallin analysis were probed with antibodies to Cx50 and Cx46. Western blot analysis of the insoluble fractions confirmed that Cx50 was absent in knockout animals from both genetic backgrounds, whereas wild-type animals continued to synthesize Cx50 protein (Fig. 6A). The expression of Cx46 was qualitatively similar in Cx50-knockout animals of both genetic backgrounds and comparable to that in wild-type

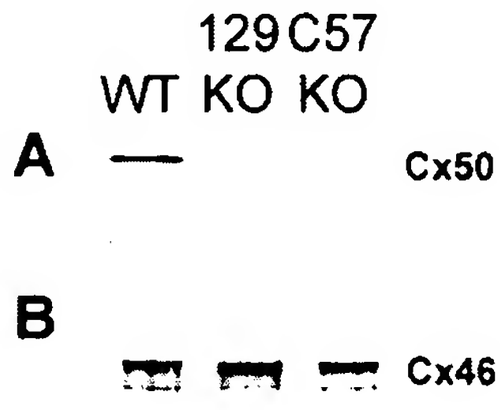

FIGURE 6. Analysis of connexin synthesis. Equal volumes of the lens fractions used in Figure 3 were probed with antibodies specific for Cx50 (**A**) and Cx46 (**B**). Cx50 was present in the insoluble fraction of wild-type animals only, confirming that the Cx50 gene was deleted. Cx46 expression levels were unchanged in all mice, independent of the deletion of Cx50.

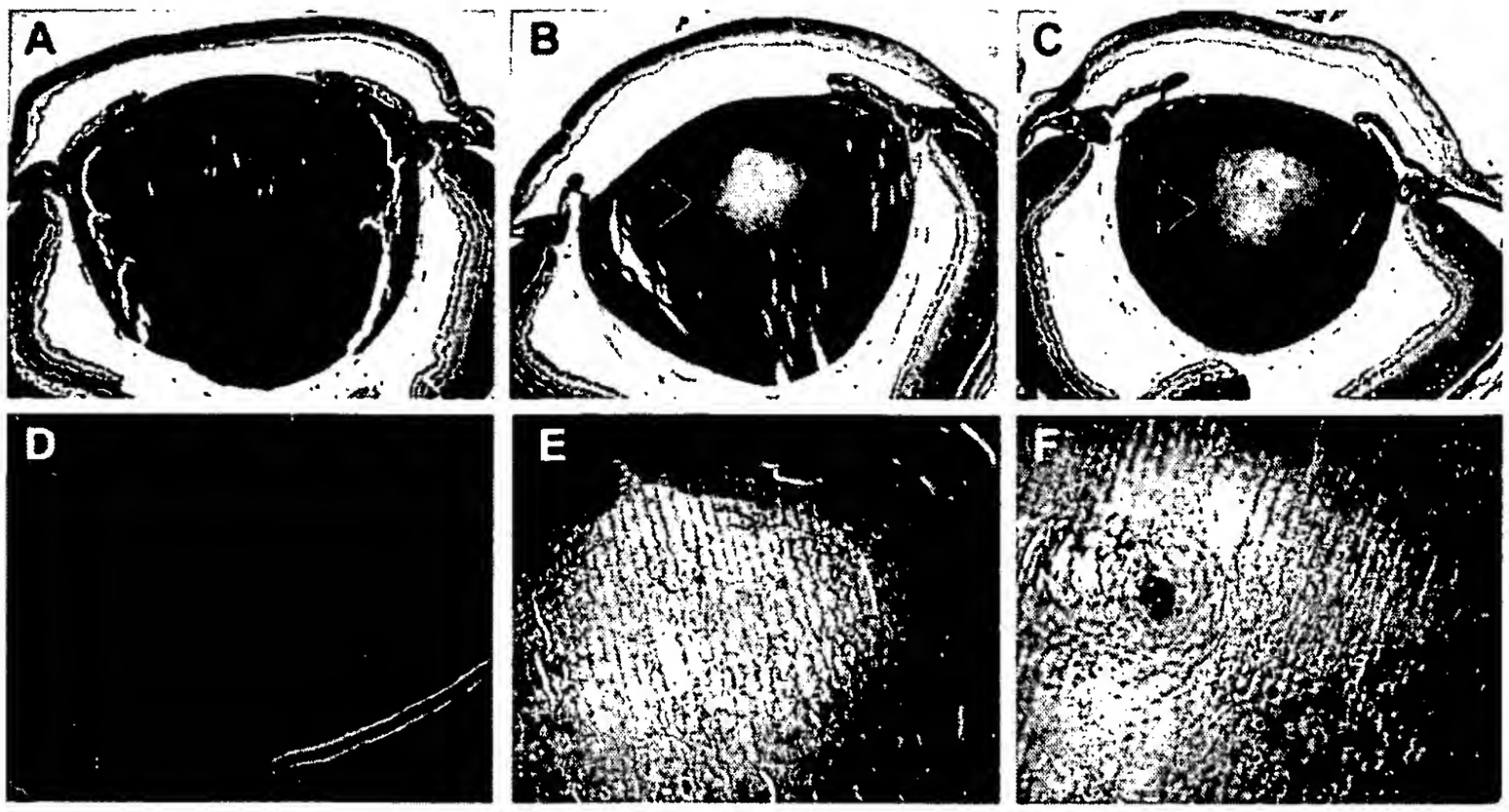

FIGURE 7. Pathologic changes in postnatal Cx50-knockout lenses. Eyes were fixed, serially sectioned, and stained with hematoxylin and eosin. (A) One-week-old wild-type eyes had normal ocular development and the lenses were uniformly stained with eosin throughout the core region. In contrast, knockout lenses exhibited a large clear zone in their nuclear region (B, C, *arrows*). At higher magnification, wild-type lens fibers were homogeneously labeled (D), whereas the clear zone in knockout lenses was composed of fiber cells that had lost the eosinophilic staining (E, F). In addition, the transition between stained and unstained regions was abrupt in the 129S6 background (B, E) and more gradual in the C57BL/6J mice (C, F).

mice (Fig. 6B). Consistent with many prior studies, there was no apparent upregulation of Cx46 in the absence of Cx50, and there were no differences in Cx46 expression between the C57BL/6J and 129S6 mice.[16,18,19,24] Thus, differential levels of Cx46 cannot explain the variation in Cx50-knockout-induced cataracts in the two mouse strains.

Lens Histology

The differences in lens opacities due to genetic background suggest that different cellular pathologic disorders may have occurred in the two genetic backgrounds. To determine pathologic differences, histologic sections of mouse eyes were stained with hematoxylin and eosin. Sections of postnatal day-7 wild-type eyes revealed normal ocular development without cellular damage (Fig. 7A), particularly in the core of the lens (Fig. 7D), where cataracts occurred in the Cx50-knockout mice. In contrast, sections of Cx50-knockout eyes displayed disruption of the normally uniform staining in the lens core (Figs. 7B, 7C, arrows) and increased cellular damage in the nuclear region with apparent differences between the two genetic backgrounds. In the 129S6 mice there was an abrupt transition between healthy fiber tissue and the disrupted core (Figs. 7B, 7E), whereas C57BL/6J lenses displayed a gradual transition into the zone of cellular damage (Figs. 7C, 7F). These histologic differences in the Cx50-knockout lenses from 129S6 or C57BL/6J backgrounds support the idea that a genetic modifier influences the cataract phenotype in Cx50-deficient mice.

DISCUSSION

Studies have shown that genetically altered mice display diverse phenotypes, which can be dependent on the genetic background of the knockout animals.[23,25] Deletion of Cx50 in mice produces mild nuclear cataracts and an approximately 42% reduction in lens size.[18,19] In the current study, Cx50-dependent growth deficiency persisted, regardless of genetic background, whereas cataracts were different in the 129S6 and C57BL/6J mice. These results suggest the two elements of the Cx50-knockout phenotype are independent of each other, and a genetic modifier influences cataractogenesis, whereas growth is strictly dependent on Cx50-mediated intercellular communication.

A genetic modifier has also been shown to influence cataractogenesis in mice with a deletion of Cx46,[23] raising the question of whether a common mechanism could be responsible, regardless of which lens connexin is deleted. Studies with Cx46-knockout mice from the 129S4 and C57BL/6J backgrounds have revealed that cataracts are also more severe in the 129S4 mice than in the C57BL/6J mice. Cataract severity also correlates well with increased cleavage of γ-crystallin in 129S4 Cx46 knockouts compared with C57BL/6J mice, suggesting that the modifier may have influenced crystallin stability.[23] However, deletion of Cx50 produces cataracts without the cleavage of γ-crystallin,[18,19] and the observed differences in cataractogenesis between strains appear to be independent of crystallin proteolysis. Therefore, if a common genetic modifier influences cataractogenesis resulting from deficient gap junctional communication, crystallin proteolysis must be a secondary consequence of its activity, because the mechanism of cataractogenesis is clearly different in Cx46- and Cx50-knockout mice.

The γ-crystallin cleavage in the 129S4 Cx46-knockouts results from an increased calcium concentration in the lens core and activity of the calcium-dependent protease Lp82.[21] The two mouse strains may differ in their ability to buffer increased concentrations of cytoplasmic calcium with different consequences in the two knockout models. In Cx50-knockouts, higher Ca^{2+} could lead to γ-crystallin precipitation without cleavage, whereas in Cx46-knockouts elevated Ca^{2+} activates Ca-dependent proteases. These diverse effects could result from differences in the magnitude or spatial arrangement of coupling provided by these two distinct connexins.[24] Thus, it is possible that a common genetic modifier contributes to cataract severity in the two knockout models by influencing calcium homeostasis. This hypothesis could be tested by measuring cytoplasmic calcium in wild-type and knockout lenses from the two models in the two mouse strains.

Although genetic modifier(s) that influence cataracts in mice with connexin deletions have been observed (Ref. 23 and the present work), their chromosomal location is not currently known. Recent evidence has shown that mutations in the Cx50 gene are also capable of generating cataracts in rats and mice,[26–29] and in one of these studies, a modifier gene was identified. Yamashita et al.,[29] found that the presence of cataracts segregated with a Cx50 mutation on rat chromosome 2 (*Uca*), but that the age of onset of cataractogenesis significantly varied between the animals. This variation was mapped to a particular region on rat chromosome 5, thus identifying a genetic modifier (*Ucad1*) on a different chromosome than Cx50, which influenced the onset of cataractogenesis caused by a Cx50 mutation. These results clearly demonstrate the presence of a genetic modifier that influences the cataract

phenotype resulting from deficient gap junctional communication. Although it is too early to tell whether the same genetic modifier influences cataract severity in the connexin-knockout animals, the corresponding *Ucad1* locus on mouse chromosome 4 would be a good candidate region to examine.

In contrast to the dissimilarity of the opacities in different strains, growth of Cx50-knockout lenses was equally impaired in either genetic background, suggesting that the growth defect was independent of cataractogenesis. In support of this view, we have recently shown that Cx46 can differentially rescue the two aspects of the Cx50-knockout phenotype. Replacement of the Cx50 coding region with Cx46 by gene knock-in restored optical clarity, but not lens growth.[22] The persistence of a growth deficiency in these mice, despite rescue of the cataract phenotype, further supports the hypothesis that although both of these defects depend on Cx50, they are independent of each other. In the present study, reductions in eye and lens size were identical in the 129S6 and C57BL/6J Cx50-knockouts at all ages examined, demonstrating that the kinetics, as well as magnitude of the growth defect were unaffected by genetic background. The precise mechanism whereby Cx50 influences lens growth remains to be elucidated; however, integration of the results of the present study with those in a growing body of work from several laboratories leads to the conclusion that Cx46 and Cx50 fulfill unique roles in lens physiology and that the lens can segregate the contributions of gap-junctional communication to the control of normal growth and to the maintenance of clarity.

Acknowledgments

The authors thank Richard Mathias for critically reading the manuscript.

References

1. Piatigorsky J. Lens differentiation in vertebrates: a review of cellular and molecular features. *Differentiation*. 1981;19:134-153.
2. McAvoy JW, Chamberlain CG, de Iongh RU, Hales AM, Lovicu FJ. Lens development. *Eye*. 1999;13:425-437.
3. Mathias RT, Rae JL, Baldo GJ. Physiological properties of the normal lens. *Physiol Rev*. 1997;77:21-50.
4. Harris AL. Emerging issues of connexin channels: biophysics fills the gap. *Q Rev Biophys*. 2001;34:325-472.
5. Bruzzone R, White TW, Paul DL. Connections with connexins: the molecular basis of direct intercellular signaling. *Eur J Biochem*. 1996;238:1-27.
6. Willecke K, Eiberger J, Degen J, et al. Structural and functional diversity of connexin genes in the mouse and human genome. *Biol Chem*. 2002;383:725-737.
7. White TW, Bruzzone R. Intercellular communication in the eye: clarifying the need for connexin diversity. *Brain Res Rev*. 2000; 32:130-137.
8. Beyer EC, Kistler J, Paul DL, Goodenough DA. Antisera directed against connexin43 peptides react with a 43-kD protein localized to gap junctions in myocardium and other tissues. *J Cell Biol*. 1989;108:595-605.
9. Musil LS, Beyer EC, Goodenough DA. Expression of the gap junction protein connexin43 in embryonic chick lens: molecular cloning, ultrastructural localization, and post-translational phosphorylation. *J Membr Biol*. 1990;116:163-175.
10. Kistler J, Kirkland B, Bullivant S. Identification of a 70,000-D protein in lens membrane junctional domains. *J Cell Biol*. 1985; 101:28-35.
11. Paul DL, Ebihara L, Takemoto LJ, Swenson KI, Goodenough DA. Connexin46, a novel lens gap junction protein, induces voltage-gated currents in nonjunctional plasma membrane of Xenopus oocytes. *J Cell Biol*. 1991;115:1077-1089.
12. White TW, Bruzzone R, Goodenough DA, Paul DL. Mouse Cx50, a functional member of the connexin family of gap junction proteins, is the lens fiber protein Mp70. *Mol Biol Cell*. 1992;3:711-720.
13. Evans CW, Eastwood S, Rains J, Gruijters WT, Bullivant S, Kistler J. Gap junction formation during development of the mouse lens. *Eur J Cell Biol*. 1993;60:243-249.
14. Reaume AG, de Sousa PA, Kulkarni S, et al. Cardiac malformation in neonatal mice lacking connexin43. *Science*. 1995;267:1831-1834.
15. Gao Y, Spray DC. Structural changes in lenses of mice lacking the gap junction protein connexin43. *Invest Ophthalmol Vis Sci*. 1998;39:1198-1209.
16. White TW, Sellitto C, Paul DL, Goodenough DA. Prenatal lens development in connexin43 and connexin50 double knockout mice. *Invest Ophthalmol Vis Sci*. 2001;42:2916-2923.
17. Gong X, Li E, Klier G, et al. Disruption of alpha3 connexin gene leads to proteolysis and cataractogenesis in mice. *Cell*. 1997;91: 833-843.
18. White TW, Goodenough DA, Paul DL. Targeted ablation of connexin50 in mice results in microphthalmia and zonular pulverulent cataracts. *J Cell Biol*. 1998;143:815-825.
19. Rong P, Wang X, Niesman I, et al. Disruption of Gja8 (alpha8 connexin) in mice leads to microphthalmia associated with retardation of lens growth and lens fiber maturation. *Development*. 2002;129:167-174.
20. Piatigorsky J. Intracellular ions, protein metabolism, and cataract formation. *Curr Top Eye Res*. 1980;3:1-39.
21. Baruch A, Greenbaum D, Levy ET, et al. Defining a link between gap junction communication, proteolysis, and cataract formation. *J Biol Chem*. 2001;276:28999-29006.
22. White TW. Unique and redundant connexin contributions to lens development. *Science*. 2002;295:319-320.
23. Gong X, Agopian K, Kumar NM, Giluli NB. Genetic factors influence cataract formation in alpha 3 connexin knockout mice. *Dev Genet*. 1999;24:27-32.
24. Baldo GJ, Gong X, Martinez-Wittinghan FJ, Kumar NM, Gilula NB, Mathias RT. Gap junctional coupling in lenses from alpha(8) connexin knockout mice. *J Gen Physiol*. 2001;118:447-456.
25. Maeda YY, Funata N, Takahama S, Sugata Y, Yonekawa H. Two interactive genes responsible for a new inherited cataract (RCT) in the mouse. *Mamm Genome*. 2001;12:278-283.
26. Steele EC Jr, Lyon MF, Favor J, Guillot PV, Boyd Y, Church RL. A mutation in the connexin 50 (Cx50) gene is a candidate for the No2 mouse cataract. *Curr Eye Res*. 1998;17:883-889.
27. Graw J, Loster J, Soewarto D, et al. Characterization of a mutation in the lens-specific MP70 encoding gene of the mouse leading to a dominant cataract. *Exp Eye Res*. 2001;73:867-876.
28. Chang B, Wang X, Hawes NL, et al. A Gja8 (Cx50) point mutation causes an alteration of alpha 3 connexin (Cx46) in semi-dominant cataracts of Lop10 mice. *Hum Mol Genet*. 2002;11:507-513.
29. Yamashita S, Furumoto K, Nobukiyo A, Kamohara M, Ushijima T, Furukawa T. Mapping of A gene responsible for cataract formation and its modifier in the UPL rat. *Invest Ophthalmol Vis Sci*. 2002; 43:3153-3159.

Exhibit B

Science
AAAS

Modification of Ocular Defects in Mouse Developmental Glaucoma Models by Tyrosinase

Richard T. Libby, *et al.*

Science **299**, 1578 (2003);
DOI: 10.1126/science.1080095

Science (print ISSN 0036-8075; online ISSN 1095-9203) is published weekly, except the last week in December, by the American Association for the Advancement of Science, 1200 New York Avenue NW, Washington, DC 20005.

tein kinase RNA-activated (PKR) (*16*), or inducible nitric oxide synthase (*17*) were no more susceptible to lethal infection than wild-type controls (Fig. 3A). More subtle contributions of these genes to MNV-1 resistance cannot be ruled out by these studies. However, mice lacking both IFNαβ and IFNγ receptors were at least 10,000-fold more susceptible to lethal infection than controls after either i.c. or i.n. inoculation (Fig. 3B, fig. S4). These data show that IFNs are essential for resistance to MNV-1 infection and that the IFNαβ and IFNγ receptors can compensate for one another.

Because RAG/STAT1$^{-/-}$ mice die (fig. S1A) whereas RAG$^{-/-}$ mice survive after MNV-1 infection (Fig. 3A) and because STAT1 is involved in signaling through both the IFNαβ and IFNγ receptors (*18*), we studied whether STAT1 is required for resistance to MNV-1 infection. STAT1 deficiency resulted in lethal MNV-1 infection in mice (i) with intact B and T cell compartments (*19*) (STAT1$^{-/-}$, Fig. 3C), (ii) lacking T and B cells (RAG/STAT1$^{-/-}$, Fig. 3D), and (iii) lacking PKR (STAT1/PKR$^{-/-}$, Fig. 3E). Therefore, STAT1 is required for survival after MNV-1 infection. Together with the survival of RAG$^{-/-}$ mice, this result strongly argues that a STAT1-dependent innate immune response is sufficient to prevent lethal MNV-1 infection.

To better understand the role of STAT1-dependent innate responses in controlling MNV-1 infection, we quantified MNV-1 RNA in tissues after p.o. infection of STAT1$^{-/-}$ or 129 wild-type mice. We measured RNA because we have been unable to measure viral infectivity by plaque assay (*3*). Wild-type mice were infected after p.o. inoculation as suggested by the presence of viral RNA in intestine, liver, and spleen one day after inoculation (Fig. 4C). Furthermore, these mice seroconverted to MNV-1 capsid protein after p.o. (Fig. 4B) or i.c. inoculation (fig. S5). However, wild-type mice did not develop symptoms or tissue pathology and cleared viral RNA from visceral and mucosal tissues by 3 days after infection (Fig. 4C), a time course consistent with clearance via innate immunity. Wild-type mice, therefore, resemble asymptomatically infected humans that have been detected during norovirus epidemics (*5*, *20*).

STAT1$^{-/-}$ mice, like wild-type mice, contained MNV-1 genome in intestine, liver, and spleen one day after inoculation (Fig. 4D). In contrast to wild-type mice, STAT1$^{-/-}$ mice had high levels of MNV-1 RNA in multiple organs, as well as substantial tissue pathology, 3 and 7 days after infection. (Fig. 4, D and E). Decreases in viral RNA between 3 and 7 days of infection suggest that STAT1-independent immune responses can have some effect on MNV-1 infection. These data confirm a critical role for STAT1-dependent innate immunity in control of acute norovirus infection and show that a norovirus can cause systemic disease in immunocompromised hosts after mucosal infection.

Our finding that MNV-1 causes disease in immunocompromised mice suggests that human caliciviruses may be important systemic pathogens in patients with hereditary or acquired immunodeficiency. It is interesting to speculate, on the basis of our demonstration of persistent infection in RAG$^{-/-}$ mice and prolonged viral infection in STAT1$^{-/-}$ mice, that persons with immune deficiencies in either adaptive or innate immunity could be chronic norovirus carriers, thereby providing a source for epidemic outbreaks. Importantly, researchers using mouse models need to consider that MNV-1 can cause tissue pathology in immunocompromised mice. Acute or chronic MNV-1 infection might, therefore, contribute to phenotypes originally attributed directly to alterations in immune function. Lastly, we speculate that immunocompromised mice may harbor additional unidentified pathogens that could be studied to elucidate mechanisms of human disease and immunity.

References and Notes

1. V. Shankaran *et al.*, *Nature* **410**, 1107 (2001).
2. U. Muller *et al.*, *Science* **264**, 1918 (1994).
3. Detailed materials and methods are available as supporting material on *Science* Online.
4. K. Pastorian, L. Hawel III, C. V. Byus, *Anal. Biochem.* **283**, 89 (2000).
5. K. Y. Green, R. M. Chanock, A. Z. Kapikian, in *Fields Virology*, D. M. Knipe, P. M. Howley, Eds. (Lippincott Williams & Wilkins, Philadelphia, 2001), vol. 1, chap. 27.
6. R. L. Fankhauser, J. S. Noel, S. S. Monroe, T. Ando, R. I. Glass, *J. Infect. Dis.* **178**, 1571 (1998).
7. S. Inouye *et al.*, *J. Infect. Dis.* **181** (suppl. 2), S270 (2000).
8. S. Karst, C. Wobus, M. Lay, J. Davidson, H. W. Virgin, unpublished observation.
9. A. Z. Kapikian *et al.*, *J. Virol.* **10**, 1075 (1972).
10. J. Treanor, R. Dolin, in *Principles and Practice of Infectious Diseases*, G. L. Mandell, J. E. Bennett, R. Dolin, Eds. (Churchill Livingstone, New York, 1995), chap. 153.
11. A. M. Hutson, R. L. Atmar, D. M. Marcus, M. K. Estes, *J. Virol.* **77**, 405 (2003).
12. A. M. Huston, R. L. Atmer, D. Y. Graham, M. K. Estes, *J. Infect. Dis.* **185**, 1335 (2002).
13. S. M. Matsui, H. B. Greenberg, *J. Infect. Dis.* **181** (suppl. 2), S331 (2000).
14. P. Mombaerts *et al.*, *Cell* **68**, 869 (1992).
15. Y. Shinkai *et al.*, *Cell* **68**, 855 (1992).
16. Y. L. Yang *et al.*, *EMBO J.* **14**, 6095 (1995).
17. J. D. MacMicking *et al.*, *Cell* **81**, 1 (1995).
18. G. R. Stark, I. M. Kerr, B. R. Williams, R. H. Silverman, R. D. Schreiber, *Annu. Rev. Biochem.* **67**, 227 (1998).
19. M. A. Meraz *et al.*, *Cell* **84**, 431 (1996).
20. D. Y. Graham *et al.*, *J. Infect. Dis.* **170**, 34 (1994).

21. Supported by NIH RO1 AI49286 to H.W.V. S.K. and C.W. were supported by training grant T32-CA09547. We acknowledge the support of E. Unanue and comments from Virgin lab members, P. Allen, K. Green, H. Greenberg, and B. Levine. We thank R. D. Schreiber for providing RAG/STAT1$^{-/-}$ mice, D. Kraemelmeyer for managing mouse colonies, W. Beatty for electron microscopy, and A. Horton and J. J. Gibson-Brown for assistance with protein alignment. Special thanks go to K. Green and S. Sosnovtsev for assistance with analyzing the MNV-1 sequence.

Supporting Online Material

www.sciencemag.org/cgi/content/full/299/5612/1575/DC1
Materials and Methods
Figs. S1 to S5
References and Notes

29 August 2002; accepted 4 February 2003

Modification of Ocular Defects in Mouse Developmental Glaucoma Models by Tyrosinase

Richard T. Libby,[1]* Richard S. Smith,[1,2]* Olga V. Savinova,[2] Adriana Zabaleta,[2] Janice E. Martin,[1,2] Frank J. Gonzalez,[3] Simon W. M. John[1,2,4]†

Mutations in the cytochrome P450 family 1, subfamily B, polypeptide 1 (*CYP1B1*) gene are a common cause of human primary congenital glaucoma (PCG). Here we show that *Cyp1b1*$^{-/-}$ mice have ocular drainage structure abnormalities resembling those reported in human PCG patients. Using *Cyp1b1*$^{-/-}$ mice, we identified the tyrosinase gene (*Tyr*) as a modifier of the drainage structure phenotype, with *Tyr* deficiency increasing the magnitude of dysgenesis. The severe dysgenesis in eyes lacking both CYP1B1 and TYR was alleviated by administration of the tyrosinase product dihydroxyphenylalanine (L-dopa). *Tyr* also modified the drainage structure dysgenesis in mice with a mutant *Foxc1* gene, which is also involved in PCG. These experiments raise the possibility that a tyrosinase/L-dopa pathway modifies human PCG, which could open new therapeutic avenues.

Glaucoma is a group of heterogeneous diseases that impair vision. There are different types of glaucoma and often they have a multifactorial etiology (*1*–*3*). Primary congenital glaucoma (PCG) is a small subset of glaucoma, but it is severe and has a high incidence in some populations (*1*, *4*). PCG results from poorly understood developmental abnormalities of the ocu-

lar drainage structures and is characterized by high intraocular pressure, corneal edema, photophobia, and ocular enlargement (*1*, *3*, *4*). Recessive inheritance of PCG is common, with almost complete penetrance in populations with a high consanguinity rate. There is often reduced penetrance (40% in some populations) and variable presentation, however, pointing to a multifactorial etiology (Online Mendelian Inheritance in Man 231300) (*4*–*6*). Although there is evidence for a modifier gene affecting the development of glaucoma in individuals homozygous for *CYP1B1* mutations, the gene or genes have not yet been identified (*7*).

To study ocular developmental abnormalities underlying PCG, we evaluated the consequences of *Cyp1b1* deficiency in mice. The development and structure of the trabecular meshwork and Schlemm's canal (iridocorneal angle drainage structures) are similar in humans and mice (*8*). Homozygous mutant mice ($Cyp1b1^{-/-}$) on a mixed 129X1/SvJ × C57BL/6J (B6) background had no gross abnormalities at ages up to 13 months (fig. S1, A and B), and their intraocular pressure was indistinguishable from that of normal littermates (*9*). However, histological and electron microscopic analyses detected angle abnormalities in all $Cyp1b1^{-/-}$ eyes but not in $Cyp1b1^{+/+}$ eyes (Fig. 1 and fig. S1C). These defects were only focally present, and much of the angle had normal morphology. The observed defects included a small or absent Schlemm's canal, basal lamina extending from the cornea over the trabecular meshwork, fibers resembling smooth muscle at anterior positions in the trabecular meshwork, and attachments of the iris to the trabecular meshwork and peripheral cornea (synechiae).These developmental abnormalities resemble those reported in human patients with PCG (*10*, *11*).

We next tested different mouse strains for strain-specific modifier genes that might suppress or enhance angle abnormalities in these mice. The *Cyp1b1* mutation was crossed onto strains 129X1/SvJ, B6, CAST/Ei, and MOLC/Rk. No gross defects or elevation in intraocular pressure were present in $Cyp1b1^{-/-}$ mice on any of these backgrounds (*9*). However, histologic studies provided initial evidence for a modifier gene (tyrosinase, the rate-limiting enzyme in the pigment production pathway). Pigmented $Cyp1b1^{-/-}$ mice of the B6 background had mild and focal angle abnormalities, including small Schlemm's canals and hypoplastic trabecular meshworks (Fig. 2). However, albino (tyrosinase-deficient) $Cyp1b1^{-/-}$ mice of the 129X1/SvJ background had more severe and extensive angle abnormalities (*9*). Examination of the segregating 129X1/SvJ × B6 background also showed that albino mice lacking tyrosinase were more severely affected than pigmented mice (Fig. 1) (*9*). Although the albino and pigmented mice of the above strains had many genetic differences, these observations suggested that the presence of tyrosinase protects against developmental abnormalities in $Cyp1b1^{-/-}$ mice.

To test whether the *Tyr* gene modifies angle abnormalities in $Cyp1b1^{-/-}$ mice, we analyzed pigmented and albino $Cyp1b1^{-/-}$ B6 mice that were genetically uniform except for the presence or absence of the mutant Tyr^{c-2J} allele that arose on this genetic background (*12*). We assessed the severity of angle abnormalities by analysis of histological sections from different regions around these eyes, and devised a severity grading protocol to allow comparisons between different eyes (*12*). Three separate angle abnormalities that contribute to glaucoma were analyzed (Fig. 2). Pigmented $Cyp1b1^{-/-}$ mice consistently had mild focal defects, whereas albino $Cyp1b1^{-/-}$ mice had severe and more extensive developmental defects (Fig. 2, A to D). These differences were consistent and significant for all assessed phenotypes (Fig. 2E; $P < 0.001$ for all).

We also analyzed albino and pigmented B6 mice ($Cyp1b1^{+/+}$) to determine whether the *Tyr* genotype alters the susceptibility of B6 eyes to anterior segment dysgenesis. Albino $Cyp1b1^{+/+}$

[1]The Jackson Laboratory, [2]The Howard Hughes Medical Institute, Bar Harbor, ME 04609, USA. [3]Laboratory of Metabolism, National Cancer Institute, Bethesda, MD 20892, USA. [4]Department of Ophthalmology, Tufts University School of Medicine, Boston, MA 02111, USA.

*These authors contributed equally to this work.
†To whom correspondence should be addressed. E-mail: swmj@jax.org

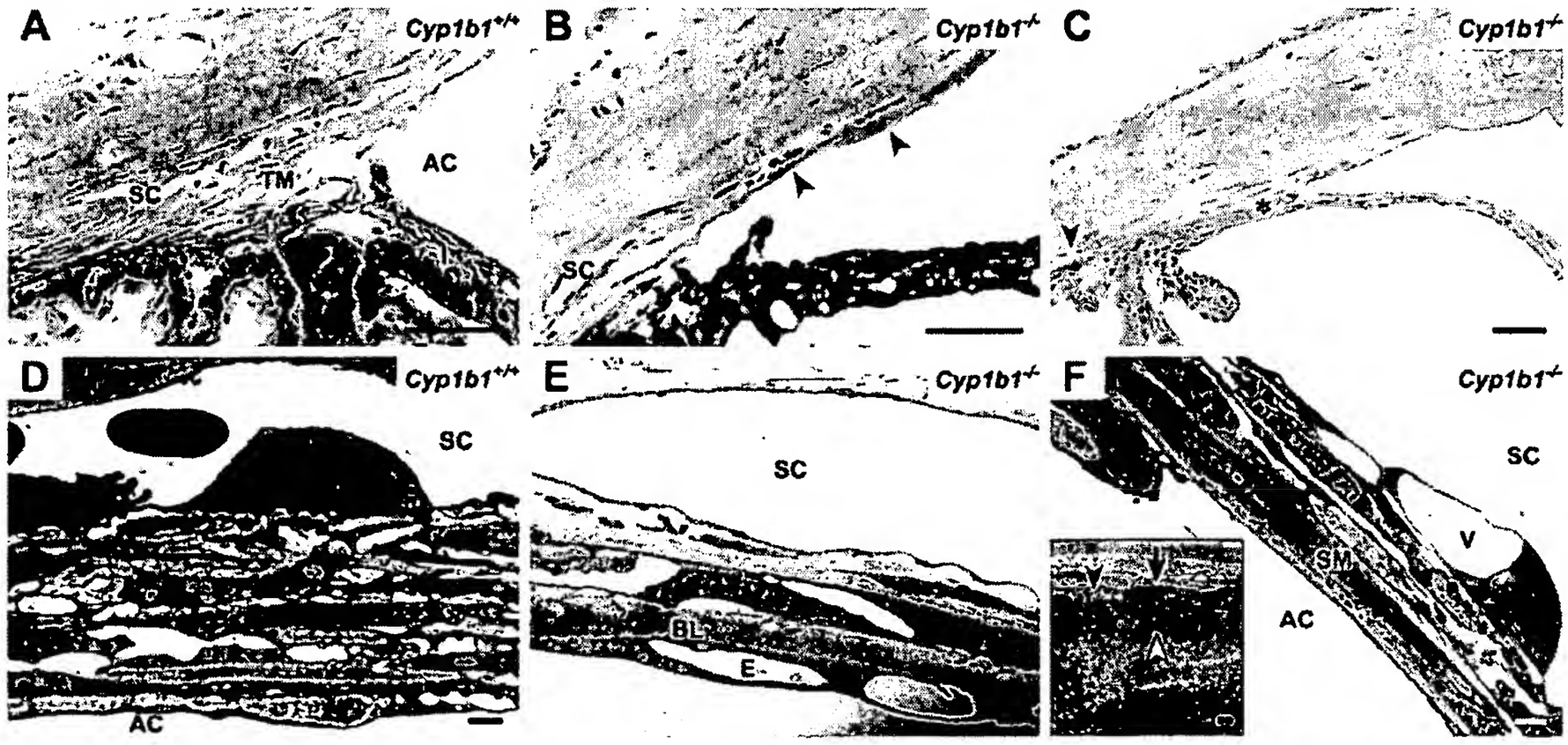

Fig. 1. Ocular abnormalities in $Cyp1b1^{-/-}$ mice. All images are from adult mice of the 129X1/SvJ × B6 mixed background. (**A**) In $Cyp1b1^{+/+}$ mice, the iridocorneal angle is well formed with an obvious Schlemm's canal of normal extent. The trabecular meshwork and iris are normal, and the deep angle recess of the anterior chamber is open. (**B**) Pigmented $Cyp1b1^{-/-}$ mice. The trabecular meshwork is hypoplastic, and material resembling Descemet's membrane (the basal lamina of the corneal endothelium, arrowheads) abnormally covers a portion of the trabecular meshwork. (**C**) Albino $Cyp1b1^{-/-}$ mice. A very small Schlemm's canal may be present (arrowhead). The trabecular meshwork cannot be identified. The deep angle recess is not open because of a synechia (*). (**D**) $Cyp1b1^{+/+}$ mice. There is an endothelial-lined Schlemm's canal and a robust trabecular meshwork with numerous well-formed trabecular beams. The internal aspect of the trabecular meshwork is demarcated by the anterior chamber. (**E**) $Cyp1b1^{-/-}$ mice. The endothelial lining of Schlemm's canal is attenuated and there is only a single trabecular beam. Access to the trabecular meshwork and Schlemm's canal is blocked by a thick basal lamina. The inner aspect of the basal lamina is covered with abnormal cells resembling endothelial cells. (**F**) $Cyp1b1^{-/-}$ mice. Schlemm's canal is lined by endothelium and contains a giant vacuole (aqueous humor drainage structure). Only one to two poorly formed trabecular beams are present. Smooth muscle is abnormally located in the trabecular meshwork. Inset: Higher magnification demonstrates the focally increased density of the plasma membrane (arrow), pinocytotic vesicles (black arrowhead), and longitudinally arranged actin filaments (white arrowhead), confirming the presence of smooth muscle. SC, Schlemm's canal; TM, trabecular meshwork; I, iris; AC, anterior chamber; BL, basal lamina; E, endothelial cells; V, vacuole; SM, smooth muscle. Scale bars in (A) to (C), 40 μm; in (D) to (F), 1 μm.

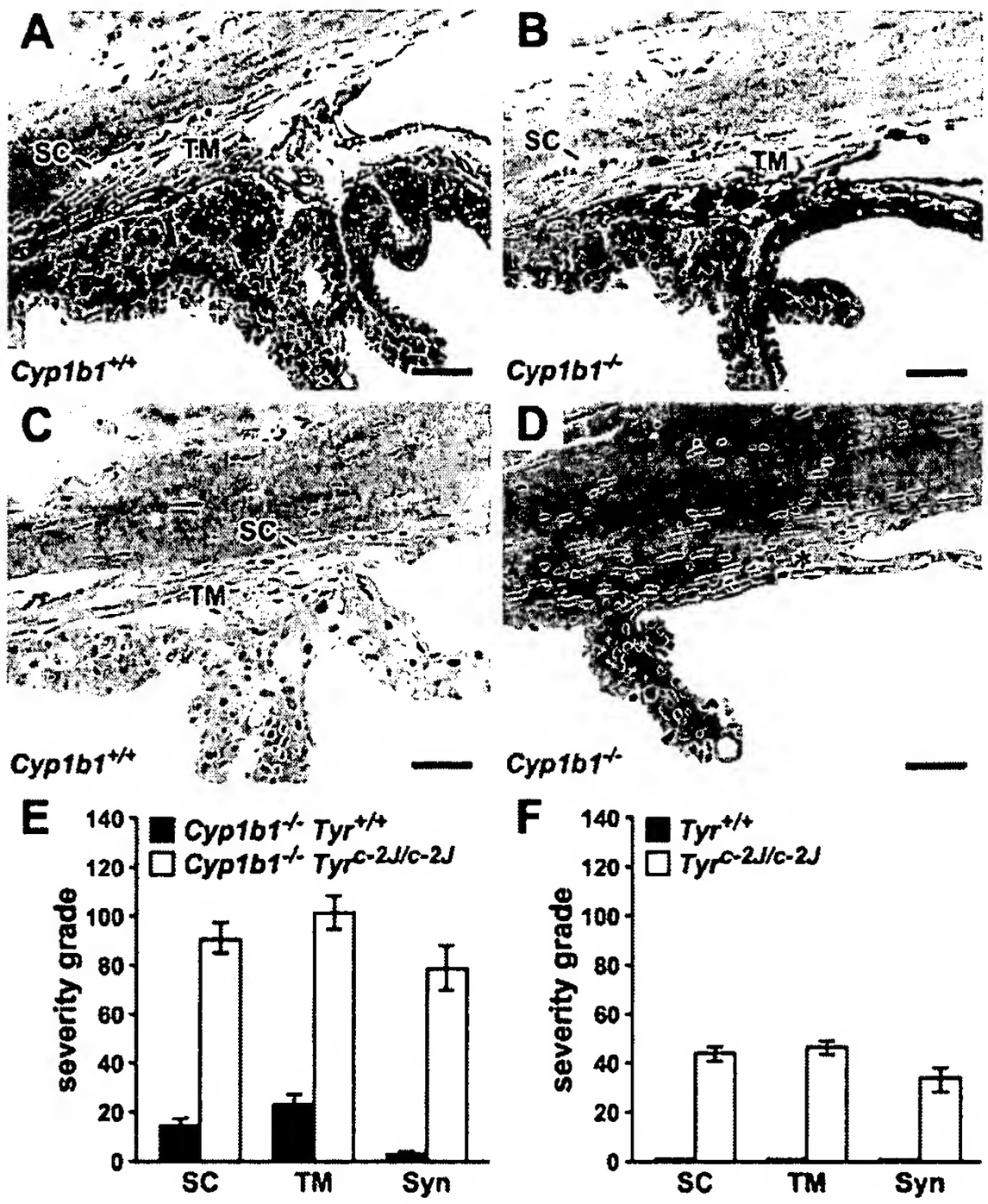

Fig. 2. Tyrosinase modifies angle defects in *Cyp1b1*$^{-/-}$ mice. All mice were adults with a B6 genetic background. Common features are shown for mice of each genotype. (**A**) *Cyp1b1*$^{+/+}$ *Tyr*$^{+/+}$ (pigmented) mice. There is a well-formed angle with a long open Schlemm's canal and robust trabecular meshwork. (**B**) *Cyp1b1*$^{-/-}$ *Tyr*$^{+/+}$ mice. Schlemm's canal and the trabecular meshwork are present. This is true around most of the eye. (**C**) *Cyp1b1*$^{+/+}$ *Tyr*$^{c-2J/c-2J}$ (albino) mice. Schlemm's canal and the trabecular meshwork are well formed. (**D**) *Cyp1b1*$^{-/-}$ *Tyr*$^{c-2J/c-2J}$ mice. Schlemm's canal and the trabecular meshwork are not identifiable. The iris is attached by a synechia (*) to the region that is normally occupied by the trabecular meshwork. (**E**) Mean severity grades demonstrate that tyrosinase activity modifies the severity of angle abnormalities in *Cyp1b1*$^{-/-}$ mice that are genetically uniform except for their *Tyr* genotypes. For an eye, the grade can be any value between 0 and 144 (*12*). A grade of zero would indicate that the angle was completely normal at all analyzed locations around the eye, whereas a score of 144 would indicate that the angle was severely affected at all locations studied. Angles with severe and extensive developmental lesions have high grades, whereas angles with less severe or less extensive lesions have lower grades. Severity was assessed for two important structures that are known to be affected by anterior segment dysgenesis in humans: Schlemm's canal and the trabecular meshwork. Also, a grade was assigned for the presence and extent of a synechia (Syn). *Cyp*$^{-/-}$ *Tyr*$^{c-2J/c-2J}$ mice had significantly more extensive dysgenesis than *Cyp*$^{-/-}$ *Tyr*$^{+/+}$ mice ($P < 0.001$ for all phenotypes assessed). (**F**) Mean severity grades demonstrated that the *Tyr* genotype affects angle development in otherwise wild-type, genetically identical B6 mice. *Cyp1b1*$^{+/+}$ *Tyr*$^{c-2J/c-2J}$ mice had focal developmental defects, whereas *Cyp1b1*$^{+/+}$ *Tyr*$^{+/+}$ mice had none ($P < 0.001$ for all phenotypes assessed). Pigmented and albino mice of each genotype were intermixed during analysis, and the grader was unaware of the genotypes. Scale bars, 40 μm.

mice were found to have mild focal developmental defects, whereas pigmented *Cyp1b1*$^{+/+}$ mice had no observed defects (Fig. 2F), thus confirming the protective effect of tyrosinase activity. The severity of abnormalities in albino *Cyp1b1*$^{-/-}$ mice was greater than could be accounted for by adding the severity values of pigmented *Cyp1b1*$^{-/-}$ and albino *Cyp1b1*$^{+/+}$ eyes (Fig. 2, E and F). Together, these results demonstrate an interaction (exacerbating angle dysgenesis) between *Tyr* and *Cyp1b1* deficiency.

Human PCG can also arise from dominant mutations in the transcription factor gene *FOXC1* (forkhead box C1, formerly *FKHL7*) (*5*). *Foxc1*$^{+/-}$ mice have anterior segment dysgenesis phenotypes resembling those in human patients (*13*, *14*). To determine whether *Tyr* activity also modifies the phenotype in *Foxc1*$^{+/-}$ mice, we compared the extent of anterior segment dysgenesis in *Foxc1*$^{+/-}$ mice that were genetically uniform except for the presence or absence of the *Tyr* mutation. Tyrosinase-deficient *Foxc1*$^{+/-}$ mice had more severe abnormalities than their pigmented counterparts (B6 background; fig. S2). Abnormalities in Schlemm's canal and the extent of synechiae were more severe in albino *Foxc1*$^{+/-}$ mice than could be accounted for by adding the severity grades for albino *Foxc1*$^{+/+}$ mice and pigmented *Foxc1*$^{+/-}$ mice, suggesting that the combined effects of *Foxc1* and *Tyr* mutation are more than additive. Together, our experiments identify a previously unknown anterior segment developmental pathway involving tyrosinase, and show that *Tyr* mutation modifies the phenotype associated with inheritance of mutant orthologs of two known human PCG genes, *Cyp1b1* and *Foxc1*.

We hypothesized that tyrosinase might affect angle development through modulation of L-dihydroxyphenylalanine (dopa) levels. Tyrosinase is a monooxygenase that converts tyrosine to L-dopa and L-dopa to dopaquinone. L-Dopa affects development and is the precursor of catecholamines, which are important developmental regulators (*15*–*17*). To investigate whether L-dopa is a critical molecule in angle development, we administered water containing L-dopa or standard drinking water to *Cyp1b1*$^{-/-}$ *Tyr*$^{c-2J/c-2J}$ (albino) double mutants throughout ocular development [their mothers received this water throughout the period of in utero development (*12*)]. L-Dopa treatment was found to prevent the severe angle dysgenesis present in untreated mice lacking both CYP1B1 and TYR (Fig. 3). This experiment demonstrates that a pathway involving L-dopa (or an L-dopa metabolite) participates in angle formation and that disturbances in this pathway can be treated by L-dopa administration. Despite the profound rescue in L-dopa –treated albino *Cyp1b1*$^{-/-}$ mice, mild abnormalities of similar severity to those observed in pigmented *Cyp1b1*$^{-/-}$ mice remained. Our experiments do not indicate whether these remaining abnormalities reflected an inability of L-dopa administration to rescue *Cyp1b1* phenotypes or whether *Cyp1b1* phenotypes were rescued but L-dopa treatment was not completely effective (possibly resulting from variability in achieved L-dopa levels at different angle locations). The alleviation of ocular defects by L-dopa suggests that other genes that are unlikely to alter pigmentation are potential candidates to affect angle formation. These include genes that affect L-dopa levels, affect the metabolism of L-dopa to other developmentally important molecules, or affect the signaling of these molecules in developmental and physiologic pathways.

Anterior segment development occurs by similar processes and is affected by many of the same genes in human and mice (*3*, *8*). Because *Tyr* function protects against angle dysgenesis in both the *Cyp1b1*$^{-/-}$ and *Foxc1*$^{+/-}$ mouse models, it is possible that mutations in multiple genes that contribute to developmental glaucoma affect L-dopa levels. L-dopa levels may be altered in the neural crest cells from which the angle structures and iris stroma derive. Conceivably, mutations in glaucoma genes affect the activity of tyrosine hydroxylase (TH), which produces L-dopa from tyrosine. Many of the genes that cause anterior segment dysgenesis and/or developmental glaucoma can pro-

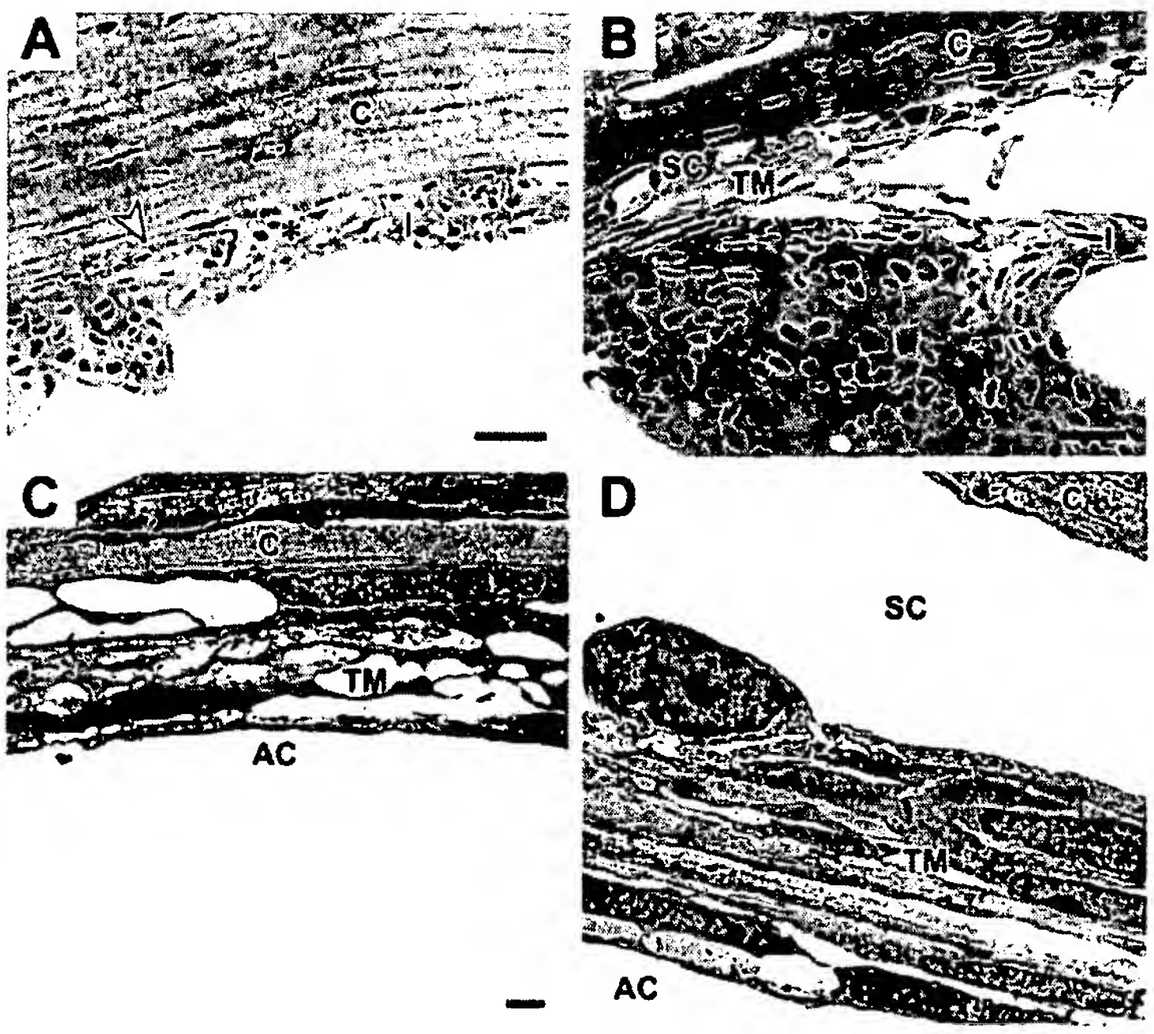

Fig. 3. L-Dopa treatment alleviates the effect of angle dysgenesis. All mice were *Cyp1B1*$^{-/-}$ *Tyr*$^{c-2J/c-2J}$ with a B6 genetic background. (**A**) In an untreated mouse, there is a severely malformed iridocorneal angle with a large synechia (*) attaching the iris (I) and the cornea (C). There is no observable Schlemm's canal or trabecular meshwork. Schlemm's canal and the trabecular meshwork normally extend to the arrowhead. (**B**) L-Dopa supplementation (1 mg/ml in drinking water) substantially prevented developmental abnormalities in the iridocorneal angle. In this representative section, there is a long endothelial-lined Schlemm's canal, the trabecular meshwork is robust, and the angle recess is open. Electron micrographs of untreated (C) and L-dopa–treated (D) mice show that L-dopa treatment rescues the ultrastructure of the trabecular meshwork. (**C**) In an untreated mouse, the Schlemm's canal is completely absent, and the trabecular meshwork is severely hypoplastic, contains little extracellular matrix, and is attached to the cornea. (**D**) In an L-dopa–treated mouse [at a similar location to that shown for the untreated mouse in (C)], Schlemm's canal is present with a normal endothelial lining and the trabecular meshwork is robust with organized trabecular beams. (**E**) Mean severity grades demonstrate that the developmental dysgenesis in *Cyp1B1*$^{-/-}$ *Tyr*$^{c-2J/c-2J}$ double mutants can be alleviated by L-dopa supplementation ($P < 0.001$ for all assessed phenotypes). The grader was not aware of which mice were from which treatment arm. Scale bars in (A) and (B), 40 μm; in (C) and (D), 1 μm.

mote either TH expression or the proliferation of TH expressing neural crest cells during the development of other tissues (*18*–*23*). PITX2 and PITX3, for example, induce *Th* expression by binding to a high-affinity regulatory site in the *Th* gene (*21*). Additionally, CYP1B1 oxidizes all-*trans*-retinol to all-*trans*-retinal, the rate-limiting step for retinoic acid biosynthesis (*24*), and retinoic acid promotes proliferation of a subset of avian neural crest cells that express TH (*25*). Together, these observations support a model in which a metabolic disturbance involving TH and L-dopa levels contributes to the anterior segment dysgenesis caused by mutations in various glaucoma genes.

Anterior segment dysgenesis and congenital glaucoma have been reported in a few humans with albinism (*26*, *27*), but this coexistence of phenotypes has typically been considered a coincidence. Our experimental data, along with a 1984 report of anterior segment dysgenesis in 7% of 86 studied albinos (*27*), suggest that tyrosinase may play a role in congenital glaucoma in humans. Abnormalities in genes other than TYR also result in decreased ocular pigmentation (*28*), and deficiency of at least one of these genes, *Tyrp1*, decreases tyrosinase stability (*29*). Our data raise the possibility that these mutations may modify the effects of developmental glaucoma genes by affecting L-dopa levels. Finally, our findings suggest that L-dopa may merit investigation as a possible therapy for reducing the incidence of glaucoma in certain high-risk families.

References and Notes

1. R. Ritch, M. B. Shields, T. Krupin, in *The Glaucomas, Clinical Science*, R. Ritch, M. B. Shields, T. Krupin, Eds. (Mosby, St. Louis, MO, ed. 2, 1996), vol. 2.
2. A. L. Vincent *et al.*, *Am. J. Hum. Genet.* **70**, 448 (2002).
3. D. B. Gould, S. W. M. John, *Hum. Mol. Genet.* **11**, 1185 (2002).
4. M. Sarfarazi, I. Stoilov, *Eye* **14**, 422 (2000).
5. D. Y. Nishimura *et al.*, *Nature Genet.* **19**, 140 (1998).
6. A. Gencik, A. Gencikova, A. Gerinec, *Clin. Genet.* **17**, 241 (1980).
7. B. A. Bejjani *et al.*, *Hum. Mol. Genet.* **9**, 367 (2000).
8. R. S. Smith, A. Zabaleta, O. V. Savinova, S. W. M. John, *BMC Dev. Biol.* **1**, 3 (2001); available at www.biomedcentral.com/1471-213X/1/3.
9. O. V. Savinova, R. S. Smith, S. W. M. John, unpublished data.
10. L. Allen, H. M. Burian, A. E. Braley, *Arch. Ophthalmol.* **53**, 783 (1955).
11. E. A. Maumenee, *Trans. Am. Ophthalmol. Soc.* **56**, 507 (1958).
12. Materials and methods are available as supporting material on *Science* Online.
13. H. K. Hong, J. H. Lass, A. Chakravarti, *Hum. Mol. Genet.* **8**, 625 (1999).
14. R. S. Smith *et al.*, *Hum. Mol. Genet.* **9**, 1021 (2000).
15. M. Ilia, G. Jeffery, *J. Comp. Neurol.* **405**, 394 (1999).
16. S. A. Thomas, A. M. Matsumoto, R. D. Palmiter, *Nature* **374**, 643 (1995).
17. Q. Y. Zhou, C. J. Quaife, R. D. Palmiter, *Nature* **374**, 640 (1995).
18. T. L. Dellovade, D. W. Pfaff, M. Schwanzel-Fukuda, *J. Comp. Neurol.* **402**, 402 (1998).
19. T. Vitalis *et al.*, *J. Neurosci.* **20**, 6501 (2000).
20. P. Cazorla, M. P. Smidt, K. L. O'Malley, J. P. Burbach, *J. Neurochem.* **74**, 1829 (2000).
21. M. Lebel, Y. Gauthier, A. Moreau, J. Drouin, *J. Neurochem.* **77**, 558 (2001).
22. J. E. Varley, G. D. Maxwell, *Exp. Neurol.* **140**, 84 (1996).
23. M. P. Smidt *et al.*, *Nature Neurosci.* **3**, 337 (2000).
24. H. Chen, W. N. Howald, M. R. Juchau, *Drug Metab. Dispos.* **28**, 315 (2000).
25. J. M. Rockwood, G. D. Maxwell, *Exp. Cell Res.* **223**, 250 (1996).
26. R. A. Catalano, L. B. Nelson, D. B. Schaffer, *Ophthalmic Paediatr. Genet.* **9**, 5 (1988).
27. D. B. van Dorp, J. W. Delleman, D. H. Loewer Sieger, *Clin. Genet.* **26**, 440 (1984).
28. R. E. Boissy, J. J. Nordlund, *Pigment Cell Res.* **10**, 12 (1997).
29. T. Kobayashi, G. Imokawa, D. C. Bennett, V. J. Hearing, *J. Biol. Chem.* **273**, 31801 (1998).
30. We thank F. Farley and J. Smith for assistance in preparing the manuscript and M. Anderson, D. Gould, T. Gridley, and T. O'Brien for critical reading of the manuscript, and L. Bechtold for assistance with electron microscopy. Scientific support services at The Jackson Laboratory are subsidized by a core grant from the National Cancer Institute (grant CA34196). S.W.M.J. is an Associate Investigator of The Howard Hughes Medical Institute.

Supporting Online Material
www.sciencemag.org/cgi/content/full/299/5612/1578/DC1
Materials and Methods
Figs. S1 and S2
References

4 November 2002; accepted 21 January 2003

Exhibit C

ELSEVIER

Mechanisms of Development 124 (2007) 551–558

www.elsevier.com/locate/modo

Heart development in fibronectin-null mice is governed by a genetic modifier on chromosome four

Sophie Astrof [a,1], Andrew Kirby [b], Kerstin Lindblad-Toh [c], Mark Daly [b,c], Richard O. Hynes [a,*]

[a] *Howard Hughes Medical Institute, Center for Cancer Research, Department of Biology, Massachusetts Institute of Technology, 77 Massachusetts Avenue, Cambridge, MA 02139, USA*
[b] *Center for Human Genetic Research, Massachusetts General Hospital, Boston, MA, USA*
[c] *Broad Institute of Harvard and MIT, Cambridge, MA, USA*

Received 21 February 2007; received in revised form 16 May 2007; accepted 28 May 2007
Available online 2 June 2007

Abstract

Absence of the fibronectin (*FN*) gene leads to early embryonic lethality in both 129S4 and C57BL/6J strains due to severe cardiovascular defects. However, heart development is arrested at different stages in these embryos depending on the genetic background. In the majority of 129S4 *FN-null* embryos, heart progenitors remain at their anterior bilateral positions and fail to fuse at the midline to form a heart tube. However, on the C57BL/6J genetic background, cardiac development progresses further and results in a centrally positioned and looped heart. To find factor(s) involved in embryonic heart formation and governing the extent of heart development in *FN-null* embryos in 129S4 and C57BL/6J strains, we performed genetic mapping and haplotype analyses. These analyses lead to identification of a significant linkage to a 1-Mbp interval on chromosome four. Microarray analysis and sequencing identified 21 genes in this region, including five that are differentially expressed between the strains, as potential modifiers. Since none of these genes was previously known to play a role in heart development, one or more of them is likely to be a novel modifier affecting cardiac development. Identification of the modifier would significantly enhance our understanding of the molecular underpinning of heart development and disease.

Keywords: Fibronectin; Heart development; Genetic modifier; Mapping

1. Introduction

The heart is the first organ to form in the developing vertebrate embryo and the survival of the embryo and the well-being of the adult are critically dependent on the integrity of the developmental program guiding heart formation (Srivastava, 2006). One of the earliest events during cardiogenesis is the coalescence of the bilateral cardiac primordia toward the midline to form a single heart tube (Buckingham et al., 2005) – the failure of this to happen leads to *cardia bifida* and lethality.

Genetic analyses in zebrafish and mice have uncovered a number of genes and processes required for the formation of a single heart tube from the paired cardiac primordia. First, cardiac mesoderm is derived from the early wave of cells migrating through the primitive streak, and the deletion of genes that affect this process (*Mesp1* and *Nap1*) gives rise to *cardia bifida* (Rakeman and Anderson, 2006; Saga et al., 1999). Second, endoderm provides an essential signal for the migration of the cardiac lateral plate mesoderm toward the midline, and genes required for endoderm specification (*cas, bon, oep*) (Alexander et al., 1999; Kikuchi et al., 2000; Schier et al., 1997) or morphogenesis (*fau, GATA4, Hrs, Furin, Foxp4*) (Komada and Soriano,

* Corresponding author. Tel.: +1 617 253 6422; fax: +1 617 253 8357.
E-mail address: rohynes@mit.edu (R.O. Hynes).
[1] Present address: Center for Molecular Cardiology, Weill Medical College of Cornell University, New York, NY, USA.

0925-4773/$ - see front matter © 2007 Elsevier Ireland Ltd. All rights reserved.
doi:10.1016/j.mod.2007.05.004

1999; Kuo et al., 1997; Li et al., 2004; Reiter et al., 1999; Roebroek et al., 1998) are required for the formation of a central heart tube. Hypoxia-regulated processes requiring HIF1α are also involved. Finally, genes important for cell migration (*paxillin, fibronectin, S1P receptor, NAP1*) (George et al., 1993; Hagel et al., 2002; Kupperman et al., 2000; Rakeman and Anderson, 2006), cell polarity (e.g. *fibronectin*, *NAP1*) (Rakeman and Anderson, 2006; Trinh and Stainier, 2004), extracellular matrix synthesis (*mtx1*) (Sakaguchi et al., 2006), or protein prenylation (*hmgcr1b*) (D'Amico et al., 2007) are essential for the formation of a centrally located heart tube.

Interestingly, the genetic makeup of laboratory mouse strains affects the phenotypes of mice carrying various knockout alleles. The most dramatic variations, from embryonic lethality in one strain to survival past birth in a different strain, are seen in mice carrying deletions in genes encoding an Rb family member p130 or EGF receptor (LeCouter et al., 1998; Threadgill et al., 1995). Heart function is also affected by strain-specific genetic variation. For example, adult wild-type mice of C57BL/6J strain possess the "heart of an athlete" compared with the hearts of A/J mice (Hoit et al., 2002). Genetic differences between strains also affect the degree of cardiac defects in some knockout mice. A deletion in the *HIF1α* gene results in *cardia bifida* in 32% of the embryos on a mixed 129X1-Swiss background while a central looped heart develops in all embryos from a mixed 129Sv/J × C57BL/6J strain (Compernolle et al., 2003; Iyer et al., 1998).

FN-null embryos have *cardia bifida* in the 129S4 strain of mice but develop a central looped heart in the C57BL/6J strain (George et al., 1997). Interestingly, the point mutant *natter* in zebrafish, which introduces a translational stop codon at the beginning of the *FN*1 message and abrogates the expression of fibronectin, also shows a strain-dependent *cardia bifida* phenotype (Trinh and Stainier, 2004). These phenomena suggest that there exist genetic factors whose identity and importance for heart development could be uncovered by performing genetic mapping analysis. Identification of new genes involved in early cardiogenesis may also facilitate our understanding of congenital heart defects. So far, mutations in a number of genes essential for embryonic heart development (e.g. *GATA4, Notch1, Nkx2.5, Tbx1, Tbx5*) have been found to underlie familial cases of congenital heart disease (Garg et al., 2003, 2005; Li et al., 1997; Merscher et al., 2001; Schott et al., 1998).

To identify new genes involved in heart development, we decided to map factor(s) governing heart formation in the *FN-null* embryos derived from F2 intercrosses between 129S4 and C57BL/6J strains. We used high-throughput genotyping of single-nucleotide polymorphisms (SNPs) and a dense SNP haplotype map of 129S4 and C57BL/6J strains (Wade and Daly, 2005) to identify a 1-Mbp interval on mouse chromosome four containing a modifier of cardiogenesis in *FN-null* embryos. Furthermore, by performing microarray analysis on wild-type, heterozygous, and *FN-null* embryos, we identified 21 candidate genes expressed in this interval, five of which were differentially expressed between 129S4 and C57BL/6J strains. This is the first example, to our knowledge, of mapping a quantitative trait locus of an embryonic lethal phenotype.

2. Results and discussion

2.1. Phenotypic analysis of FN-null embryos

All *FN-null* embryos from the C57BL/6J background developed a centrally located and looped heart by e9.3 (Fig. 1c and f). However, in 72% of 129S4 *FN-null* embryos, heart development stopped following the migration of cardiac primordia to their anterior–lateral positions (Fig. 1a and d). In the remaining 129S4 *FN-null* embryos, the heart primordia migrated and fused to form a central heart ball (Fig. 1b and e); however, none of the 129S4 *FN-null* embryos developed a looped heart tube (Table S1). Analysis of 62 *FN-null* embryos from F1 crosses between 129S4 and C57BL/6J, showed that, similar to 129S4 embryos, the largest group among the *FN-null* F1 embryos (37 out of 62) had bilateral cardiac primordia.

2.2. Genetic mapping

To perform genetic mapping analyses, we collected two independent sets of *FN-null* embryos from F2 intercrosses (there were 175 and 165 embryos in each set) and classified them into three groups according to their heart phenotypes (Fig. 1). Group 1 comprised embryos with unfused bilateral heart primordia, group 2 included embryos with a small- or medium-sized heart in the shape of a ball, and group 3 comprised embryos that developed a looped heart. Both sets of F2 embryos had similar distributions of phenotypes (Table S2). Each embryo was then genotyped using a genome-wide panel of SNP markers spaced about 20 cM apart on each chromosome. Each set of embryos was genotyped with a different set of genetic markers. These genome-wide scans indicated a potential linkage to the distal arm of chromosome four (Fig. 2a). We performed linkage analysis on the first and second sets of F2 embryos independently, and observed linkage to chromosome four in similar locations in each case (Fig. S1). An additional panel of SNP markers placed on chromosome four allowed us to narrow down the position of the modifier to a 5-Mbp interval (Fig. 2a and b). Other genomic regions did not show significant linkage (Fig. 2a). Furthermore, we did not detect genetic interactions between the locus on chromosome four and other chromosomal loci with LOD scores above 2.5 (Table S3).

We reasoned that the genetic modifier on chromosome four could affect either of two processes: migration of the lateral primordia to the midline or subsequent morphogenesis of the heart tube. In an attempt to distinguish between these two possibilities, we performed linkage analysis using different combinations of phenotypic groups. For example,

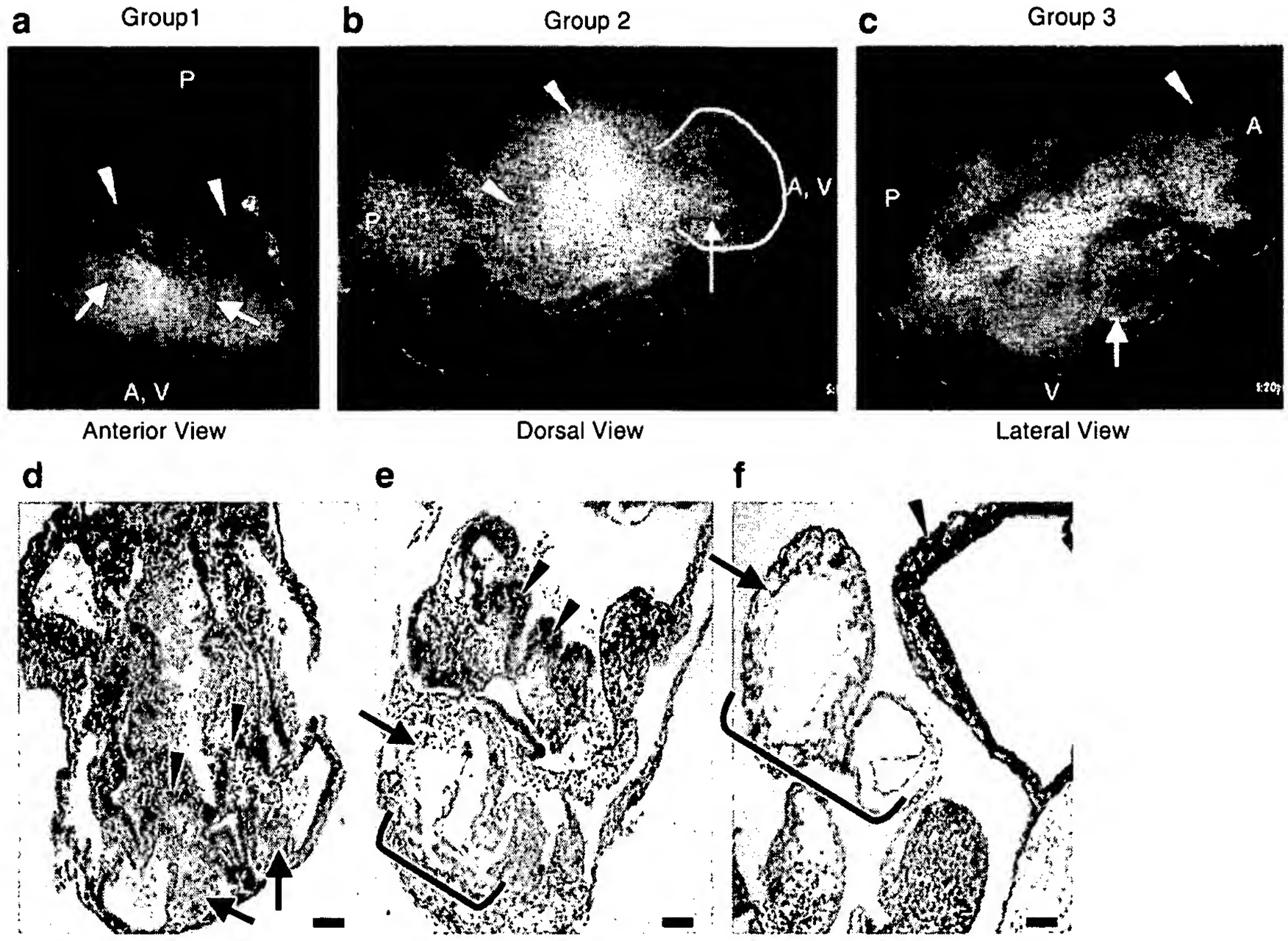

Fig. 1. Phenotypes of *FN-null* embryos. (a and d) A whole-mount view and a transverse section through an embryo representative of the majority of *FN-null* embryos from the 129S4 strain and of F2 embryos belonging to group 1. Arrows point to the two cardiac primordia, arrowheads point to the head folds. Anterior (A) and ventral (V) are at the bottom and posterior (P) is at the top. (b and e) A whole-mount view and a transverse section through a representative F2 embryo from group 2. Arrow points to the single heart ball outlined in B and encompassed by the bracket (e). Arrowheads point to headfolds. Anterior is to the right in (b) and at the bottom in (e). (c and f) A whole-mount view and a sagittal section through an embryo representative of *FN-null* embryos from C57BL/6J strain and F2 embryos belonging to group 3. Anterior is to the right in (c) and at the top right corner in (f). Arrow points to the central heart which is also delineated by a bracket in (f). Arrowhead points to the head. Scale bars in (d, e and f) are 65 μm.

to determine whether the modifier on chromosome four affected the progression from the bilateral cardiac primordia stage to a central heart, we analyzed embryos from group 1 against embryos from combined groups 2 and 3. While our analysis showed that the peak on chromosome four was mainly due to the genetic differences between groups 1 and 3 (Table S4), we obtained the highest LOD score, 5.5, when the three phenotypic classes were combined into two groups, one group contained embryos with unfused lateral heart primordia (group 1), while the other group consisted of embryos in which fusion of the primordia occurred (groups 2 and 3). This suggested that we were mapping a modifier affecting the event of coalescence of the two heart primordia into a single heart tube, a migration process that ordinarily happens during normal heart development (Buckingham et al., 2005).

The peak on chromosome four spanned five megabases (Mbp) (Fig. 2b) between 134 and 140 Mbp (2004 genome assembly). The LOD score of 5.5 corresponds to a pointwise (two-sided) p value of 2.5×10^{-6} and a genome-wide significance level of 0.003 (0.003 is the number of times that a linkage of LOD 5.5 could have been found fortuitously). These values comprise significant evidence (Lander and Kruglyak, 1995) that this region of chromosome four is linked to a gene(s) affecting heart development in *FN-null* embryos, and we term this locus modifier influencing single heart assembly (*Misha-1*).

The highest predicted LOD score (5.5) within the peak is 2 cM away from the closest genotyped marker, w4_13753, at 138 Mbp (Fig. 2b). Those embryos having two C57BL/6J alleles at the w4_13753 locus are approximately twofold more likely to develop a centrally located heart than to arrest at the bilateral primordia stage, and embryos homozygous or heterozygous for the 129S4 allele at w4_13735 have a 50/50 chance either to develop a central heart or to arrest at the bilateral primordia stage (Table S5). This suggests that, while a locus within the 5-Mbp region on chromosome four contains the major modifier of *FN-null* phenotype, there exist other quantitative trait loci, which contribute to strain-specific differences in heart development of *FN-null* mice.

While our experiments suggested that the locus on chromosome four contains one or more modifiers affecting the coalescence of the bilateral primordia into a single heart tube, the heart phenotype is not the only difference between these two groups, another notable

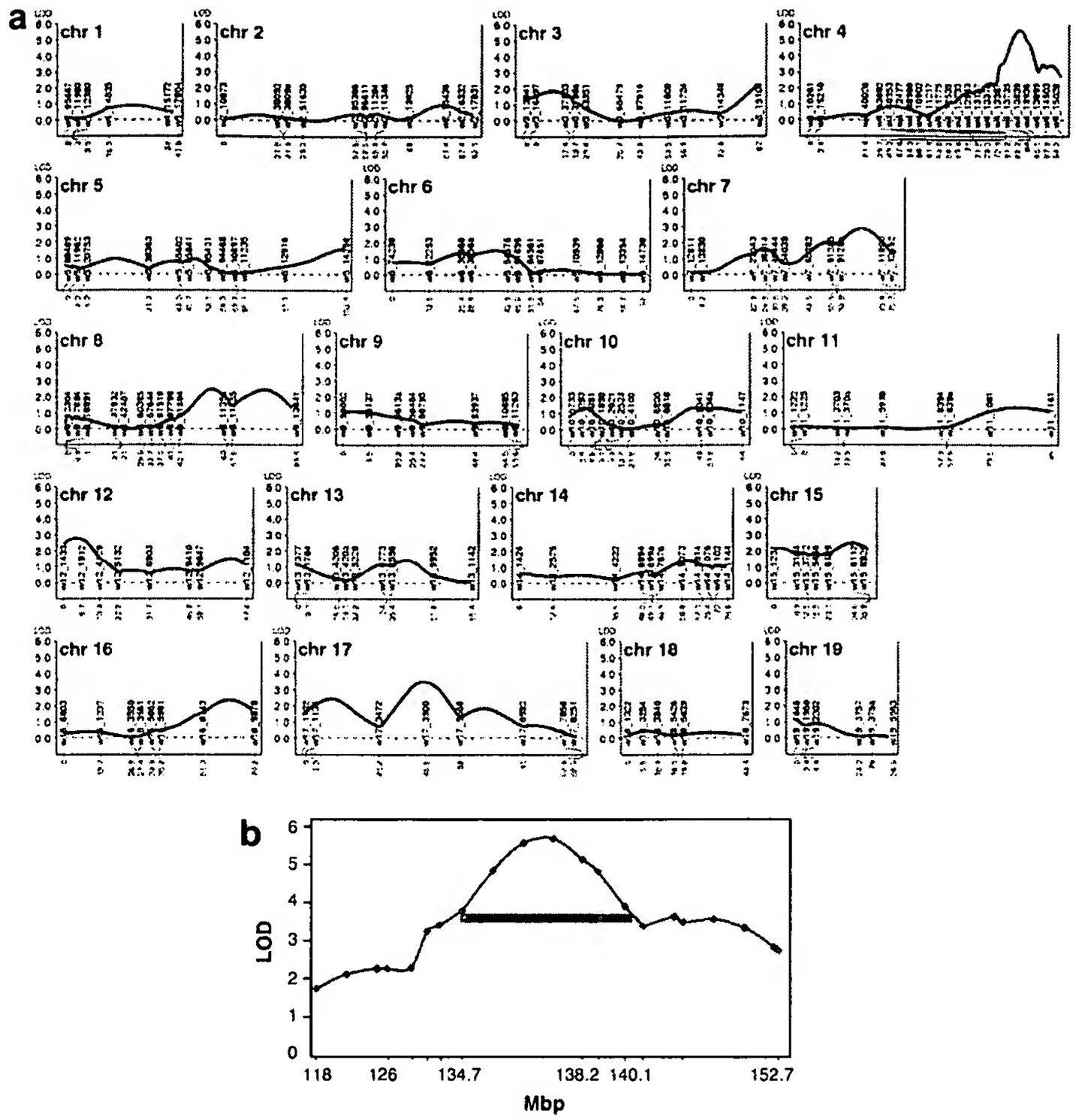

Fig. 2. A genetic modifier of heart development in *FN-null* mice is linked to the distal arm of chromosome four. (a) Genomescan of 341 F2 samples identified a linkage peak on chromosome four. For each chromosome, positions of the SNP markers in cM are plotted on the *x*-axis and LOD scores are plotted on the *y*-axis. Penetrance scan is shown, representing analysis of embryos from group 1 against embryos from combined groups two and three. Peaks on chromosomes eight and seventeen are not reproducible between the two sets of embryos and probably result from combining two different sets of markers used for the genome-wide scan. Chromosome four was genotyped with a single set of markers for all of the 341 embryo samples. (b) Linkage peak and haplotype map of the region on chromosome four. Embryos were pooled into two phenotypic groups (group 1 vs. groups 2 and 3) and analyzed using penetrance scan. Red marks and red points on the graph indicate positions of genotyped SNPs. Blue points on the curve show the points calculated by the MapmakerQTL. Blue bar – haplotype block shared between 129X1, 129S1, 129S4 and C57BL/6J strains based on the genotyping of 298 SNPs in this region (see Section 3). Marker w4_13753 at 138.2 Mb is the only polymorphism detected in this region. Red bars – regions containing SNPs between the 129S4 and C57BL/6J strains.

difference is the presence of vessels in embryos with at least a central heart ball, in contrast to those embryos without a heart (George et al., 1997). Therefore it is possible that the modifier locus affects an earlier stage in embryogenesis, correlating with the extent of the heart development. In order to understand the role of this locus in embryogenesis and heart formation, we need to identify the gene within it that acts as modifier.

2.3. Further analyses of the region

To narrow down the region containing the candidate modifier(s), we determined those areas within the 5-Mbp interval that contain polymorphisms between 129S4 and C57BL/6J strains, using a mouse SNP chip (Wade and Daly, 2005). This experiment showed that none of the 298 genotyped markers located between 134.8 and 139.1 Mbp was polymorphic between 129S4 and C57BL/6J strains (http://www.broad.mit.edu/~mjdaly/mousehapmap).

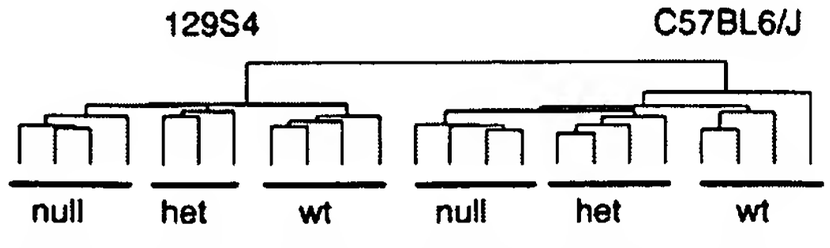

Fig. 3. Gene expression analysis of wild-type, heterozygous and *FN-null* embryos from 129S4 and C57BL/6J strains. Hierarchical unsupervised clustering of gene expression profiles distinguishes embryos from 129S4 and C57BL/6J strains and they cluster according to the number of wild-type *FN* alleles and according to genetic background.

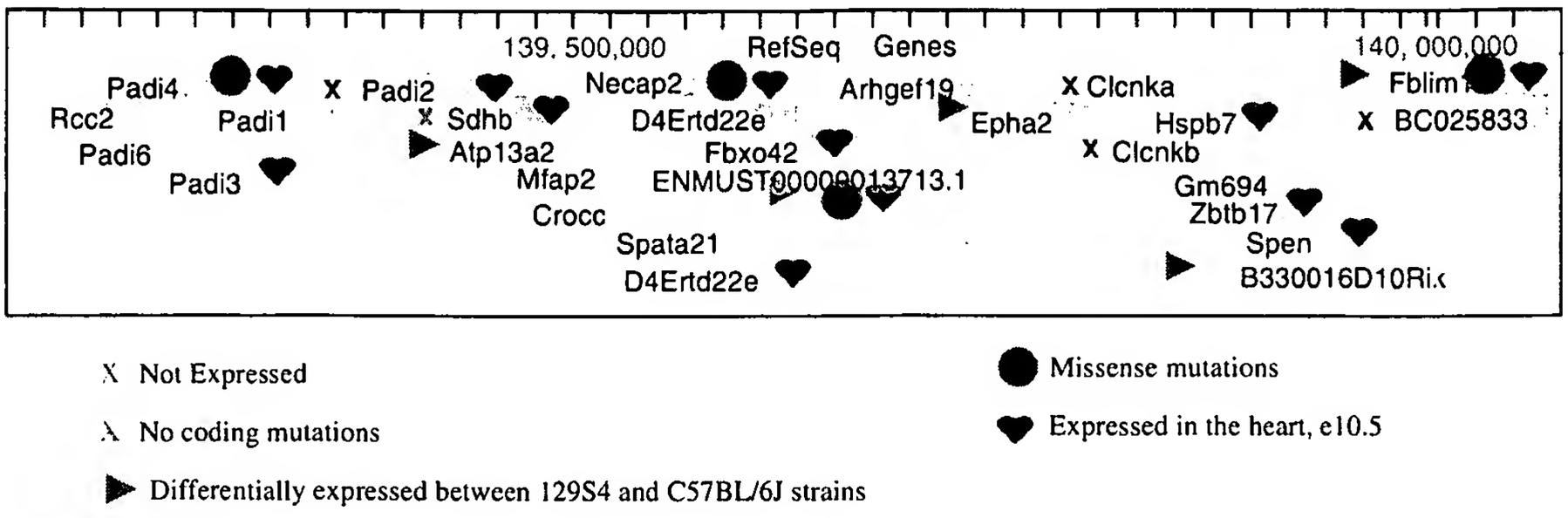

Fig. 4. Candidate modifier genes. There are 26 genes annotated in this 1-Mbp region of chromosome four. Twenty-five of them are annotated by RefSeq and are shown in the figure; the expression of one additional gene, ENMUST00000013713.1, is detected by the Affymetrix probe 1459714 at 139.67 Mbp. Genes expressed in the hearts of e10.5 embryos were found by mining the Entrez GEO database. Missense mutations were found by using the Perlegen database and by direct sequencing of cDNAs (see Section 3 and Table 1). Genes not expressed in the region were determined using Affymetrix absence and presence calls.

Table 1
Candidate modifier genes – expression and polymorphisms

	Affymetrix probe No.	Gene name/symbol	Expressed at e8.0	Differentially expressed	Expressed in the heart at e10.5	Missense mutations
1	1426897_at	RCC2	Yes	No	No	NS
2	1437084_at	PADi6	Yes	No	No	NS
3	1422760_at	PADi4	Yes	No	Yes	A573V
4	1419767_at	PADi3	Yes	No	Yes	NS
5	1419323_at	PADi1	Yes	No	No	NS
6	1418252_at	PADi2	No	No	Yes	NS
7	1418005_at	Sdhb*	Yes	No	Yes	None*
8	1428340_at	ATP13a2	Yes	Up in 129S4	Yes	NS
9	1417359_at	Mfap2	Yes	No	Yes	NS
10	1427338_at	Rootletin	Yes	No	No	T289A, E360G, V811M, S845N
11	1418961_at	NECAP2	Yes	No	Yes	I104L
12	1455718_at	Spata21	Yes	No	No	NS
13	1434482_at	D4Ertd22e	Yes	No	Yes	NS
14	1453382_at	Fbxo42	Yes	No	Yes	NS
15	1459714_at	ENMUST 00000013713.1*	Yes	Up in C57BL/6J	Yes	L40I, C106R, L168I, A107E*
16	1437629_at	ArhGEF19*	Yes		No	G492S*
17	1421151_at	EphA2	Yes	Up in C57BL/6J	No	NS
18	1457076_at	Gm693	Yes	No	No	NS
19	1455677_at	Clcnka	No	No	No	NS
20	1450340_at	Clcnkb	No	No	No	A380V, I431V, A554T, V571M, L637P, S667F
21	1421290_at	Hspb7	Yes	No	Yes	NS
22	1416224_at	Zbtb17	Yes	No	Yes	NS
23	1420397_at	Spen	Yes	No	Yes	NS
24	1455492_at	B330016D10Rik	Yes	Up in C57BL/6J	No	NS
25	1418569_at	Fblim1*	Yes	Up in C57BL/6J	Yes	I159R*
26	1451528_at	BC025833	No	No	No	NS

There are 26 genes annotated in the 1-Mbp region of chromosome four. Microarray analysis showed that 22 of these genes are expressed in e8.0 embryos and five of these genes are differentially expressed between the strains. Genes expressed in the hearts of e10.5 embryos were found by browsing Entrez GEO database. Missense mutations (C57BL/6J –> 129S4) were found by mining the Perlegen database and by direct sequencing. NS, not sequenced; these genes did not contain coding SNPs in the Perlegen database. Asterisks denote genes whose cDNAs were sequenced at 8× coverage from 129S4 and C57BL/6J strains.

Clearly this is a conserved haplotype block shared between the two strains. We resequenced several putative polymorphisms in this region – only one, w4_13753, was a true polymorphism and is the only known polymorphic marker in this region. We initially hoped that w4_13753 might help identify the modifier. However, there are no known or predicted genes in the near vicinity of w4_13753. The closest gene to the left of this marker

(TIR2) is 60 kb away and the closest gene on the right (Pax7) is 25 kb away. Neither gene is differentially expressed between 129S4 and C57BL/6J strains. While we cannot absolutely rule out the possibility that a rare polymorphism in this region could contribute to the modifier effect, this analysis suggests that the modifier(s) is more likely located within the 100 kbp on the left and/or 1 Mbp on the right sides of the peak, regions that do differ between strains (shown in red in Fig. 2b). We hypothesize that it is most likely that the potential modifier lies in the 1-Mbp region since it is closer to the two genotyped markers (at 138.2 and 139.1 Mbp) with the highest LOD scores (Fig. 2b).

The potential modifier must be a gene expressed in the embryos we analyzed. It could be either a differentially expressed gene, whose levels depend on the genetic strain or on the number of wild-type *FN*-alleles, or it could be a gene carrying a missense mutation. Since the levels of FN protein depend on the number of functional *FN* alleles (George et al., 1993), we determined gene expression profiles of *FN-null*, *FN*-heterozygous, and wild-type embryos at e8.0 of development, from both 129S4 and C57BL/6J strains by performing microarray analyses. Our analyses indicated that the expression profiles were segregated according to the strain and the genotype of the embryos (Fig. 3) and that 22 out of 26 annotated genes in the 1-Mbp region were expressed (Fig. 4 and Table 1). Among the expressed genes, five were differentially expressed between 129S4 and C57BL/6J strains. We did not find any genes in this interval that were differentially regulated by FN. Limited sequence analysis of the candidate genes (see Section 3) together with data from Perlegen (http://mouse.perlegen.com) showed that at least seven of the genes in the region contained missense mutations (Fig. 4 and Table 1), and that one gene, *Sdhb*, a potential tumor suppressor known to regulate HIF1α (Gottlieb and Tomlinson, 2005), does not have any coding SNPs, leaving 21 candidate modifier genes.

A potential modifier could be one of the genes differentially expressed between strains, such as *Fblim1*. *Fblim1* is a presumptive transcription factor that shuttles between the nucleus and the cytoplasm in response to Ca^{2+} and binds to Nkx2.5 (Akazawa et al., 2004), a transcription factor involved in heart development. This protein is interesting, because in the cytoplasm, it associates with actin stress fibers (Takafuta et al., 2003), appearance of which is modulated by the cellular adhesion to extracellular matrix proteins including fibronectin. Fblim1 contains three LIM domains and harbors a SNP between 129S4 and C57BL/6J strains located N-terminal to the first LIM domain leading to a missense mutation of Ile 159 (C57BL/6J) to Arg (129S4). A second interesting differentially expressed gene is the previously unidentified ENMUST00000013713.1. This gene has a GTPase domain, which harbors four SNPs between 129S4 and C57BL/6J strains leading to missense mutations in this domain (Table 1).

Alternatively, the modifier may not be differentially expressed between the strains but could have altered function due to a mutation. One such gene could be *ArhGEF19*, a novel gene with a predicted guanidine nucleotide exchange factor (GEF) domain and harboring Gly 492 (C57BL/6J) to Ser (129S4) mutation in this domain.

To identify the candidate modifier gene, we have tried to modify the levels of differentially expressed genes directly in 129S4 or C57BL/6J *FN-null* embryos, and used *FN-null* ES cells from 129S4 or C57BL/6J strains to generate tetraploid chimeras. These chimeras result from injecting diploid ES cells into tetraploid blastocysts, giving rise to embryos that are mainly derived from the ES cells and to extraembryonic tissues, derived from the tetraploid blastocysts. Even though fibronectin is a secreted protein, we hoped that its incorporation into the insoluble extracellular matrix of extraembryonic tissues would not lead to its distribution within the embryo. However this was not the case – the tetraploid chimeras made with *FN-null* ES cells of either strain, contained fibronectin within the embryo and developed hearts (data not shown). This was possibly due to the FN protein derived from rare wild-type tetraploid cells contributing to the embryo (Eakin et al., 2005) or, perhaps more likely, from diffusion of FN from the tetraploid extraembryonic tissues. While this approach was not useful to identify the modifier of *FN-null* phenotype, it would be useful for identifying a modifier of an embryonic lethal phenotype of a cell-autonomous gene such as integrin α5 (Yang et al., 1993).

Several approaches are available to identify the modifier of heart development in *FN-null* embryos from among the candidate genes. One could use RNAi to decrease the levels of differentially expressed genes: *ATP13a2* in 129S4 $FN^{+/-}$ ES cells or *Fblim1*, *ENMUST00000013713.1*, *Epha2*, and *B330016D10Rik* in C57BL/6J $FN^{+/-}$ ES cells. These modified ES cells would then be used to generate transgenic mice. Alternatively, $FN^{+/-}$ mice carrying BACs spanning the 1-Mbp region of chromosome four could be generated. However, these experiments are beyond the scope of the present paper.

2.4. Conclusion

It has been known for a long time that knockouts of some genes produce variable phenotypes depending on the mouse strain. This is interesting and could potentially allow identification of new and/or unexpected players in a particular process. We took advantage of the difference in heart formation in *FN-null* embryos from 129S4 and C57BL/6J strains with the aim of identifying new factors involved in heart development. Using a high-throughput SNP genotyping technology, which requires only nanogram quantities of genetic material, together with the recently available haplotype map of mouse strains and genome-wide expression analysis, we have narrowed the search to 21 primary candidate genes and outlined strategies that should be useful in identifying the candidate modifier.

3. Experimental procedures

3.1. Embryo samples

The *FN-null* allele was generated in 129S4 ES cells (George et al., 1993). 129S4 *FN-null* embryos were directly derived from the germline transmission of these cells. *FN-null* allele in the C57BL/6J strain was obtained by backcrossing *FN*-heterozygous mice from 129S4 strain to C57BL/6J mice for thirteen generations. *FN-null* embryos were isolated from *FN*-heterozygous crosses on the morning of embryonic day (e) 9.3 *post coitum* (p.c.), photographed and assigned a grade of one through three, depending on the heart phenotype. $FN^{+/-}$ mice and embryos of either strain are phenotypically normal. DNA was prepared using the DNeasy Qiagen kit according to the manufacturer's instructions and stored at −80 °C. Embryos were genotyped by PCR to confirm the homozygosity of the *FN-null* allele (George et al., 1993), and the presence of the Y chromosome using primers 5′-GCGCCCCAT GAATGCATTTAT G-3′ and 5′-CCCTCCGATGAGGCTG-3′ to detect the SRY gene.

3.2. Sample genotyping

Samples were genotyped to detect single-nucleotide polymorphisms (SNPs) (http://www.broad.mit.edu/~mjdaly/mousehapmap database) using the Sequenom MassArray (San Diego, CA, USA) mass spectrometry system as described previously (Petryshen et al., 2005). The data were analyzed using Mapmaker and MapmakerQTL (Kruglyak and Lander, 1995) using penetrance scan (Hamilton et al., 1997). Linkage to chromosome one was analyzed starting at 95 Mbp since all C57BL/6J *FN-null* embryos possess a significant amount of 129S4 genome carried over with the *FN-null* allele (*fibronectin* is situated at 70 mb on chromosome one).

3.3. Genotyping polymorphisms between 129S4 and C57BL/6J strains

DNA from 129S4 and C57BL/6J strains was hybridized to the mouse SNP chips as described (Wade and Daly, 2005). The results are available at http://www.broad.mit.edu/~mjdaly/mousehapmap web site. All genomic coordinates are according to the 2004 assembly of UCSC Genome Browser (http://genome.ucsc.edu).

3.4. Gene expression profiling

Total RNA was collected from six-somite wild-type, heterozygous, and *FN-null* embryos from 129S4 and C57BL/6J strains in the morning of the ninth day p.c. and purified using Trizol (Invitrogen). All wild-type and heterozygous embryos had crescent-shaped hearts, *FN-null* embryos from 129S4 strain had *cardia bifida* and those from C57BL/6J strain had hearts in the shape of a ball. *FN-null* embryos do not develop somites and thus we collected these embryos at the same day and time of development as the wild-type embryos. We obtained about 1 μg of total RNA from each embryo and used 100 ng to amplify and label mRNA according to the Affymetrix instructions (www.affymetrix.com). The labeled mRNA was hybridized to the Affymetrix 430 2.0 arrays. Data were analyzed using S-plus and GenePattern software packages.

3.5. Sequence analysis

cDNA was generated from total RNA isolated from 129S4 and C57BL/6J embryos at day e8.0. Guided by the sequence of the C57BL/6J mouse genome, we designed primers to amplify and sequence cDNAs encoding a few candidate modifier genes: *ArhGEF19*, *SdhB*, *ENMUST00000013713.1*, and *Fblim1*. *ENMUST00000013713.1* and *Fblim1* are two of the five genes differentially expressed between 129S4 and C57BL/6J strains, corresponding to Affymetrix probe Nos. 1459714 and 1418569. We determined that the probe set 1459714 assayed the expression of *ENMUST00000013713.1* since we amplified the cDNA corresponding to this gene using probe sequences from this probe set as reverse primers and primers lying in the predicted exons of *ENMUST00000013713.1* as forward primers. These cDNAs were isolated and sequenced from each of the two parental strains (results given in Table 1).

Acknowledgements

We thank Jeremy Hearn, Mary Connolly, and Aaron Cook for help with mouse dissections and mouse colony management, Charlie Whittaker and Steve Shen for help with microarray analysis, James Whittle for script to analyze Perlegen data, and Nathan Astrof for helpful discussions. We also thank E.J. Kulbocas, Tara Biagi, and Christine Curley for performing SNP genotyping, Brendan Blumenstiel for performing SNP chip hybridization, and Clare Wade for providing Perlegen data and helpful suggestions. This work was supported in part by grants from the NIH (PO1-HL66105) and the Howard Hughes Medical Institute, of which R.O.H. is an Investigator.

Appendix A. Supplementary data

Supplementary data associated with this article can be found, in the online version, at doi:10.1016/j.mod.2007.05.004.

References

Akazawa, H., Kudoh, S., Mochizuki, N., Takekoshi, N., Takano, H., Nagai, T., Komuro, I., 2004. A novel LIM protein Cal promotes cardiac differentiation by association with CSX/NKX2-5. J. Cell Biol. 164, 395–405.

Alexander, J., Rothenberg, M., Henry, G.L., Stainier, D.Y., 1999. Casanova plays an early and essential role in endoderm formation in zebrafish. Dev. Biol. 215, 343–357.

Buckingham, M., Meilhac, S., Zaffran, S., 2005. Building the mammalian heart from two sources of myocardial cells. Nat. Rev. Genet. 6, 826–835.

Compernolle, V., Brusselmans, K., Franco, D., Moorman, A., Dewerchin, M., Collen, D., Carmeliet, P., 2003. Cardia bifida, defective heart development and abnormal neural crest migration in embryos lacking hypoxia-inducible factor-1alpha. Cardiovasc. Res. 60, 569–579.

D'Amico, L., Scott, I.C., Jungblut, B., Stainier, D.Y., 2007. A mutation in zebrafish hmgcr1b reveals a role for isoprenoids in vertebrate heart-tube formation. Curr. Biol. 17, 252–259.

Eakin, G.S., Hadjantonakis, A.K., Papaioannou, V.E., Behringer, R.R., 2005. Developmental potential and behavior of tetraploid cells in the mouse embryo. Dev. Biol. 288, 150–159.

Garg, V., Kathiriya, I.S., Barnes, R., Schluterman, M.K., King, I.N., Butler, C.A., Rothrock, C.R., Eapen, R.S., Hirayama-Yamada, K., Joo, K., et al., 2003. GATA4 mutations cause human congenital heart defects and reveal an interaction with TBX5. Nature 424, 443–447.

Garg, V., Muth, A.N., Ransom, J.F., Schluterman, M.K., Barnes, R., King, I.N., Grossfeld, P.D., Srivastava, D., 2005. Mutations in NOTCH1 cause aortic valve disease. Nature 437, 270–274.

George, E.L., Baldwin, H.S., Hynes, R.O., 1997. Fibronectins are essential for heart and blood vessel morphogenesis but are dispensable for initial specification of precursor cells. Blood 90, 3073–3081.

George, E.L., Georges-Labouesse, E.N., Patel-King, R.S., Rayburn, H., Hynes, R.O., 1993. Defects in mesoderm, neural tube and vascular development in mouse embryos lacking fibronectin. Development 119, 1079–1091.

Gottlieb, E., Tomlinson, I.P., 2005. Mitochondrial tumour suppressors: a genetic and biochemical update. Nat. Rev. Cancer 5, 857–866.

Hagel, M., George, E.L., Kim, A., Tamimi, R., Opitz, S.L., Turner, C.E., Imamoto, A., Thomas, S.M., 2002. The adaptor protein paxillin is essential for normal development in the mouse and is a critical transducer of fibronectin signaling. Mol. Cell Biol. 22, 901–915.

Hamilton, B.A., Smith, D.J., Mueller, K.L., Kerrebrock, A.W., Bronson, R.T., van Berkel, V., Daly, M.J., Kruglyak, L., Reeve, M.P., Nemhauser, J.L., et al., 1997. The vibrator mutation causes neurodegeneration via reduced expression of PITP alpha: positional complementation cloning and extragenic suppression. Neuron 18, 711–722.

Hoit, B.D., Kiatchoosakun, S., Restivo, J., Kirkpatrick, D., Olszens, K., Shao, H., Pao, Y.H., Nadeau, J.H., 2002. Naturally occurring variation in cardiovascular traits among inbred mouse strains. Genomics 79, 679–685.

Iyer, N.V., Kotch, L.E., Agani, F., Leung, S.W., Laughner, E., Wenger, R.H., Gassmann, M., Gearhart, J.D., Lawler, A.M., Yu, A.Y., et al., 1998. Cellular and developmental control of O2 homeostasis by hypoxia-inducible factor 1 alpha. Genes Dev. 12, 149–162.

Kikuchi, Y., Trinh, L.A., Reiter, J.F., Alexander, J., Yelon, D., Stainier, D.Y., 2000. The zebrafish bonnie and clyde gene encodes a Mix family homeodomain protein that regulates the generation of endodermal precursors. Genes Dev. 14, 1279–1289.

Komada, M., Soriano, P., 1999. Hrs, a FYVE finger protein localized to early endosomes, is implicated in vesicular traffic and required for ventral folding morphogenesis. Genes Dev. 13, 1475–1485.

Kruglyak, L., Lander, E.S., 1995. A nonparametric approach for mapping quantitative trait loci. Genetics 139, 1421–1428.

Kuo, C.T., Morrisey, E.E., Anandappa, R., Sigrist, K., Lu, M.M., Parmacek, M.S., Soudais, C., Leiden, J.M., 1997. GATA4 transcription factor is required for ventral morphogenesis and heart tube formation. Genes Dev. 11, 1048–1060.

Kupperman, E., An, S., Osborne, N., Waldron, S., Stainier, D.Y., 2000. A sphingosine-1-phosphate receptor regulates cell migration during vertebrate heart development. Nature 406, 192–195.

Lander, E., Kruglyak, L., 1995. Genetic dissection of complex traits: guidelines for interpreting and reporting linkage results. Nat. Genet. 11, 241–247.

LeCouter, J.E., Kablar, B., Whyte, P.F., Ying, C., Rudnicki, M.A., 1998. Strain-dependent embryonic lethality in mice lacking the retinoblastoma-related p130 gene. Development 125, 4669–4679.

Li, Q.Y., Newbury-Ecob, R.A., Terrett, J.A., Wilson, D.I., Curtis, A.R., Yi, C.H., Gebuhr, T., Bullen, P.J., Robson, S.C., Strachan, T., et al., 1997. Holt-Oram syndrome is caused by mutations in TBX5, a member of the Brachyury (T) gene family. Nat. Genet. 15, 21–29.

Li, S., Zhou, D., Lu, M.M., Morrisey, E.E., 2004. Advanced cardiac morphogenesis does not require heart tube fusion. Science 305, 1619–1622.

Merscher, S., Funke, B., Epstein, J.A., Heyer, J., Puech, A., Lu, M.M., Xavier, R.J., Demay, M.B., Russell, R.G., Factor, S., et al., 2001. TBX1 is responsible for cardiovascular defects in velo-cardio-facial/DiGeorge syndrome. Cell 104, 619–629.

Petryshen, T.L., Kirby, A., Hammer Jr., R.P., Purcell, S., O'Leary, S.B., Singer, J.B., Hill, A.E., Nadeau, J.H., Daly, M.J., Sklar, P., 2005. Two quantitative trait loci for prepulse inhibition of startle identified on mouse chromosome 16 using chromosome substitution strains. Genetics 171, 1895–1904.

Rakeman, A.S., Anderson, K.V., 2006. Axis specification and morphogenesis in the mouse embryo require Napl, a regulator of WAVE-mediated actin branching. Development 133, 3075–3083.

Reiter, J.F., Alexander, J., Rodaway, A., Yelon, D., Patient, R., Holder, N., Stainier, D.Y., 1999. Gata5 is required for the development of the heart and endoderm in zebrafish. Genes Dev. 13, 2983–2995.

Roebroek, A.J., Umans, L., Pauli, I.G., Robertson, E.J., van Leuven, F., Van de Ven, W.J., Constam, D.B., 1998. Failure of ventral closure and axial rotation in embryos lacking the proprotein convertase Furin. Development 125, 4863–4876.

Saga, Y., Miyagawa-Tomita, S., Takagi, A., Kitajima, S., Miyazaki, J., Inoue, T., 1999. MesP1 is expressed in the heart precursor cells and required for the formation of a single heart tube. Development 126, 3437–3447.

Sakaguchi, T., Kikuchi, Y., Kuroiwa, A., Takeda, H., Stainier, D.Y., 2006. The yolk syncytial layer regulates myocardial migration by influencing extracellular matrix assembly in zebrafish. Development 133, 4063–4072.

Schier, A.F., Neuhauss, S.C., Helde, K.A., Talbot, W.S., Driever, W., 1997. The one-eyed pinhead gene functions in mesoderm and endoderm formation in zebrafish and interacts with no tail. Development 124, 327–342.

Schott, J.J., Benson, D.W., Basson, C.T., Pease, W., Silberbach, G.M., Moak, J.P., Maron, B.J., Seidman, C.E., Seidman, J.G., 1998. Congenital heart disease caused by mutations in the transcription factor NKX2-5. Science 281, 108–111.

Srivastava, D., 2006. Making or breaking the heart: from lineage determination to morphogenesis. Cell 126, 1037–1048.

Takafuta, T., Saeki, M., Fujimoto, T.T., Fujimura, K., Shapiro, S.S., 2003. A new member of the LIM protein family binds to filamin B and localizes at stress fibers. J. Biol. Chem. 278, 12175–12181.

Threadgill, D.W., Dlugosz, A.A., Hansen, L.A., Tennenbaum, T., Lichti, U., Yee, D., LaMantia, C., Mourton, T., Herrup, K., Harris, R.C., et al., 1995. Targeted disruption of mouse EGF receptor: effect of genetic background on mutant phenotype. Science 269, 230–234.

Trinh, L.A., Stainier, D.Y., 2004. Fibronectin regulates epithelial organization during myocardial migration in zebrafish. Dev. Cell 6, 371–382.

Wade, C.M., Daly, M.J., 2005. Genetic variation in laboratory mice. Nat. Genet. 37, 1175–1180.

Yang, J.T., Rayburn, H., Hynes, R.O., 1993. Embryonic mesodermal defects in alpha 5 integrin-deficient mice. Development 119, 1093–1105.

Exhibit D

Research article

The potential role of glutamate transporters in the pathogenesis of normal tension glaucoma

Takayuki Harada,[1,2,3] Chikako Harada,[1,2] Kazuaki Nakamura,[2] Hun-Meng A. Quah,[1] Akinori Okumura,[2] Kazuhiko Namekata,[2] Tadashiro Saeki,[4] Makoto Aihara,[4] Hiroshi Yoshida,[3] Akira Mitani,[5] and Kohichi Tanaka[1,6,7]

[1]Laboratory of Molecular Neuroscience, School of Biomedical Science and Medical Research Institute, Tokyo Medical and Dental University, Tokyo, Japan. [2]Department of Molecular Neurobiology, Tokyo Metropolitan Institute for Neuroscience, Fuchu, Japan. [3]Department of Neuro-ophthalmology, Tokyo Metropolitan Neurological Hospital, Fuchu, Japan. [4]Department of Ophthalmology, University of Tokyo School of Medicine, Tokyo, Japan. [5]Human Health Science, Graduate School of Medicine, Kyoto University, Kyoto, Japan. [6]Precursory Research for Embryonic Science and Technology, Japan Science and Technology Agency, Kawaguchi, Japan. [7]Center of Excellence Program for Brain Integration and its Disorders, Tokyo Medical and Dental University, Tokyo, Japan.

Glaucoma, a progressive optic neuropathy due to retinal ganglion cell (RGC) degeneration, is one of the leading causes of irreversible blindness. Although glaucoma is often associated with elevated intraocular pressure (IOP), IOP elevation is not detected in a significant subset of glaucomas, such as normal tension glaucoma (NTG). Moreover, in some glaucoma patients, significant IOP reduction does not prevent progression of the disease. Thus, understanding IOP-independent mechanisms of RGC loss is important. Here, we show that mice deficient in the glutamate transporters GLAST or EAAC1 demonstrate spontaneous RGC and optic nerve degeneration without elevated IOP. In GLAST-deficient mice, the glutathione level in Müller glia was decreased; administration of glutamate receptor blocker prevented RGC loss. In EAAC1-deficient mice, RGCs were more vulnerable to oxidative stress. These findings suggest that glutamate transporters are necessary both to prevent excitotoxic retinal damage and to synthesize glutathione, a major cellular antioxidant and tripeptide of glutamate, cysteine, and glycine. We believe these mice are the first animal models of NTG that offer a powerful system for investigating mechanisms of neurodegeneration in NTG and developing therapies directed at IOP-independent mechanisms of RGC loss.

Introduction

It is estimated that glaucoma affects nearly 70 million individuals worldwide, with at least 6.8 million bilaterally blind (1). The disease is characterized by a slow progressive degeneration of retinal output neurons (retinal ganglion cells [RGCs]) and their axons, which is usually associated with elevated intraocular pressure (IOP). The common adult-onset glaucoma is primary open-angle glaucoma (POAG), which is probably caused by a reduction in outflow of aqueous humor through the trabecular outflow pathways (2). Normal tension glaucoma (NTG), a subset of POAG that indicates statistically normal IOP, also shows glaucomatous optic neuropathy and relevant visual field defect. Several population studies have suggested that NTG represents 20%–90% of all POAG, with percentages seeming to vary according to race (3–5). Interestingly, IOP still seems to play a role in NTG because a substantial number of patients with NTG as well as other forms of POAG benefit from lowering of IOP (6). Thus, NTG may be caused by the vulnerability of optic nerves to normal range of IOP. However, it should be noted that some of NTG patients are still progressive in spite of sufficient IOP reduction. All these observations suggest a possibility that factors not dependent on IOP may contribute to disease progress and that elucidating such factors would be necessary to understand the pathogenesis of glaucoma and guide efforts toward improved therapeutics.

Recent studies have shown that glaucoma is affected by multiple genetic and environmental factors (7, 8), and this complexity can make it difficult to reach definitive conclusions (especially in human studies, in which many factors cannot be controlled). Animal studies complement human studies and can provide important insights into genetic etiology and molecular mechanisms for further assessment in people. There are now several published mouse models of pressure-induced RGC death. These include inherited and experimentally induced models (9). However, no animal model for NTG is currently known and available for research.

Besides more extensively investigated factors, such as reduced ocular blood flow, ocular vascular dysregulation, and systemic blood pressure alterations, excessive stimulation of the glutamatergic system, specifically the NMDA subtypes, has been proposed to contribute to death of RGCs in glaucoma. Glutamate transporter is the only mechanism for the removal of glutamate from the extracellular fluid in the retina (10). Therefore, it is hypothesized that the increase in glutamate may result from a failure of the glutamate transporters adjacent to RGCs. In the inner plexiform layer where synapses on RGCs exist, there are 3 transporters involved in this task: glutamate transporter 1 (GLT-1), located in the bipolar cell terminals; excitatory amino acid carrier 1 (EAAC1) in retinal neurons including RGCs; and glutamate/aspartate transporter (GLAST) in Müller cells (11). However, there is still debate on whether excitotoxic damage is involved in the pathophysiology of glaucoma (12). Here, we utilized mice in which 1 of each of these 3 glutamate transporters has been knocked out

Nonstandard abbreviations used: EAAC1, excitatory amino acid carrier 1; GCL, ganglion cell layer; GLAST, glutamate/aspartate transporter; GLT-1, glutamate transporter 1; GS, glutamine synthetase; INL, inner nuclear layer; IOP, intraocular pressure; 2K, second-order kernel; mfERG, multifocal electroretinogram; NTG, normal tension glaucoma; ONL, outer nuclear layer; POAG, primary open-angle glaucoma; RGC, retinal ganglion cell.

Conflict of interest: The authors have declared that no conflict of interest exists.

Citation for this article: *J. Clin. Invest.* 117:1763–1770 (2007). doi:10.1172/JCI30178.

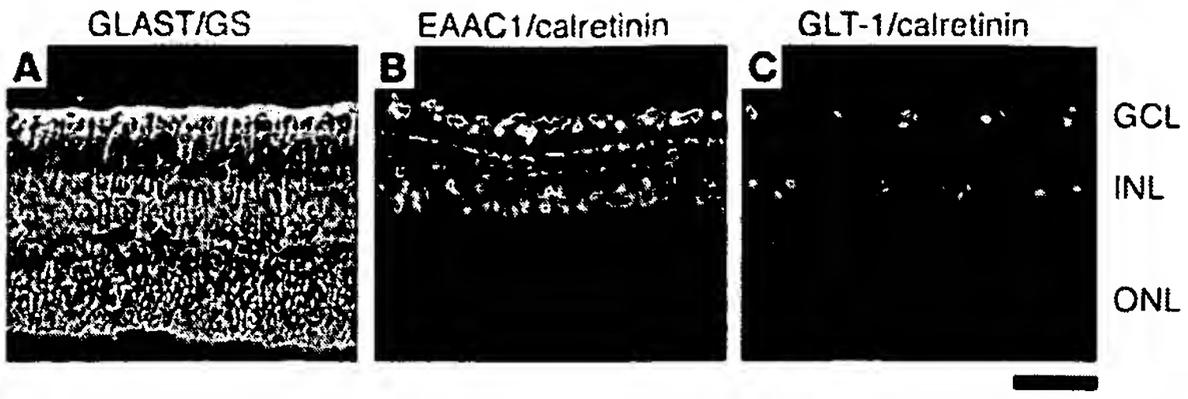

Figure 1
Expression of glutamate transporters in the retina. Immunohistochemical analysis of mouse retina double-stained with GLAST and GS, a specific marker for Müller glial cells (**A**); EAAC1 and calretinin, a specific marker for RGCs and amacrine cells (**B**); and GLT-1 and calretinin antibodies (**C**). Scale bar: 50 μm.

and examined the long-term effect of retinal morphology during postnatal development on RGC survival in vivo. We found that GLAST- and EAAC1-knockout mice showed spontaneously occurring RGC death and typical glaucomatous damage of the optic nerve without elevated IOP. To our knowledge, these glutamate transporter knockout mice are the first animal models of NTG, which offer a powerful system for determining mechanisms and evaluating new treatments of NTG.

Results

Degeneration of RGCs in GLAST- and EAAC1-deficient mice. Immunohistochemical studies demonstrated the presence of 3 subtypes of glutamate transporters in the inner plexiform layer of the rat retina. GLAST is expressed on Müller cells, GLT-1 on the bipolar cell terminals, and EAAC1 on ganglion cells (11). We verified that these localizations are also true for the mouse. As we previously reported (13), GLAST immunoreactivity is present throughout the retina and double-labeled by glutamine synthetase (GS), a specific marker for Müller glial cells (Figure 1A). EAAC1 and GLT-1 are neural-type glutamate transporters; however, their distribution is different. EAAC1 is mainly localized to the inner retinal layer and double-labeled by calretinin, a specific marker for RGCs and amacrine cells (Figure 1B). On the other hand, GLT-1 immunoreactivity is present in a small fraction of photoreceptors in the outer nuclear layer (ONL) in addition to bipolar cells but not in RGCs (Figure 1C). The findings are in agreement with those reported by Rauen for rat retina (11). The retinae of GLAST (14) and EAAC1 (15) mutant mice have normal organization at birth (Figure 2A). However, we noticed severe retinal degeneration in 8-month-old GLAST$^{-/-}$ mice (see also Figure 3, A and B), in

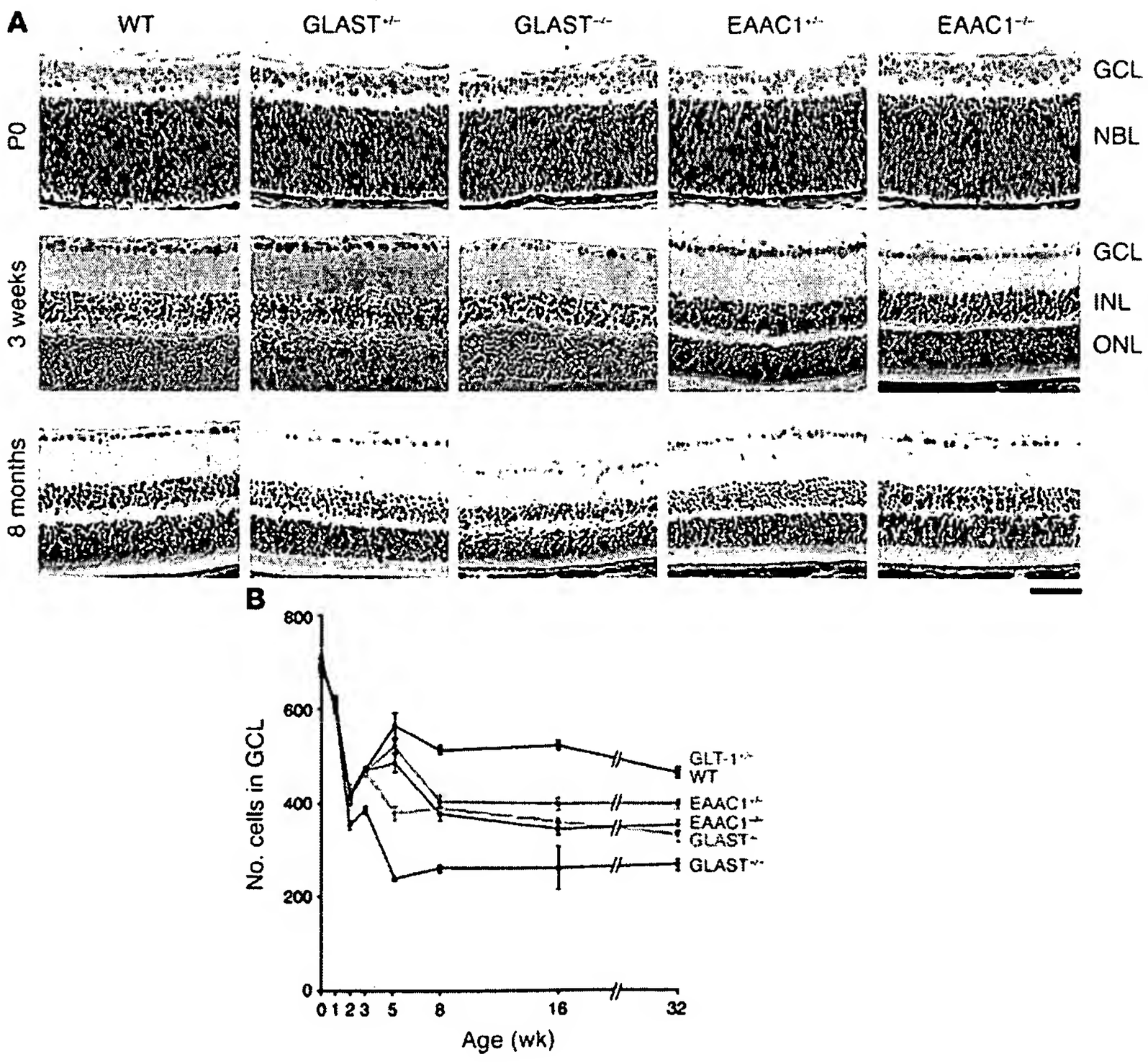

Figure 2
RGC degeneration in glutamate transporter mutant mice. (**A**) H&E staining of retinal sections during postnatal development. WT, GLAST$^{+/-}$, and GLAST$^{-/-}$ mice are littermates. EAAC1$^{+/-}$ and EAAC1$^{-/-}$ mice are littermates. (**B**) Quantification of RGC number in glutamate transporter mutant mice. The number of neurons in the GCL was counted in the retinal section from one ora serrata through the optic nerve to the other ora serrata at 0, 1, 2, 3, 5, 8, 16, and 32 weeks of age. Each plot represents the results of 3 to 6 independent experiments. Scale bar: 50 μm (**A**). NBL, neuroblast layer.

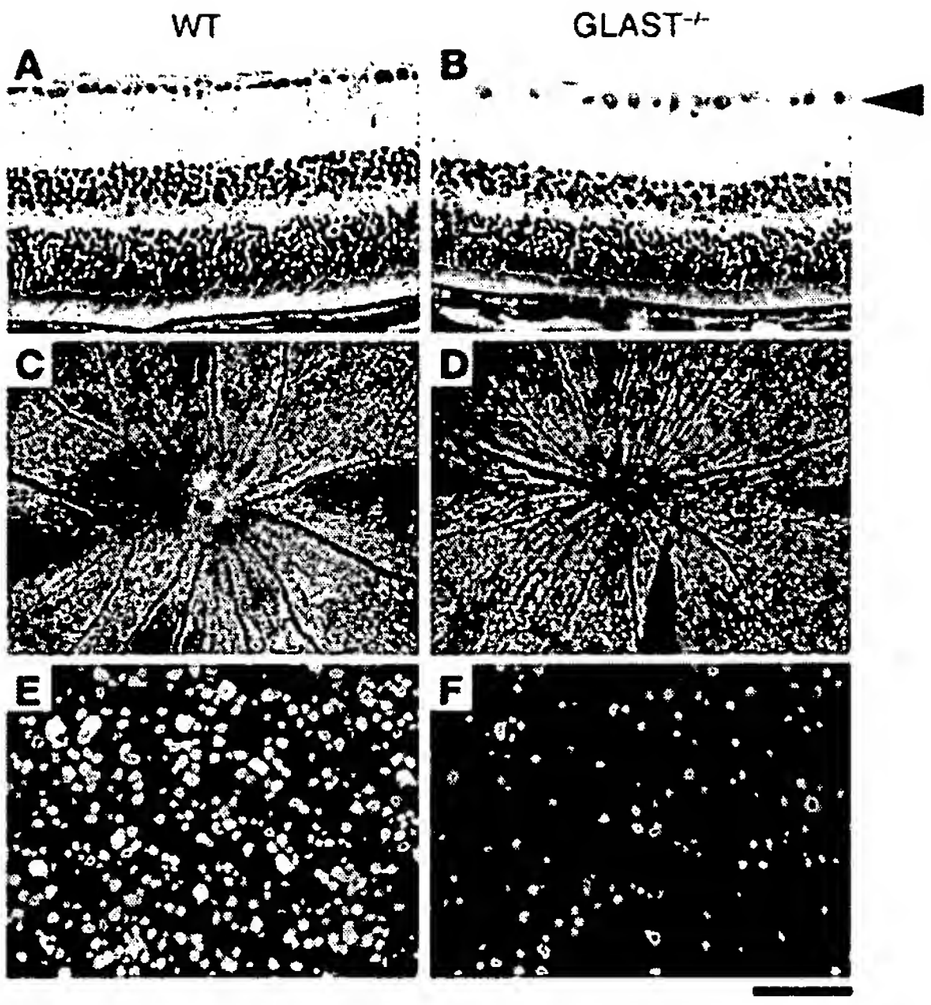

Figure 3
RGC degeneration in GLAST$^{-/-}$ mice. H&E-stained sections show a decreased number of cells in the GCL in GLAST$^{-/-}$ mouse (arrowhead) (**A** and **B**). Retrogradely labeled RGCs in GLAST$^{-/-}$ mouse were decreased compared with those in WT mouse (**C** and **D**). **E** and **F** are magnified images of **C** and **D**, respectively. Scale bar: 100 μm (**A**, **B**, **E**, and **F**); 500 μm (**C** and **D**).

which cell number was decreased in the ganglion cell layer (GCL) (53% ± 6%; $n = 6$, $P < 0.0001$) and the inner nuclear layer (INL) (81% ± 11%; $n = 6$, $P < 0.05$) but not in the ONL (97% ± 5%; $n = 6$, $P = 0.34$). As nearly half of the cells in the rodent GCL are displaced amacrine cells, we distinguished RGCs from displaced amacrine cells by retrograde labeling (16). The number of RGCs per mm^2 in retinae of 8-month-old GLAST$^{-/-}$ mice (2022 ± 48; $n = 18$) was significantly reduced compared with that in WT mice (4011 ± 106; $n = 18$, $P < 0.0001$) (Figure 3, C–F). We also examined RGC number by counting the cells located in the GCL. Because quantification of RGC loss by GCL cell count (49% ± 2%; $n = 6$) was consistent with that by RGC labeling (50% ± 1%; $n = 18$, $P = 0.89$) in 8-month-old GLAST$^{-/-}$ mice, we examined the GCL cell number from P0 to 8 months in all mutant mice (Figure 2B). Significant RGC loss was also observed in GLAST$^{-/-}$ mice after 2 weeks of age, GLAST$^{+/-}$ mice after 5 weeks, and EAAC1$^{+/-}$ and EAAC1$^{-/-}$ mice after 8 weeks. We were unable to examine 8-month-old GLT-1$^{-/-}$ mice (17) because most of them died within 3 weeks; however, RGC number in 8-month-old GLT-1$^{+/-}$ mice was normal compared with that in WT mice (101% ± 2%; $n = 10$; Figure 2B and Figure 4). Thus, GLT-1 mutant mice were not evaluated further.

Degeneration of optic nerve in GLAST- and EAAC1-deficient mice. Degeneration of the optic nerve is one of the hallmarks of glaucoma. Consistent with severe RGC loss, optic nerve cupping (Figure 5B) and thinning of the optic nerve (Figure 5D) were apparent in 8-month-old GLAST$^{-/-}$ mutants. Quantitative analysis revealed that optic nerve area in GLAST$^{-/-}$ mice (0.074 ± 0.002 mm^2; $n = 6$) was significantly decreased compared with that in WT mice (0.096 ± 0.005 mm^2; $n = 6$, $P = 0.0019$). To analyze morphological changes in the optic nerve, semithin transverse sections were cut and stained with toluidine blue. The degenerating axons in 5-week-old GLAST$^{-/-}$ mutants had abnormally dark axonal profiles (Figure 5F). In addition, compared with WT mice (Figure 5E), the density of axons through the optic nerve was clearly declined in GLAST$^{-/-}$ mice (Figure 5F). We next examined the iridocorneal angle in GLAST$^{-/-}$ mutants and found that it was well formed with an obvious Schlemm canal and a normal extent of trabecular meshwork (Figure 5H). EAAC1$^{-/-}$ mutants also showed excavation of the optic nerve and normal iridocorneal angle morphology (data not shown).

IOP measurement in GLAST- and EAAC1-deficient mice. GLAST and EAAC1 mutant mice showed POAG-like phenotype, which suggests the involvement of increased IOP. Therefore, we examined the IOPs of WT, EAAC1$^{-/-}$, and GLAST$^{-/-}$ mice. IOP measurement was carried out for both young (4 week) and adult (9 to 11 month) mice around 9 pm, when IOP is highest in mouse eyes (18). The IOPs of EAAC1$^{-/-}$ and GLAST$^{-/-}$ mice were not significantly increased compared with WT at both time points (Figure 5I). These results suggest that RGC loss and glaucomatous-like changes of the optic nerve in these mutants are IOP-independent.

Impaired visual function in GLAST-deficient mice. To determine whether the observed degeneration of RGCs and the optic nerve is functionally significant, we analyzed multifocal electroretinograms (mfERGs) of GLAST$^{-/-}$ mouse retina. RGCs contribute to the human mfERG response, and the second-order kernel (2K), which appears to be a sensitive indicator of inner retinal dysfunction (19), is impaired in glaucoma patients (20). The averaged 2K responses of 10 mice are shown in Figure 6A. The response topography demonstrated that the 2K component derived from GLAST$^{-/-}$ mice tended to be shorter in all visual fields compared with that of WT mice (Figure 6B). Quantitative analysis revealed that the 2K amplitude was reduced by about half in GLAST$^{-/-}$ mice compared with that in WT mice ($P < 0.005$) (Figure 6C), suggesting that RGC loss is functionally significant in GLAST$^{-/-}$ mice.

Role of glutamate neurotoxicity in RGC degeneration in GLAST-deficient mice. To determine the contribution of excitotoxicity to RGC death in these models, we first measured the intravitreal glutamate concentration in WT and mutant mice. Glutamate concentration was not significantly increased in GLAST or EAAC1 mutant mice (Figure 7A). Because an increase in glutamate concentration in the extracellular space just adjacent to RGCs might be obscured due to dilution within the vitreous (21), failure to detect glutamate elevation in the vitreous fluid does not necessarily exclude glutamate involvement in RGC degeneration in the mutants. To assess glu-

Figure 4
Normal retinal structure in GLT-1$^{+/-}$ mouse. H&E-stained sections show the absence of RGC degeneration in an 8-month-old GLT-1$^{+/-}$ mouse. Scale bar: 50 μm.

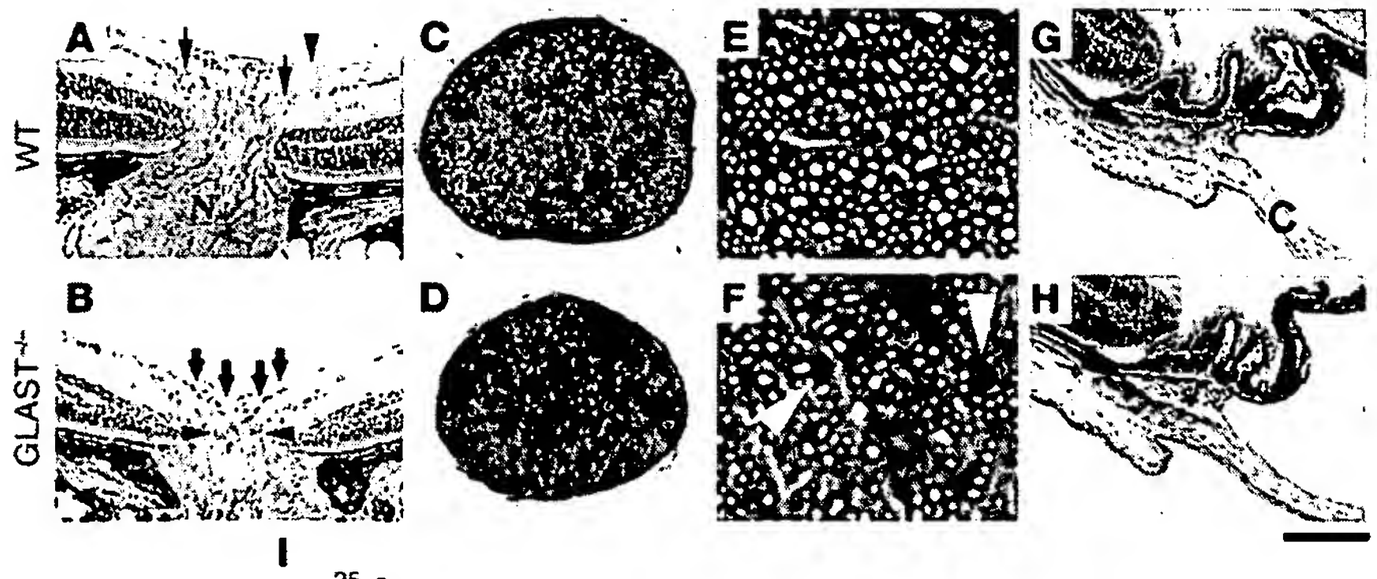

Figure 5

Optic nerve degeneration and normal IOP in glutamate transporter mutant mice. (**A** and **B**) Optic nerve atrophy in 8-month-old GLAST$^{-/-}$ mice. In WT mice (**A**), the nasal and temporal nerve fibers (arrows) are beneath the internal limiting membrane (arrowhead) and enter a well-formed optic nerve (N). In GLAST$^{-/-}$ mice (**B**), the nerve fiber layer has become thin and almost absent as it enters the nerve (bold arrows). Cupping extends to the posterior aspect of the inner retinal layer (arrowheads). (**C** and **D**) Thinning of optic nerve is apparent in GLAST$^{-/-}$ (**D**) compared with WT (**C**) mice. (**E** and **F**) Staining of semithin sections with toluidine blue reveals the presence of abnormally dark axonal profiles (arrowheads) and decline of axons in GLAST$^{-/-}$ (**F**) compared with WT (**E**) mice. (**G** and **H**) Aqueous humor drainage structures in WT (**G**) and GLAST$^{-/-}$ (**H**) mice. Iridocorneal angle in GLAST$^{-/-}$ mice is normal with an obvious Schlemm's canal (arrow) and trabecular meshwork (asterisk) compared with those in WT mice. The angle recess between the cornea (C) and iris is wide open. (**I**) IOP of young (4 weeks old) and adult (9–11 months old) mice. Sample numbers are indicated in parentheses. Scale bar: 200 μm (**A**, **B**, **G**, and **H**); 130 μm (**C** and **D**); 9 μm (**E** and **F**).

tamate involvement in RGC degeneration, we next examined the effect of the NMDA receptor antagonist memantine (22) on RGC degeneration in GLAST mutants. Memantine (10 mg/kg injected daily) prevented RGC loss when applied from P7 to P13 (Figure 7B), and the RGC number in GLAST$^{-/-}$ mice was normal at P14 (Figure 7C). The protective effect of glutamate receptor antagonist suggests that glutamate neurotoxicity is partly involved in RGC loss in GLAST mutant mice. However, since glutamate concentration in the vitreous fluid was normal, other factors, in addition to glutamate neurotoxicity, might contribute to RGC degeneration of GLAST-deficient mice.

Role of oxidative stress in RGC degeneration of GLAST- and EAAC1-deficient mice. In addition to excitotoxicity, oxidative stress has also been proposed to contribute to RGC death in glaucoma (23, 24). In adult GLAST$^{-/-}$ and EAAC1$^{-/-}$ mice, lipid hydroperoxides were increased in retinae, suggesting the involvement of oxidative stress in RGC loss (Figure 8A). Previous studies demonstrated that glutathione, a tripeptide of glutamate, cysteine, and glycine, has a central role in protecting RGCs against oxidative stress and that glutamate uptake is a rate-limiting step in glial glutathione synthesis (25, 26). Because retinal glutathione was specifically distributed in Müller cells (Figure 8B), we hypothesized that oxidative stress may result from impaired glial glutathione synthesis in GLAST$^{-/-}$ mice. In agreement with this hypothesis, glutathione content in the retina and in cultured Müller cells was decreased in GLAST$^{-/-}$ mice (Figure 8C). A similar reduction in glutathione level was recently reported in the plasma of human POAG patients (27). To confirm that the reduction in Müller cell glutathione levels makes RGCs more vulnerable to oxidative stress, we examined the effect of H_2O_2 on WT RGCs in a mixed culture with Müller cells from GLAST$^{-/-}$ or WT mice. We used a concentration of H_2O_2 that does not induce Müller cell death. RGC loss was significantly higher when RGCs were mixed with Müller cells from GLAST$^{-/-}$ mice than when mixed with Müller cells from WT mice (Figure 8D). These results indicate that GLAST deficiency leads to glaucomatous-like RGC loss in 2 ways: first, by excessive stimulation of NMDA receptors and second, by reducing the glutathione levels in Müller cells, thus making RGCs more vulnerable to oxidative stress.

Unlike glial GLAST, neuronal EAAC1 does not play a major role in clearing glutamate from the extracellular space (15, 28). Instead, EAAC1 can transport cysteine, an obligate precursor for neuronal glutathione synthesis, far more effectively than GLAST (29). Aoyama et al. recently reported that EAAC1 deficiency leads to impaired neuronal glutathione metabolism and age-dependent brain atrophy (29). In EAAC1$^{-/-}$ mutant mice, retinal glutathione content was not decreased (Figure 8C). These measurements represent bulk glutathione content in retinal homogenates from

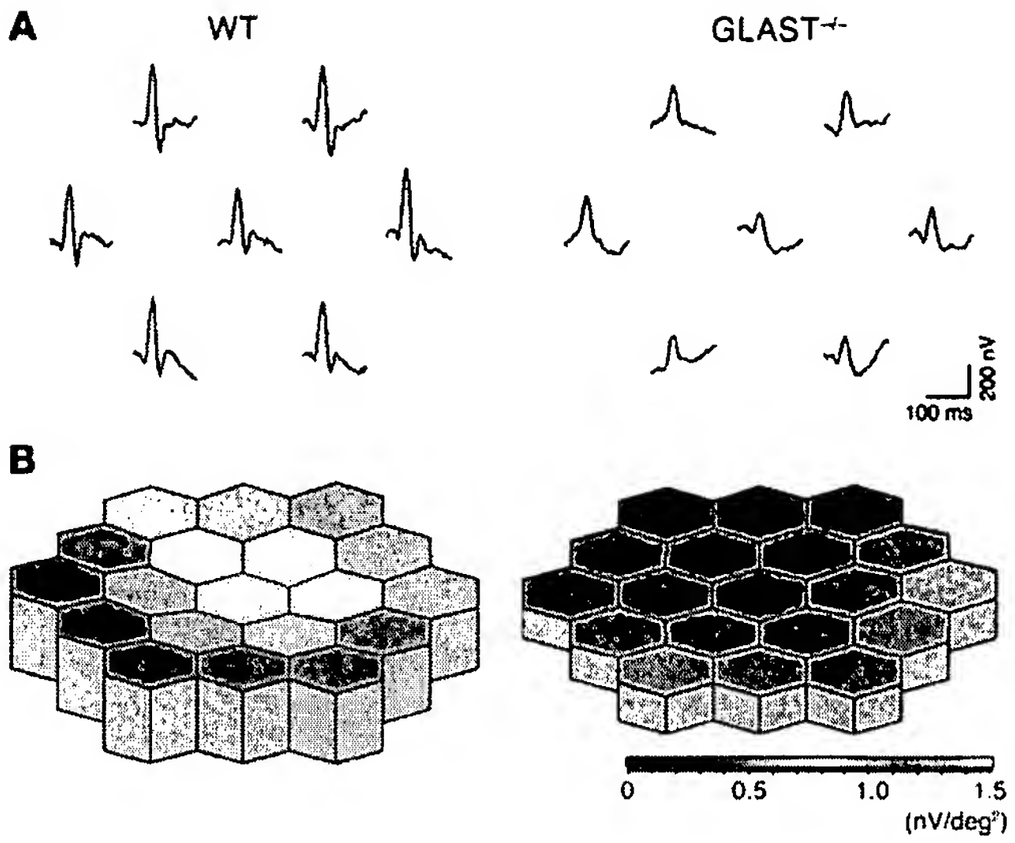

Figure 6
Impaired multifocal electroretinogram in GLAST$^{-/-}$ mice. (**A**) Averaged responses of 2K from 10 mice. The visual stimulus was applied to 7 different areas in the retina. The 7 individual traces demonstrate the average responses to the visual stimulus at the corresponding stimulus area. (**B**) Three-dimensional plots showing the amplitude variation across the arrays in **A**. (**C**) Quantitative analysis of 2K amplitude. The response amplitudes for each stimulus element were added and the result was divided by the total area of the visual stimulus. $n = 10$ per group; $^*P < 0.005$. Values in **B** and **C** are given in nV per square degree (nV/deg^2).

EAAC1$^{-/-}$ and WT mice. Thus, glutathione deficiency in RGCs of EAAC1$^{-/-}$ mice may not be apparent because a large share of retinal glutathione is localized to Müller cells (26), which do not express EAAC1. To directly determine the vulnerability of EAAC1$^{-/-}$ RGCs to oxidants, primary cultures of mutant and WT RGCs were treated with H_2O_2. Cultured RGCs from EAAC1$^{-/-}$ mice were susceptible to H_2O_2 compared with those from WT mice (Figure 8E). These findings suggest that EAAC1 deficiency makes RGCs more vulnerable to oxidative stress.

Discussion

Here, we show that GLAST- and EAAC1-knockout mice show progressive RGC loss and glaucomatous optic nerve degeneration without elevated IOP. Our study raises the possibility that dysfunction of the glutamate transporters GLAST (EAAT1 in humans) and EAAC1 (EAAT3 in humans) plays a role in RGC death in human NTG. It is reported that EAAT1 is downregulated in human glaucoma (30). In addition, a decrease of EAAT1 has been shown in fibroblasts from patients with Alzheimer disease (31). Considering the high frequency of POAG in Alzheimer disease patients (32), common mechanisms, such as GLAST dysfunction, might contribute to the 2 diseases. These findings indicate that GLAST- and EAAC1-knockout mice are useful as models of NTG.

Because GLAST is a major glutamate transporter in the mammalian retina, loss of GLAST is expected to render the retina highly susceptible to excitotoxic damage. However, we previously reported that the GLAST$^{-/-}$ retina showed no signs of RGC degeneration although it was more sensitive to prolonged ischemia than normal retina (13). In the present study, GLAST$^{-/-}$ mice showed spontaneous RGC loss and glaucomatous optic nerve degeneration. What factors account for this discrepancy? One possibility is the genetic background of the mice used. In previous studies, we used GLAST$^{-/-}$ mice on a mixed C57BL/6 × 129 genetic background. During the course of backcrossing to a C57BL/6 strain, GLAST$^{-/-}$ mice showed spontaneous NTG-like RGC degeneration. This finding can allow us to identify strain-specific modifier genes that might suppress or enhance RGC degeneration. It is intriguing that the C57BL/6J mice with mutations in the optineurin (*OPTN*) gene, which have been associated with human POAG and NTG, show extensive RGC loss (33). Thus, the C57BL/6J strain may have a potentially pathogenic allele of *Optn*. Although more studies are needed to determine whether the NTG-like phenotype in GLAST$^{-/-}$ mice on a C57BL/6J strain is related to *Optn*, such studies will identify new candidate molecules/pathways that may contribute to RGC survival.

The results of the present study suggest that glial GLAST and neuronal EAAC1 play differential roles in preventing RGC degeneration. GLAST is essential not only to keep the extracellular glutamate concentration below the neurotoxic level, but also to maintain the glutathione levels in Müller cells by transporting glutamate, the substrate for glutathione synthesis, into the cells. In contrast, the main role of EAAC1 is to transport cysteine into RGCs as a precursor for neuronal glutathione synthesis. Thus, GLAST deficiency leads to RGC degeneration caused by both excitotoxicity and oxidative stress whereas EAAC1 deficiency induces RGC loss mainly through oxidative stress. In the present paper, we demonstrate that the availability of glutamate is limiting for the maintenance of normal intracellular glutathione level in Müller cells. This observation differs from findings in other tissues, where cysteine was identified as the rate-limiting substance (34, 35). How can this be explained? Previous studies demonstrated that Müller cells possess a very fast glutamate turnover (36). A major part of the available intracellular glutamate is used for glutamine synthesis catalyzed by the enzyme GS, which is exclusively located in Müller cells (37). This makes the intracellular glutamate concentration of Müller cells strongly dependent on glutamate uptake via the glutamate transporter GLAST. In contrast, the cysteine turnover of Müller cells seems to be rather slow (36). Therefore, the rate-limiting factor for glutathione levels in Müller cells is not the cystine supply to the cells but rather the provision of glutamate.

Glutamate excitotoxicity and oxidative stress have been proposed to contribute to retinal damage in various eye diseases, including retinal ischemia, glaucoma, diabetic retinopathy, and age-related macular degeneration (38–40). Therefore, the design of compounds capable of activating glutamate uptake by GLAST represents a novel strategy for the management of glaucoma and various forms of retinopathy (41, 42). We also showed that RGCs

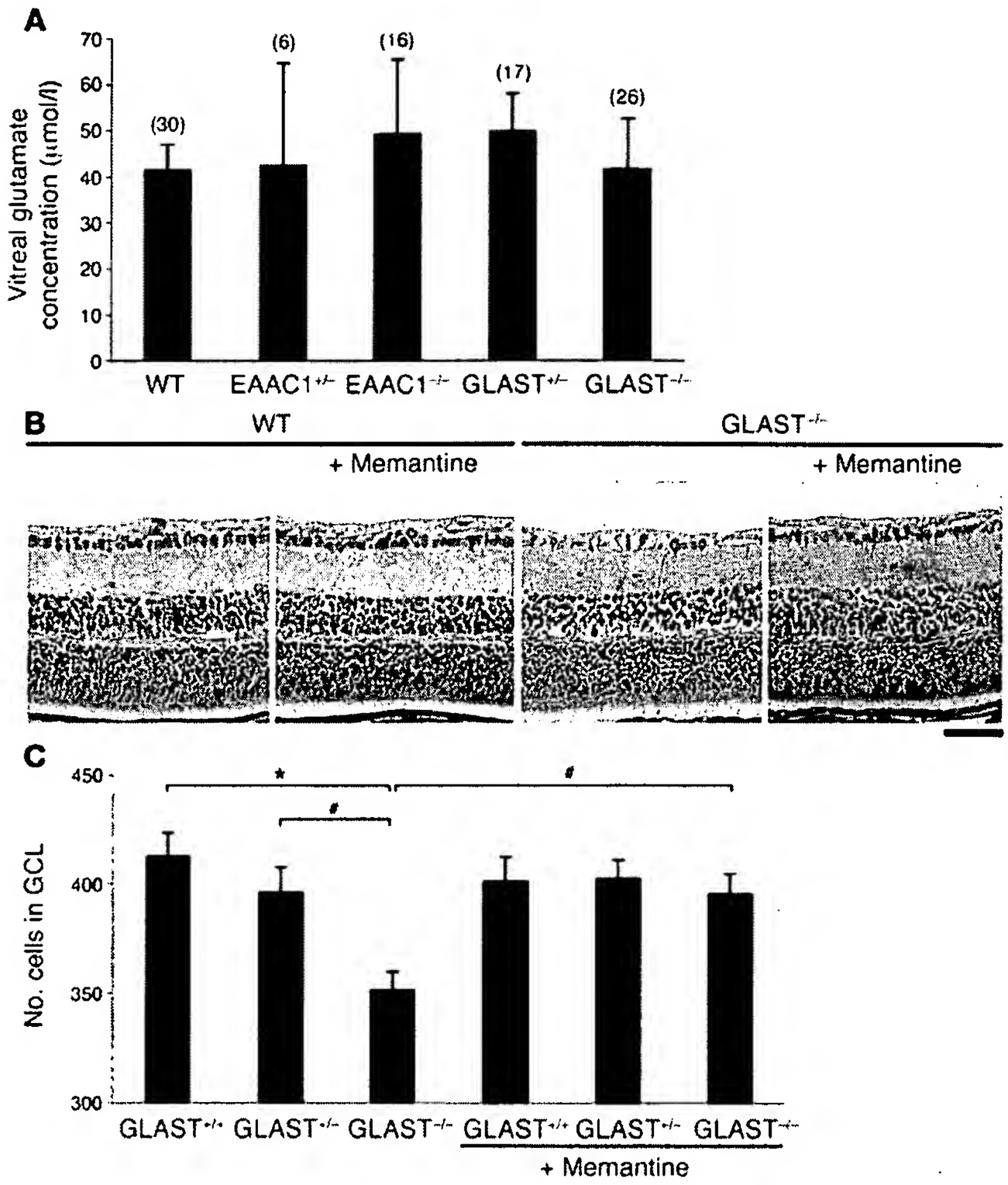

Figure 7
Effect of glutamate neurotoxicity on RGC degeneration. (**A**) Intravitreal glutamate concentration in glutamate transporter mutant mice. Sample numbers are indicated in parentheses. (**B**) H&E-stained P14 retinal sections from WT and GLAST$^{-/-}$ mice with or without treatment with memantine (10 mg/kg, i.p.) daily from P7 to P13. (**C**) Quantitative analysis of RGC number following memantine administration. The number of neurons in the GCL was counted in the retinal section from one ora serrata through the optic nerve to the other ora serrata. n = 6 per group. $^{\#}P < 0.05$; $^{*}P < 0.005$. Scale bar: 50 μm (**B**).

cocultured with Müller cells from GLAST$^{-/-}$ mice are susceptible to free radical stimulation (Figure 8D). We previously reported that neurotrophins alter the production of some trophic factors in Müller cells, which indirectly leads to neural cell survival during photoreceptor degeneration (43, 44). We suggest that such a glia-neuron network is functional in various forms of neurodegenerative diseases, and the messengers between glia and neurons may be different according to the situation. In addition, each single Müller cell extends from the outer to the inner surface of the retina. This allows the Müller cells to form elaborate intimate contacts with the somata of all types of retinal neurons as well as with the fibers and synapses in the neuropile of the 2 plexiform layers. Their ubiquitous presence makes the Müller cells a suitable target for drug delivery and gene therapy in retinal degenerative diseases. Furthermore, recent studies have shown that Müller cells could proliferate after neurotoxic damage and produce bipolar cells and rod photoreceptors in the adult mammalian retina (45, 46). Therefore, Müller cells may be a new therapeutic target for both neuroprotection and regeneration in retinal degenerative diseases (47, 48).

Methods

Mice. Experiments were performed using EAAC1$^{+/-}$, EAAC1$^{-/-}$ (15), GLT-1$^{+/-}$ (17), GLAST$^{+/}$, and GLAST$^{-/}$ (14) mice with approval from the Institutional Animal Care and Use Committee of Tokyo Medical and Dental University and the Tokyo Metropolitan Institute for Neuroscience. All the mice used in this study were backcrossed with C57BL/6 more than 8 times.

Immunohistochemistry. Frozen 12-μm–thick retinal sections were incubated with 1 of 4 sets of primary antibody mix. Primary antibodies used were mouse anti-GS (Chemicon International) and rabbit anti-GLAST (13) or anti-glutathione (Signature Immunologics); and mouse anti-calretinin (Chemicon International) and rabbit anti-EAAC1 (49) or anti–GLT-1 (13). Fluorescence immunohistochemistry was performed using Cy2-conjugated donkey anti-mouse IgG and Cy3-conjugated donkey anti-rabbit IgG (Jackson ImmunoResearch Laboratories Inc.). Sections were examined by fluorescence microscopy (Olympus).

Histological and morphometric studies. Paraffin sections (7-μm thick) of retinal specimens were cut through the optic nerve and stained with H&E. RGC number and the extent of retinal degeneration were quantified in 3 ways. First, the cell density of each layer was analyzed (50). Second, in the same sections, the number of neurons in the GCL was counted from one ora serrata through the optic nerve to the other ora serrata. Third, RGCs were retrogradely labeled from the superior colliculus with Fluoro-Gold (Fluorochrome) (16). Seven days after Fluoro-Gold application, eyes were enucleated and retinas were detached and prepared as flattened whole mounts in 4% paraformaldehyde in 0.1 M PBS solution. GCL was examined in whole-mounted retinae with fluorescence microscopy to determine the RGC density. Four standard areas (0.04 mm^2) of each retina at the point of 0.1 mm from the optic disc were randomly chosen, labeled cells were counted by observers

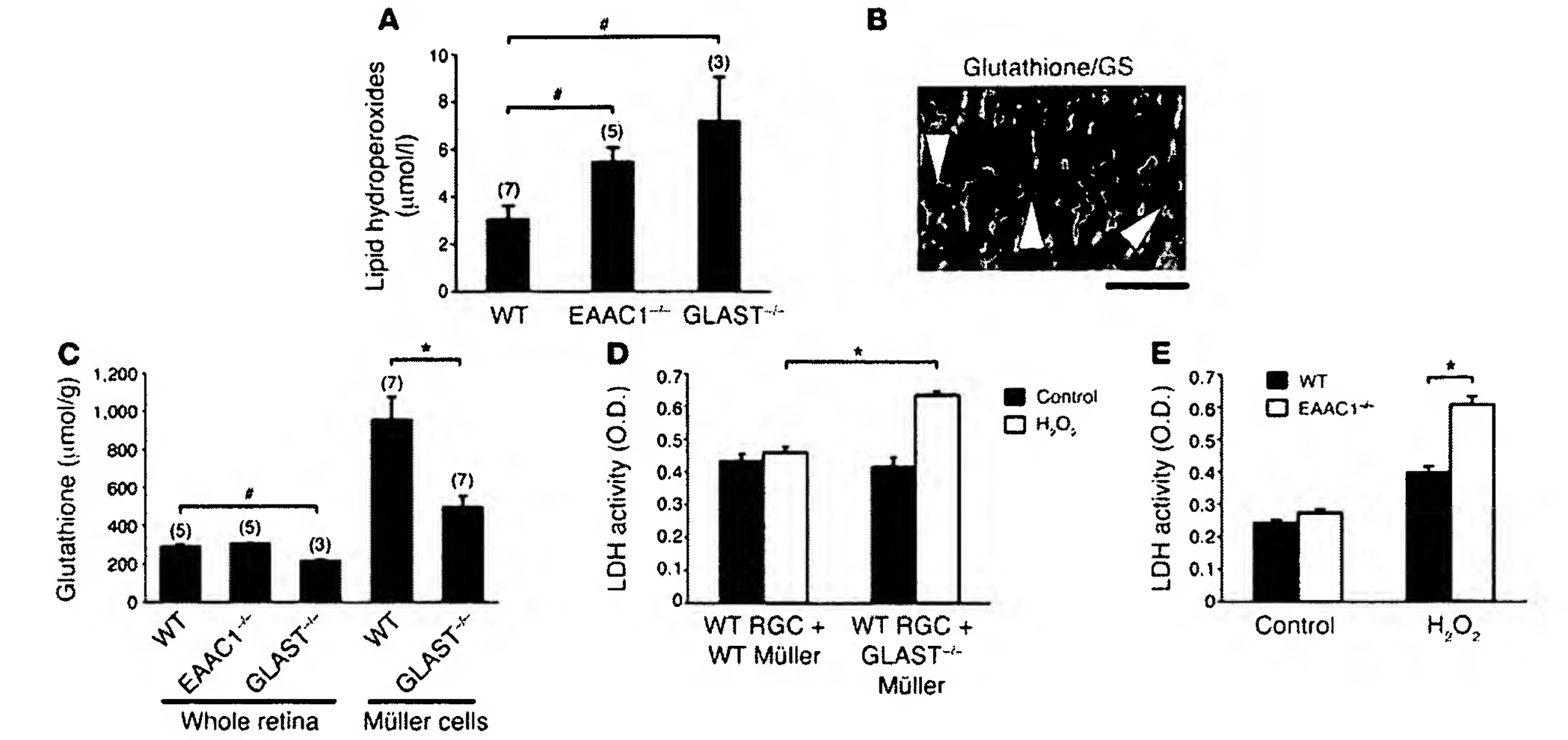

Figure 8
Increased oxidative stress in glutamate transporter mutant mice. (**A**) Lipid hydroperoxide concentration in whole retina of WT, EAAC1$^{-/-}$, and GLAST$^{-/-}$ mice. Sample numbers are indicated in parentheses. (**B**) Immunohistochemical analysis of mouse retina double-stained with glutathione and GS. Glutathione-like immunoreactivity was observed in Müller glial cells (arrowheads). Scale bar: 20 μm. (**C**) Mean glutathione concentration in whole retina and cultured Müller cells. Sample numbers are indicated in parentheses. (**D**) Lactate dehydrogenase (LDH) release from H_2O_2-treated RGCs cocultured with WT or GLAST$^{-/-}$ Müller cells. $n = 3$ per group. (**E**) Lactate dehydrogenase release from H_2O_2-treated RGCs from WT or EAAC1$^{-/-}$ mice. $n = 4$ per group. $^{\#}P < 0.05$; $^{*}P < 0.005$.

blinded to the identity of the mice, and the average number of RGCs/mm^2 was calculated. The changes in RGC number were expressed as percentages of the WT control eyes. In some experiments, memantine (10 mg/kg; Merz) was injected i.p. into GLAST$^{-/-}$ mice and their littermates daily from P7 to P13. These mice were sacrificed on P14 and processed for RGC count.

For the analysis of the optic nerve, frozen 10-μm–thick sections were cut at 2.5 mm from the eyeball and stained with H&E. Quantitative analysis of the optic nerve area was carried out using a computerized image analysis program (Scion Image Beta 4.0.3; Scion Corporation). For detailed morphological analysis, optic nerves were fixed in 2% glutaraldehyde and 2% paraformaldehyde in 0.1 M phosphate buffer overnight at 4°C. After dissection, the pieces of tissue were placed in 1% osmium tetroxide. After dehydration, the pieces were embedded in EPON (Nisshin EM). Transversal semithin (1 μm) sections were stained with 0.2% toluidine blue in 1.0% sodium borate.

IOP measurement. IOP was directly measured by a microneedle method in anesthetized mice as described previously (18, 51). The microneedle was connected to a pressure transducer, which relayed its signal to a bridge amplifier and then to an analog-to-digital converter and a computer (World Precision Instruments). The microneedle tip was inserted through the cornea and the data were automatically collected online into a computer database. To minimize variation, data were collected during a time window 4–6 minutes after injection of anesthetic, during which time IOP plateaued (51). Animal age was 4 weeks or 9–11 months, and body weight ranges were 13–24 g or 28–36 g at the time of IOP measurement, respectively. Since 24-hour IOP pattern in mouse eyes is biphasic and IOP is highest around 9:00 pm (18), we examined IOP between 8:00 pm and 11:00 pm.

mfERGs. Mice (12–16 weeks old) were anesthetized by i.p. injection of a mixture of xylazine (10 mg/kg) and ketamine (25 mg/kg). Pupils were dilated with 0.5% phenylephrine hydrochloride and 0.5% tropicamide. mfERGs were recorded using a VERIS 5.1 system (Electro-Diagnostic Imaging Inc.). The visual stimulus consisted of 7 hexagonal areas scaled with eccentricity. The stimulus array was displayed on a high-resolution black and white monitor driven at a frame rate of 100 Hz. The 2K, which is impaired in patients with glaucoma (20), was analyzed.

Glutamate assay. Vitreous samples (5–10 μl) were surgically extracted from adult mice, and glutamate was analyzed by serial enzymatic reactions as previously reported (52).

Cell culture. RGCs (16) and Müller cells (44) were prepared from P7 mice. In some experiments, WT RGCs were cocultured with Müller cells from GLAST$^{-/-}$ mice or their WT littermates. These culture cells were stimulated with 200 μM H_2O_2 for 16 hours, and RGC death rate was analyzed using a lactate dehydrogenase cytotoxic test kit (Wako) as previously reported (16).

Lipid peroxidation and glutathione assay. The concentrations of lipid peroxides and glutathione were measured using Bioxytech LPO-560 (Oxis Health Products Inc.) and Glutathione assay kit (Cayman Chemical) per the manufacturers' protocols.

Statistics. For statistical comparison of 2 samples, we used a 2-tailed Student's *t* test or Mann-Whitney *U* test. In other cases, we also used 1-factor ANOVA and Tukey-Kramer test. Data are presented as the mean ± SEM. $P < 0.05$ was regarded as statistically significant.

Acknowledgments

We thank X. Guo, K. Ajiki, and M. Ichikawa for technical assistance. This study was supported in part by grants from the Ministry of Education, Culture, Sports, Science and Technology of Japan, the Tokyo Biochemical Research Foundation, the Naito

Foundation, and the Uehara Memorial Foundation (to T. Harada). C. Harada was supported by a fellowship from Japan Society for the Promotion of Science for Young Scientists.

Received for publication August 28, 2006, and accepted in revised form April 24, 2007.

Address correspondence to: Kohichi Tanaka, Laboratory of Molecular Neuroscience, School of Biomedical Science and Medical Research Institute, Tokyo Medical and Dental University, 1-5-45 Yushima, Bunkyo-ku, Tokyo 113-8510, Japan. Phone: 81-3-5803-5846; Fax: 81-3-5803-5843; E-mail: tanaka.aud@mri.tmd.ac.jp.

1. Quigley, H.A. 1996. Number of people with glaucoma worldwide. *Br. J. Ophthalmol.* **80**:389–393.
2. Weinreb, R.N., and Khaw, P.T. 2004. Primary open-angle glaucoma. *Lancet.* **363**:1711–1720.
3. Klein, B.E., et al. 1992. Prevalence of glaucoma. The Beaver Dam Eye Study. *Ophthalmology.* **99**:1499–1504.
4. Bonomi, L., et al. 1998. Prevalence of glaucoma and intraocular pressure distribution in a defined population. The Egna-Neumarkt Study. *Ophthalmology.* **105**:209–215.
5. Iwase, A., et al. 2004. The prevalence of primary open-angle glaucoma in Japanese: the Tajimi Study. *Ophthalmology.* **111**:1641–1648.
6. Anderson, D.R. 2003. Collaborative normal tension glaucoma study. *Curr. Opin. Ophthalmol.* **14**:86–90.
7. Wiggs, J.L. 2007. Genetic etiologies of glaucoma. *Arch. Ophthalmol.* **125**:30–37.
8. Osborne, N.N., Lascaratos, G., Bron, A.J., Chidlow, G., and Wood, J.P. 2006. A hypothesis to suggest that light is a risk factor in glaucoma and the mitochondrial optic neuropathies. *Br. J. Ophthalmol.* **90**:237–241.
9. Lindsey, J.D., and Weinreb, R.N. 2005. Elevated intraocular pressure and transgenic applications in the mouse. *J. Glaucoma.* **14**:318–320.
10. Danbolt, N.C. 2001. Glutamate uptake. *Prog. Neurobiol.* **65**:1–105.
11. Rauen, T. 2000. Diversity of glutamate transporter expression and function in the mammalian retina. *Amino Acids.* **19**:53–62.
12. Dalton, R. 2001. Private investigations. *Nature.* **411**:129–130.
13. Harada, T., et al. 1998. Functions of the two glutamate transporters GLAST and GLT-1 in the retina. *Proc. Natl. Acad. Sci. U. S. A.* **95**:4663–4666.
14. Watase, K., et al. 1998. Motor discoordination and increased susceptibility to cerebellar injury in GLAST mutant mice. *Eur. J. Neurosci.* **10**:976–988.
15. Peghini, P., Janzen, J., and Stoffel, W. 1997. Glutamate transporter EAAC-1-deficient mice develop dicarboxylic aminoaciduria and behavioral abnormalities but no neurodegeneration. *EMBO J.* **16**:3822–3832.
16. Harada, C., et al. 2006. Role of apoptosis signal-regulating kinase 1 in stress-induced neural cell apoptosis in vivo. *Am. J. Pathol.* **168**:261–269.
17. Tanaka, K., et al. 1997. Epilepsy and exacerbation of brain injury in mice lacking the glutamate transporter GLT-1. *Science.* **276**:1699–1702.
18. Aihara, M., Lindsey, J.D., and Weinreb, R.N. 2003. Twenty-four-hour pattern of mouse intraocular pressure. *Exp. Eye Res.* **77**:681–686.
19. Hasegawa, S., Ohshima, A., Hayakawa, Y., Takagi, M., and Abe, H. 2001. Multifocal electroretinograms in patients with branch retinal artery occlusion. *Invest. Ophthalmol. Vis. Sci.* **42**:298–304.
20. Sutter, E.E., and Bearse, M.A., Jr. 1999. The optic nerve head component of the human ERG. *Vision Res.* **39**:419–436.
21. Adachi, K., et al. 1998. Mechanisms of the pathogenesis of glutamate neurotoxicity in retinal ischemia. *Graefes Arch. Clin. Exp. Ophthalmol.* **236**:766–774.
22. Lipton, S.A. 2004. Paradigm shift in NMDA receptor antagonist drug development: molecular mechanism of uncompetitive inhibition by memantine in the treatment of Alzheimer's disease and other neurologic disorders. *J. Alzheimers Dis.* **6**(6 Suppl.):S61–S74.
23. Klein, J.A., et al. 2002. The harlequin mouse mutation downregulates apoptosis-inducing factor. *Nature.* **419**:367–374.
24. Tezel, G. 2006. Oxidative stress in glaucomatous neurodegeneration: mechanisms and consequences. *Prog. Retin. Eye Res.* **25**:490–513.
25. Schulz, J.B., Lindenau, J., Seyfried, J., and Dichgans, J. 2000. Glutathione, oxidative stress and neurodegeneration. *Eur. J. Biochem.* **267**:4904–4911.
26. Huster, D., Reichenbach, A., and Reichelt, W. 2000. The glutathione content of retinal Müller (glial) cells: effect of pathological conditions. *Neurochem. Int.* **36**:461–469.
27. Gherghel, D., Griffiths, H.R., Hilton, E.J., Cunliffe, I.A., and Hosking, S.L. 2005. Systemic reduction in glutathione levels occurs in patients with primary open-angle glaucoma. *Invest. Ophthalmol. Vis. Sci.* **46**:877–883.
28. Sarthy, V.P., et al. 2005. Glutamate transporter in retinal Müller cells from glutamate/aspartate transporter (GLAST) knockout mice. *Glia.* **49**:184–196.
29. Aoyama, K., et al. 2006. Neuronal glutathione deficiency and age-dependent neurodegeneration in the EAAC1 deficient mouse. *Nat. Neurosci.* **9**:119–126.
30. Naskar, R., Vorwerk, C.K., and Dreyer, E.B. 2000. Concurrent downregulation of a glutamate transporter and receptor in glaucoma. *Invest. Ophthalmol. Vis. Sci.* **41**:1940–1944.
31. Zoia, C.P., et al. 2005. Fibroblast glutamate transport in aging and in AD: correlations with disease severity. *Neurobiol. Aging.* **26**:825–832.
32. Tamura, H., et al. 2006. High frequency of open-angle glaucoma in Japanese patients with Alzheimer's disease. *J. Neurol. Sci.* **246**:79–83.
33. Libby, R.T., Gould, D.B., Anderson, M.G., and John, S.W. 2005. Complex genetics of glaucoma susceptibility. *Annu. Rev. Genomics Hum. Genet.* **6**:15–44.
34. Dringen, R., Pfeiffer, B., and Hamprecht, B. 1999. Synthesis of the antioxidant glutathione in neurons: supply by astrocytes of CysGly as precursor for neuronal glutathione. *J. Neurosci.* **19**:562–569.
35. Wu, G., Fang, Y.Z., Yang, S., Lupton, J.R., and Turner, N.D. 2004. Glutathione metabolism and its implications for health. *J. Nutr.* **134**:489–492.
36. Reichelt, W., Stabel-Burow, J., Pannicke, T., Weichert, H., and Heinemann, U. 1997. The glutathione level of retinal Müller glial cells is dependent on the high-affinity sodium-dependent uptake of glutamate. *Neuroscience.* **77**:1213–1224.
37. Riepe, R.E., and Norenburg, M.D. 1977. Müller cell localisation of glutamine synthetase in rat retina. *Nature.* **268**:654–655.
38. Li, Q., and Puro, D.G. 2002. Diabetes-induced dysfunction of the glutamate transporter in retinal Müller cells. *Invest. Ophthalmol. Vis. Sci.* **43**:3109–3116.
39. Ohia, S.E., Opere, C.A., and LeDay, A.M. 2005. Pharmacological consequences of oxidative stress in ocular tissues. *Mutation Res.* **579**:22–36.
40. Lipton, S.A. 2001. Retinal ganglion cells, glaucoma and neuroprotection. *Prog. Brain Res.* **131**:712–718.
41. Yamashita, H., Kawakami, H., Zhang, Y.X., Tanaka, K., and Nakamura, S. 1995. Neuroprotective mechanism of bromocriptine. *Lancet.* **346**:1305.
42. Tanaka, K. 2005. Antibiotics rescue neurons from glutamate attack. *Trends Mol. Med.* **11**:259–262.
43. Harada, T., et al. 2000. Modification of glial-neuronal cell interactions prevents photoreceptor apoptosis during light-induced retinal degeneration. *Neuron.* **26**:533–541.
44. Harada, T., et al. 2002. Microglia-Müller glia cell interactions control neurotrophic factor production during light-induced retinal degeneration. *J. Neurosci.* **22**:9228–9236.
45. Ooto, S., et al. 2004. Potential for neural regeneration after neurotoxic injury in the adult mammalian retina. *Proc. Natl. Acad. Sci. U. S. A.* **101**:13654–13659.
46. Harada, T., Harada, C., and Parada, L.F. 2007. Molecular regulation of visual system development: more than meets the eye. *Genes Dev.* **21**:367–378.
47. Bringmann, A., et al. 2006. Müller cells in the healthy and diseased retina. *Prog. Retin. Eye Res.* **25**:397–424.
48. Harada, C., Mitamura, Y., and Harada, T. 2006. The role of cytokines and trophic factors in epiretinal membranes: involvement of signal transduction in glial cells. *Prog. Retin. Eye Res.* **25**:149–164.
49. Rothstein, J.D., et al. 1994. Localization of neuronal and glial glutamate transporters. *Neuron.* **13**:713–725.
50. Fontaine, V., et al. 2002. Neurodegenerative and neuroprotective effects of tumor necrosis factor (TNF) in retinal ischemia: opposite roles of TNF receptor 1 and TNF receptor 2. *J. Neurosci.* **22**:RC216.
51. Aihara, M., Lindsey, J.D., and Weinreb, R.N. 2002. Reduction of intraocular pressure in mouse eyes treated with latanoprost. *Invest. Ophthalmol. Vis. Sci.* **43**:146–150.
52. Mitani, A., and Tanaka, K. 2003. Functional changes of glial glutamate transporter GLT-1 during ischemia: an in vivo study in the hippocampal CA1 of normal mice and of mutant mice lacking GLT-1. *J. Neurosci.* **23**:7176–7182.

Exhibit E

Proc. Natl. Acad. Sci. USA
Vol. 95, pp. 4663–4666, April 1998
Neurobiology

Functions of the two glutamate transporters GLAST and GLT-1 in the retina

TAKAYUKI HARADA*†, CHIKAKO HARADA*†, MASAHIKO WATANABE‡, YOSHIRO INOUE‡, TAKASHI SAKAGAWA§, NAOKI NAKAYAMA¶, SHOJI SASAKI¶, SHIGERU OKUYAMA‖, KEI WATASE*, KEIJI WADA*, AND KOHICHI TANAKA*,**

*Department of Degenerative Neurological Diseases, National Institute of Neuroscience, NCNP, Kodaira, Tokyo 187-8502, Japan; Departments of †Ophthalmology and ‡Anatomy, Hokkaido University School of Medicine, Sapporo 060-8638, Japan; and §Laboratory of Animal Center, ¶Toxicology Laboratory, Pharmaceutical Research Laboratories, and ‖1st Laboratory, Medicinal Research Laboratories, Taisho Pharmaceutical Company, Ltd., Ohmiya, Saitama 330-8530, Japan

Edited by John E. Dowling, Harvard University, Cambridge, MA, and approved February 9, 1998 (received for review October 15, 1997)

ABSTRACT **In the retina, the glutamate transporter GLAST is expressed in Müller cells, whereas the glutamate transporter GLT-1 is found only in cones and various types of bipolar cells. To investigate the functional role of this differential distribution of glutamate transporters, we have analyzed GLAST and GLT-1 mutant mice. In GLAST-deficient mice, the electroretinogram b-wave and oscillatory potentials are reduced and retinal damage after ischemia is exacerbated, whereas GLT-1-deficient mice show almost normal electroretinograms and mild increased retinal damage after ischemia. These results demonstrate that GLAST is required for normal signal transmission between photoreceptors and bipolar cells and that both GLAST and GLT-1 play a neuroprotective role during ischemia in the retina.**

L-Glutamate is the major excitatory neurotransmitter in the mammalian retina (1). High-affinity glutamate transporters are believed to be essential for terminating synaptic transmission as well as for keeping the extracellular glutamate concentration below neurotoxic levels (1, 2). Five subtypes of glutamate transporter (GLAST, GLT-1, EAAC1, EAAT4, and EAAT5) (3–8) have been cloned, but the contributions of individual transporter subtypes to retinal function are poorly understood. Studies have been hampered by the lack of subtype-selective glutamate transporter drugs. As an alternative approach, we have analyzed GLAST- and GLT-1-deficient mice (9, 10). Our results demonstrate that GLAST is required in retinal signal transmission at the level of the photoreceptor and bipolar cell and that GLAST and GLT-1 are crucial for the protection of retinal cells from glutamate neurotoxicity.

MATERIALS AND METHODS

Immunohistochemistry. Mice were anesthetized with diethyl ether and perfused transcardially with saline, followed by 4% paraformaldehyde in 0.1 M sodium phosphate buffer containing 0.5% picric acid at room temperature. Eyes were removed and postfixed overnight in the same fixative, and 7-μm-thick paraffin or frozen sections were cut and mounted onto gelatin- and poly-L[D]-lysine-coated slides. The sections were incubated overnight with an affinity-purified rabbit polyclonal antibody against the carboxyl-terminal sequence of the mouse GLAST (1.0 μg/ml) (KKPYQLIAQDNEPEKPVADSETKM) (11, 12), an affinity-purified rabbit polyclonal antibody against the rat GLT-1 (0.2 μg/ml) [anti-B12; gift from N. C. Danbolt] (13), or a mouse monoclonal antibody against glutamate synthetase (GS) (2.0 μg/ml) (Chemicon) at room temperature. The sections were then incubated with biotinylated goat anti-rabbit IgG (Nichirei, Tokyo) for GLAST and GLT-1 or biotinylated rabbit anti-mouse IgG (Nichirei) for GS for 1 hr, followed by further incubation with streptavidin-Texas red (NEN) for 30 min at room temperature. Sections were examined by a confocal laser scanning microscope (Molecular Dynamics).

Electroretinograms (ERGs). Mice (9–11 weeks old) were anesthetized by intraperitoneal injection of a mixture of xylazine (10 mg/kg) and ketamine (25 mg/kg). The pupils were dilated with 0.5% phenylephrine·hydrochloride and 0.5% tropicamide. A carbon fiber electrode was placed on the corneal surface, and a reference electrode was attached subcutaneously on the forehead. Single-flash ERGs were recorded after dark adaptation for more than 30 min. The animal's position was secured with a bite board and head holder to ensure a 30-cm distance between the photostimulator (SLS-3100, Nihon Kohden, Tokyo) and both eyes for all experiments. White test flashes of 10-μs duration, with an intensity of 0.6 or 1.2 J, were presented. A bandpass frequency setting of 50–1000 Hz and 1–1000 Hz on the amplifier (Nihon Kohden, MEB-5304) was used to record the oscillatory potentials (OPs) and the a- and b-waves, respectively. The two responses were averaged with an averager (Nihon Kohden, MEB-5304). The a-wave amplitude was determined from the baseline to the bottom of the a-wave. The b-wave amplitude was determined from the baseline to the top of the b-wave. The OPs consisted of three to four wavelets (OP1-OP4). Because the third and fourth wavelets (OP3 and OP4) were missing in some instances, we limited the measurement to the constantly recordable OP1 and OP2 wavelets.

Induction of Retinal Ischemia. Adult mice (7–10 weeks old) were anesthetized with intraperitoneal injections of pentobarbital (60 mg/kg). Ischemia was achieved and the animals were treated essentially as described (14). Briefly, we instilled sterile saline into the anterior chamber of the right eye at 150 cm H_2O pressure for 60 min while the left eye served as nonischemic control. The animals were sacrificed 7 days after reperfusion, and eyes were enucleated for histological and morphometric study.

Histology and Morphometric Studies. The enucleated eyes were fixed in 4% paraformaldehyde and 1% glutaraldehyde buffered with 0.2 M sodium cacodylate (pH 7.4), followed by 10% paraformaldehyde in 0.1 M sodium phosphate buffer (pH 7.4) and embedded in paraffin. The posterior part of the eyes was sectioned sagittaly at 7 μm thickness through the optic

The publication costs of this article were defrayed in part by page charge payment. This article must therefore be hereby marked "*advertisement*" in accordance with 18 U.S.C. §1734 solely to indicate this fact.

This paper was submitted directly (Track II) to the *Proceedings* office.
Abbreviations: GS, glutamate synthetase; ERG, electroretinogram; INL, inner nuclear layer; IPL, inner plexiform layer; OPL, outer plexiform layer.

**To whom reprint requests should be addressed at: Department of Degenerative Neurological Diseases, National Institute of Neuroscience, NCNP, 4-1-1 Ogawahigashi-cho, Kodaira, Tokyo 187-8502, Japan. e-mail: tanaka@ncnaxp.ncnp.go.jp.

nerve, mounted, and stained with hematoxylin and eosin. For the estimation of the thickness of the inner retinal layer, measurements were performed with a calibrated reticle at 80× magnification (Kontron Elektronik, Imaging System KS100). Four sections of each eye were used for measurements. Five animals were used in each group. Results are presented as mean ± SEM and n is the number of eyes examined for each group. Student's t test was used to estimate the significance of the results.

RESULTS

Localization of Glutamate Transporters GLAST and GLT-1 in the Mouse Retina. In the brain, GLAST and GLT-1 are localized in the glia (13, 15). However, in the rat retina, GLAST is expressed in Müller cells (16, 17), whereas GLT-1 is expressed only in a specialized and restricted set of neuronal cells (mainly cone photoreceptors and cone bipolar cells) (17, 18). We verified that these localizations are also true for the mouse. Fig. 1 presents vertical sections through a mouse retina immunostained with GLAST or GLT-1 antibody. GLAST immunoreactivity is present throughout the retina, from the inner limiting membrane to the outer limiting membrane (Fig. 1 *D* and *F*). Antibodies raised against GS, a specific marker for Müller cells (16), showed a very similar staining pattern (Fig. 1 *J–L*), indicating that GLAST is predominantly expressed in Müller cells. GLT-1 immunoreactivity is present in a small fraction of photoreceptors (Fig. 1, *G* and *H*). The sparse population of their cell bodies and the termination of their axons in pedicles suggests that they are cones. In the INL, bipolar cell bodies are labeled. The findings are in agreement with those reported by Rauen and Kanner for the rat retina (18).

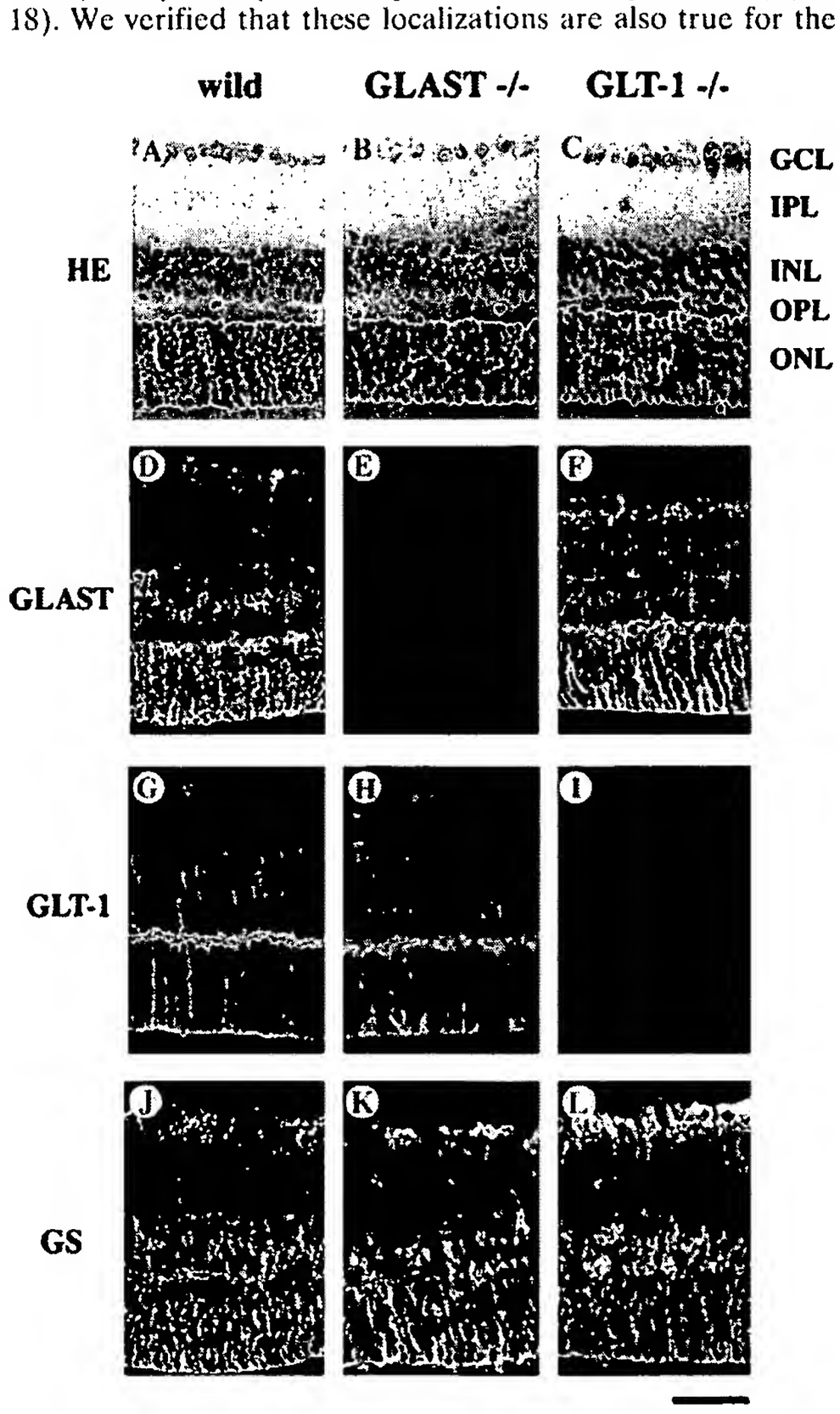

FIG. 1. Histological and immunohistochemical analyses of the retinae of the wild-type and GLAST and GLT-1 mutant mice. (*A–C*) Vertical sections of the adult mouse retinae from wild-type (*A*) and GLAST (*B*) and GLT-1 (*C*) mutant mice were stained with hematoxylin and eosin. GCL, ganglion cell layer; IPL, inner plexiform layer; INL, inner nuclear layer; OPL, outer plexiform layer; ONL, outer nuclear layer; HE, hematoxylin and eosin. (*D–L*) Sections of wild-type (*D*, *G*, and *J*) and GLAST (*E*, *H*, and *K*) and GLT-1 (*F*, *I*, and *L*) mutant mouse retinae were immunostained with the GLAST antibody (*D–F*), the GLT-1 antibody (*G–I*), and the GS antibody (*J–L*). (Scale bar = 50 μm.)

Histological and Immunohistochemical Analyses of the Retinae of GLAST- and GLT-1-Deficient Mice. We next examined whether the absence of GLAST or GLT-1 affects the anatomical organization of the retina by histological and immunohistochemical analyses. Hematoxylin and eosin staining revealed the retinae of GLAST or GLT-1 mutant mice to be normally organized, consisting of several different cell layers (Fig. 1 *A–C*). In the GLAST or GLT-1 mutant animal, immunoreactivity for GLAST or GLT-1, respectively, observed in the wild-type animal was completely absent (Fig. 1 *E* and *I*). Müller cells in the two mutant mice appeared normal when they were analyzed with the GS antibody (Fig. 1, *J–L*). Thus, there are no gross anatomical changes in the retina of GLAST- and GLT-1-deficient mice.

ERGs of GLAST- and GLT-1-Deficient Mice. To examine the physiological function of GLAST and GLT-1 in visual synaptic transmission *in vivo*, we analyzed single-flash ERG patterns of GLAST and GLT-1 mutant mice. The ERG response to a light flash can be divided into three waves, named a-wave, b-wave, and OPs (19). The a-wave arises principally from photoreceptors, whereas the b-wave and OPs originate mainly in ON bipolar cells and the amacrine/interplexiform cells, respectively (19–21). Although the GLAST mutant mice had a normal a-wave amplitude, their b-waves and OPs were attenuated by more than 50% compared with the wild-type mice (Fig. 2*A* and Table1). The ratio of b-wave to a-wave amplitude (b/a ratio) was significantly lower in GLAST mutant mice than in the wild-type mice (Table 1). In contrast, no apparent difference was found in the amplitudes of a-wave, b-wave, and OPs and b/a ratio between GLT-1 mutant and wild-type mice (Fig. 2*B* and Table 1). In both GLAST and GLT-1 mutant mice, the latency of a- and b-wave was slightly prolonged (Fig. 2). The same results were also obtained at a lower illumination intensity. These results suggest that GLAST is essential for proper neurotransmission of the light response from photoreceptors to bipolar cells.

Ischemia-Induced Retinal Damage in GLAST- and GLT-1- Deficient Mice. Glutamate transporters are thought to play a major role in keeping the extracellular glutamate concentration below neurotoxic levels (1, 2). To investigate this pathological role of GLAST and GLT-1 *in vivo*, we subjected GLAST and GLT-1 mutant mice to retinal ischemia. Retinal ischemia was induced by increasing intraocular pressure above systolic pressure for 60 min, and retinal injury was evaluated morphologically and morphometrically by measuring the thickness of the inner retinal layers (IRL, between the internal limiting membrane and the interface of the OPL and the outer nuclear layer). The representative qualitative pictures of the changes induced by ischemia in wild-type and GLAST and GLT-1 mutant mice are shown in Fig. 3. Seven days after pressure-induced ischemia, a decrease of the thickness in the inner plexiform layer (IPL), disorganization of the INL, and few and atypical ganglion cells were seen in the wild-type mice (Fig. 3 *A* and *B*). In GLAST mutant mice, the degenerative changes in IRL were more severe than those in the wild-type mice. Almost

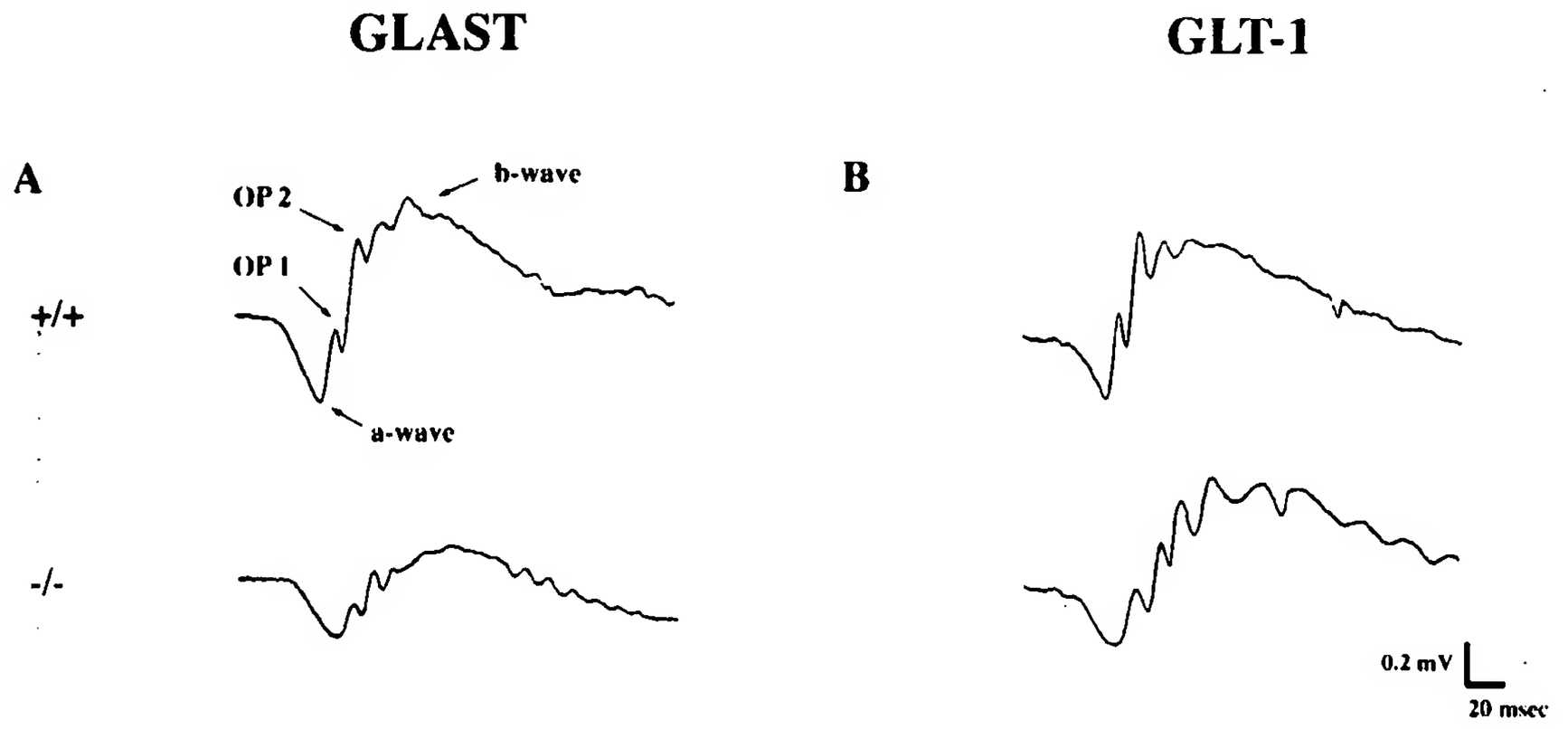

FIG. 2. ERGs of the wild-type and GLAST and GLT-1 mutant mice. (*A*) Dark-adapted ERG responses from the wild-type mouse (+/+) and GLAST mutant mouse (−/−). (*B*) Dark-adapted ERG responses from the wild-type mouse (+/+) and GLT-1 mutant mouse (−/−).

complete disappearance of the cells of the INL was observed in GLAST mutant mice. Furthermore, the nerve fiber layer, the IPL, and the OPL were thinner in GLAST mutant mice than in the wild-type siblings (Fig. 3*D*). In GLT-1 mutant mice, the ischemic degenerative changes were more severe than those in the wild-type mice, but clearly milder than those of the GLAST knockout mice (Fig. 3*C*).

Quantification of the effects of ischemia revealed that the thickness of IRL decreased from 101 ± 3 μm in untreated controls (n = 5) to 71 ± 4 μm in ischemic eyes of the wild-type mice (n = 5)(Fig. 3*E*). In GLAST mutant mice, a significant increase in ischemic damage was observed ($P < 0.05$). The IRL of ischemic eyes from GLAST mutant mice was 36 ± 2 μm (n = 5). In contrast, GLT-1 mutant mice showed a significantly higher IRL (53 ± 3 μm; n = 5; $P < 0.05$) than GLAST mutant mice. These data indicate that both GLAST and GLT-1 play an active role in preventing excitotoxic retinal damage after ischemia, but that GLAST participates more actively in the protection from ischemia than does GLT-1.

DISCUSSION

In the brain, GLAST is most abundantly expressed in the processes of Bergmann glia (15), cerebellar astrocytes associated with Purkinje cells (PCs). Bergmann glial processes surround the two distinct glutamatergic synapses onto PCs (i.e., parallel fiber and climbing fiber to PC synapses) (22). However, GLAST is not the dominant factor that determines the kinetics of excitatory postsynaptic synaptic currents at these synapses (10). In contrast, GLAST plays an essential role in the proper signal transmission in the retina. This finding is of interest because terminals of photoreceptors and bipolar cells have specific structural and functional features. They contain dense bars or ribbons anchored to the presynaptic membrane and covered with a layer of synaptic vesicles (23). In contrast to conventional synapses (i.e., parallel fiber and climbing fiber to PC synapses), which release neurotransmitter transiently, these ribbon synapses release neurotransmitter continuously (24). At the onset of a bright light, photoreceptors diminish their release of glutamate. Transmission of this effect to postsynaptic cells (bipolar cells) requires that the glutamate in the synaptic cleft be removed by either diffusion or reuptake. Therefore, GLAST is not required for proper synaptic transmission at conventional synapses but is essential for normal synaptic transmission at the photoreceptor synapse.

Our observation of the greater excitotoxic retinal damage in GLAST mutant mice than in GLT-1 mutant mice is compatible with the previous finding that accumulation of L[D]-[^{3}H]glutamate occurred predominantly in Müller cells (25). Furthermore, the occurrence of ischemic damage not only in IPL but also in OPL of GLAST mutant mice is in agreement with the previous finding that GLAST is expressed in Müller cell processes that ramify extensively in both IPL and OPL (16, 17). The results of our investigation indicate that both GLAST and GLT-1 play a neuroprotective role against ischemic retinal injury, but that GLAST participates more actively in the prevention of glutamate neurotoxicity after ischemia in the retina than does GLT-1. The neuroprotective role of GLAST and GLT-1 is in agreement with the previous finding that antisense knockout of GLAST and GLT-1 resulted in neurodegeneration characteristic of excitotoxicity (26). It has been suggested that under ischemia, glutamate neurotoxicity is exacerbated because of reversal of glutamate transport (27). However, our result indicates that GLAST and GLT-1 play a neuroprotective role during ischemia. Ischemic injury is implicated in a number of pathological states, such as central retinal artery occlusion, glaucoma, diabetic retinopathy, etc. Accordingly, the present results raise intriguing possibilities for the management of these pathological conditions with glutamate transporter activators, such as bromocryptine (28, 29).

Table 1. ERG responses

Mice	n	a-wave amplitude, μV	b-wave amplitude, μV	b/a amplitude ratio	OP1 amplitude, μV	OP2 amplitude, μV
Wild type	16	237.5 ± 26.2	461.9 ± 33.8	2.15 ± 0.19	173.8 ± 14.7	264.4 ± 17.7
GLAST −/−	8	253.8 ± 29.6	217.5 ± 30.9*	0.98 ± 0.21*	72.8 ± 7.6*	114.3 ± 12.4*
GLT-1 −/−	4	267.5 ± 66.9	475.0 ± 72.2	2.27 ± 0.78	137.5 ± 18.9	225.0 ± 23.6

All data are expressed as mean ± SEM; *, $P < 0.005$ (two-tailed t test).

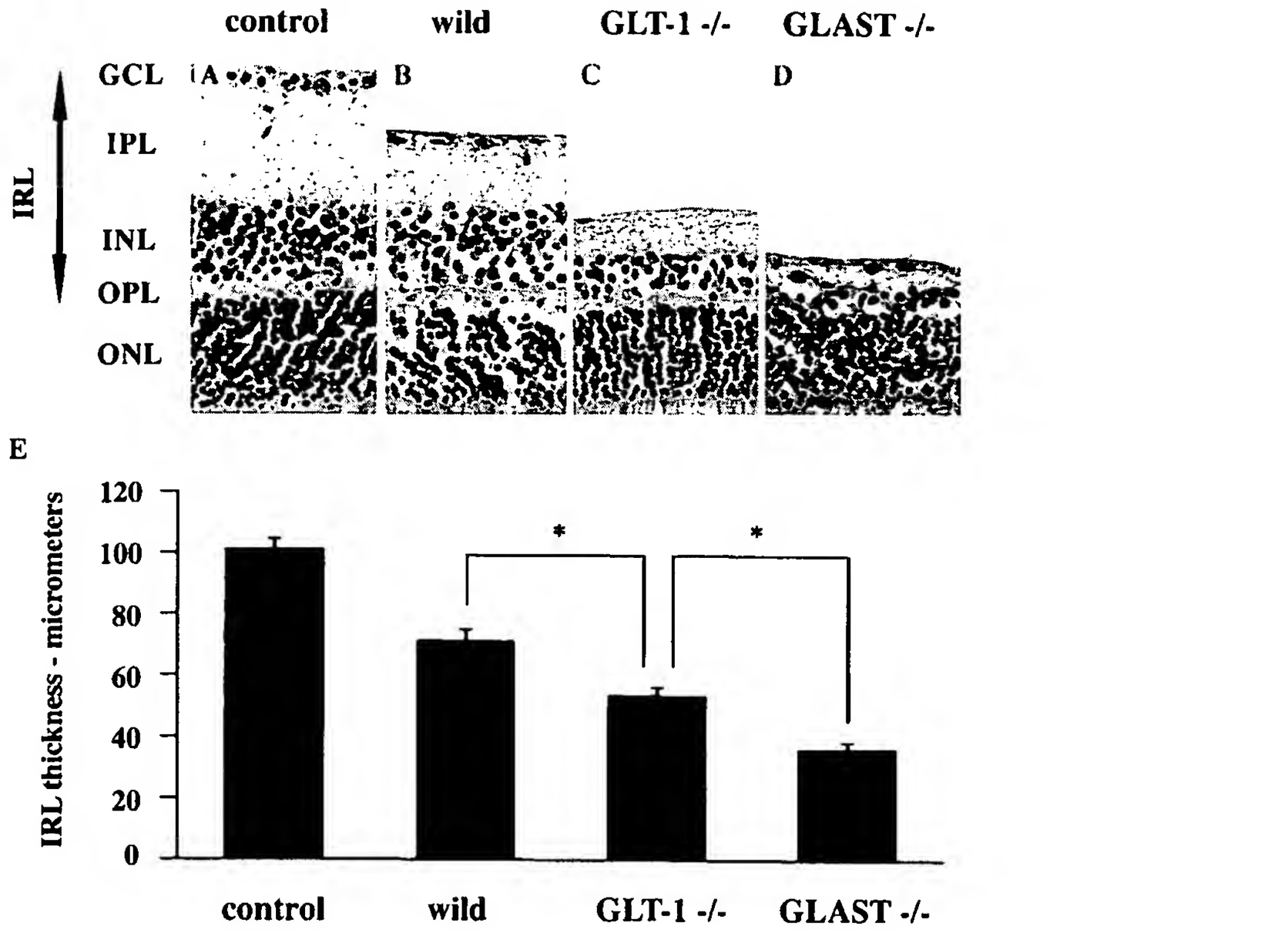

FIG. 3. The ischemic retinal changes in the wild-type and GLAST and GLT-1 mutant mice. (*A*) Micrograph of a section of a retina in the control eye taken from the wild-type mouse. (*B–D*) Ischemic retinae from the wild-type (*B*) and GLT-1 (*C*) and GLAST (*D*) mutant mouse. IRL, inner retinal layer; other abbreviations as in Fig. 1. (*E*) Mean thickness of the inner retinal layers of the retinae in control eyes from the wild-type mice and in ischemic eyes from the wild-type and GLT-1 and GLAST mutant mice. Columns and error bars represent mean ± SEM (*, $P < 0.05$).

To date, research on glutamate transporters in the retina has been conducted largely in isolated cells. Thus, GLAST and GLT-1 mutant mice will provide *in vivo* models for studying the role of glutamate transporters in retinal function.

We thank Dr. N. C. Danbolt for providing the antibodies to GLT-1. This work was supported in part by research grants from the Ministry of Education, Science, and Culture of Japan, the Ministry of Health and Welfare of Japan, the Science and Technology Agency of Japan, and the Japan Foundation for Neuroscience and Mental Health.

1. Barnstable, C. J. (1993) *Curr. Opin. Neurobiol.* **3,** 520–525.
2. Newman, E. & Reichenbach, A. (1996) *Trends Neurosci.* **19,** 307–312.
3. Storck, T., Schulte, S., Hofmann, K. & Stoffel, H. (1992) *Proc. Natl. Acad. Sci. USA* **89,** 10955–10959.
4. Pines, D., Danbolt, N. C., Bjoras, M., Zhang, Y., Bendahan, A., Eide, L., Koepsell, H., Storm, M. J., Seeberg, E. & Kanner, B. I. (1992) *Nature (London)* **360,** 464–467.
5. Kanai, Y. & Hediger, M. A. (1992) *Nature (London)* **360,** 467–471.
6. Tanaka, K. (1993) *Neurosci. Res.* **16,** 149–153.
7. Fairman, W. A., Vandenberg, R. J., Arriza, J. L., Kavanaugh, M. P. & Amara, S. G. (1995) *Nature (London)* **375,** 599–603.
8. Arriza, J. L., Eliasof, S., Kavanaugh, M. P. & Amara, S. G. (1997) *Proc. Natl. Acad. Sci. USA* **94,** 4155–4160.
9. Tanaka, K., Watase, K., Manabe, T., Yamada, K., Watanabe, M., Takahashi, K., Iwama, H., Nishikawa, T., Ichihara, N., Kikuchi, T., Okuyama, S., Kawashima, N., Hori, S., Takimoto, M. & Wada, K. (1997) *Science* **276,** 1699–1702.
10. Watase, K., Hashimoto, K., Kano, M., Yamada, K., Watanabe, M., Inoue, Y., Okuyama, S., Sakagawa, T., Ogawa, S., Kawashima, N., Hori, S., Takimoto, M., Wada, K. & Tanaka, K. (1998) *Eur. J. Neurosci.* **10,** 976–988.
11. Tanaka, K. (1993) *Neurosci. Lett.* **159,** 183–186.
12. Shibata, T., Yamada, K., Watanabe, M., Ikenaka, K., Wada, K., Tanaka, K. & Inoue, Y. (1997) *J. Neurosci.* **17,** 9212–9219.
13. Lehre, K. P., Levy, L. M., Ottersen, O. P., Storm-Mathisen, J. & Danbolt, N. C. (1995) *J. Neurosci.* **15,** 1835–1853.
14. Takahashi, K., Lam, T. T., Edward, D. P., Buchi, E. R. & Tso, M. O. M. (1992) *Arch. Ophthalmol.* **110,** 862–870.
15. Rothstein, J. D., Martin, L., Levey, A. I., Dykes-Hoberg, M., Jin, L., Wu, D., Nash, N. & Kuncl, R. W. (1994) *Neuron* **13,** 713–725.
16. Derouiche, A. & Rauen, T. (1995) *J. Neurosci. Res.* **42,** 131–143.
17. Rauen, T., Rothstein, J. D. & Wässle, H. (1996) *Cell Tissue Res.* **286,** 325–336.
18. Rauen, T. & Kanner, B. I. (1994) *Neurosci. Lett.* **169,** 137–140.
19. Steinberg, R. H., Frishman, L. J. & Sieving, P. A. (1991) in *Progress in Retinal Research*, eds. Osborne, N. N. & Chader, G. J. (Pergamon, Oxford), Vol. 10, pp. 121–160.
20. Masu, M., Iwakabe, H., Tagawa, Y., Miyoshi, T., Yamashita, M., Fukuda, Y., Sasaki, H., Hiroi, K., Shigemoto, R., Takada, M., Nakamura, K., Nakao, K., Katsuki, M. & Nakanishi, S. (1995) *Cell* **80,** 757–765.
21. Speros, P. & Price, A. J. (1981) *Surv. Ophthalmol.* **25,** 237–252.
22. Ito, M. (1984) *The Cerebellum and Neural Control* (Raven, New York).
23. Burns, M. E. & Augustine, G. J. (1995) *Cell* **83,** 187–194.
24. Juusola, M., French, A. S., Uusitalo, R. O. & Weckström, M. (1996) *Trends Neurosci.* **19,** 292–297.
25. Ehinger, B. & Flack, B. (1971) *Brain Res.* **33,** 157–172.
26. Rothstein, J. D., Dykes-Hoberg, M., Pardo, C. A., Bristol, L. A., Jin, L., Kuncl, R. W., Kanai, Y., Hediger, M. A., Wang, Y., Schieke, J. P. & Welty, D. F. (1996) *Neuron* **16,** 675–686.
27. Nicholls, D. & Attwell, D. (1990) *Trends Neurosci.* **11,** 462–468.
28. Yamashita, H., Kawakami, H., Zhang, Y.-X., Tanaka, K. & Nakamura, S. (1995) *Lancet* **346,** 1305.
29. Yamashita, H., Kawakami, H., Zhang, Y.-X., Tanaka, K. & Nakamura, S. (1998) *J. Neurol. Sci.,* in press.